TAMPEREEN TEKNILLINEN YLIOPISTO
TAMPERE UNIVERSITY OF TECHNOLOGY

Virpi Tunninen

Parathyroid Scintigraphy

Optimization of ^{99m}Tc-sestamibi/^{123}I subtraction SPECT/CT

Julkaisu 1500 • Publication 1500

Tampere 2017

Tampereen teknillinen yliopisto. Julkaisu 1500
Tampere University of Technology. Publication 1500

Virpi Tunninen

Parathyroid Scintigraphy

Optimization of ^{99m}Tc-sestamibi/^{123}I subtraction SPECT/CT

Thesis for the degree of Doctor of Philosophy to be presented with due permission for public examination and criticism in Auditorium 126, at Tampere University of Technology - Pori, on the 13th of October 2017, at 12 noon.

Tampereen teknillinen yliopisto - Tampere University of Technology
Tampere 2017

Doctoral candidate: Virpi Tunninen
Department of Nuclear Medicine
Satakunta Central Hospital
Finland

Supervisor: Hannu Eskola, Professor
Faculty of Biomedical Sciences and Engineering
Tampere University of Technology
Finland

Instructors: Tomi Kauppinen, Adjunct Professor
Helsinki University Central Hospital
Finland

Matti Koskinen, Adjunct Professor
Finland

Pre-examiners: Jari Heikkinen, Adjunct Professor
Department of Medical Physics
The Social and Health Care Joint Authority of South Savo,
Mikkeli Central Hospital
University of Eastern Finland
Finland

Piotr Slomka, Professor
Artificial Intelligence In Medicine Program
Department of Imaging, Cedars-Sinai Medical Center
David Geffen School of Medicine, University of California
Los Angeles
USA

Opponent: Mika Teräs, Professor
University of Turku, Institute of Biomedicine
Turku University Hospital, Department of Medical Physics
Finland

ISBN 978-952-15-4011-0 (printed)
ISBN 978-952-15-4021-9 (PDF)
ISSN 1459-2045

Tiivistelmä

Lisäkilpirauhasten liikatoiminnassa eli hyperparatyreoosissa yksi tai useampi lisäkilpirauhanen tuottaa verenkiertoon liikaa lisäkilpirauhashormonia, mikä johtaa seerumin kalsiumpitoisuuden nousuun. Potilaalla voi olla monentyyppisiä oireita, joista tavanomaisin on osteoporoosi. Lisäkilpirauhasten liikatoiminnan ainoa parantava hoito on leikkaus, joka tehdään tavallisesti mini-invasiivista tekniikkaa käyttäen. Edellytys tälle on liikatoimisen lisäkilpirauhasen tarkka paikantaminen.

Liikatoimisen lisäkilpirauhasen paikantaminen tehdään tavallisesti isotooppitutkimusmenetelmällä. Käytettävissä on yksi tutkimusaine, ^{99m}Tc-sestamibi, joka ei kuitenkaan ole spesifinen lisäkilpirauhaskudokselle vaan kertyy lisäksi esimerkiksi kilpirauhaseen. Lisäkilpirauhasen erottamiseksi kilpirauhasesta on kehitetty erilaisia menetelmiä ja käytettävissä on myös erilaisia kuvaustekniikoita. Lopputuloksena on suuri määrä erilaisia tutkimusprotokollia, joiden herkkyys ja spesifisyys vaihtelevat suuresti.

Tämän väitöskirjatyön tavoitteena oli löytää optimaalinen tutkimusprotokolla liikatoimisen lisäkilpirauhasen paikantamiseen isotooppimenetelmiä käyttäen. Suomessa käytössä olevat tutkimusprotokollat selvitettiin ja erilaisia protokollia testattiin potilaiden avulla. Lupaavimmaksi osoittautunutta menetelmää optimoitiin erilaisten testikohteiden eli fantomien avulla.

Työssä osoitettiin, että kaksoisisotooppimenetelmä ^{99m}Tc-sestamibi- ja ^{123}I-merkkiaineita käyttäen on ylivoimainen yhden isotoopin käyttöön verrattuna. ^{99m}Tc-sestamibi/^{123}I -SPECT/CT –protokolla on erittäin herkkä ja spesifinen tutkimusmenetelmä liikatoimisten lisäkilpirauhasten paikantamisessa. Tutkimusmenetelmästä saatava kolmiulotteinen anatominen informaatio edesauttaa lisäksi adenooman tarkassa paikantamisessa.

Kuvauksessa ja kuvankäsittelyssä käytetyillä menetelmillä on merkittävä vaikutus ^{99m}Tc-sestamibi/^{123}I SPECT/CT –tutkimuksen lopputulokseen. Tarkasti optimoitu ^{99m}Tc-sestamibi/^{123}I SPECT/CT –tutkimus on yksinään riittävä menetelmä liikatoimisen lisäkilpirauhasen paikantamiseen, eikä lisäkuvauksia tarvita. Käytettävä menetelmä on kuitenkin syytä testata tunnettuja fantomeja käyttäen kussakin sairaalassa optimaalisen lopputuloksen saavuttamiseksi. Tämän väitöskirjatyön tuloksia hyödynnetään lisäkilpirauhasten gammakuvauksen suosituksen laatimisessa.

Abstract

Hyperparathyroidism is a common endocrine disorder caused by one or more hyperfunctioning parathyroid glands secreting excess amounts of parathyroid hormone. This leads to hypercalcemia that may lead to numerous clinical manifestations, such as osteoporotic fractures. Surgery is the only curative treatment, with current trends towards minimally invasive operations. A prerequisite for targeted operation is a sensitive and specific preoperative localization that is, also capable of identifying ectopic glands and multiple gland disease.

Preoperative localization is performed using nuclear medicine, i.e., scintigraphic techniques, with ^{99m}Tc-sestamibi being the imaging agent of choice. Unfortunately, ^{99m}Tc-sestamibi is not a specific agent for parathyroid tissue, and several protocols are in use with variable sensitivity and specificity figures.

The aim of this thesis was to find the optimal protocol for parathyroid scintigraphy with the highest sensitivity and specificity. Subsequently, the national status of protocols was investigated. These protocols were tested in the clinical environment and finally the protocol of choice was optimized with the use of phantoms.

Our results indicate that the dual-isotope method with ^{99m}Tc-sestamibi and ^{123}I is superior when compared with the use of ^{99m}Tc-sestamibi alone. ^{99m}Tc-sestamibi/^{123}I subtraction SPECT/CT is a highly sensitive and specific protocol for parathyroid scintigraphy and should be preferred over planar acquisition techniques due to important anatomical 3D information. However, acquisition and processing parameters have a profound effect on the outcome of ^{99m}Tc-sestamibi/^{123}I subtraction SPECT/CT. The protocol should therefore be tested with known anthropomorphic phantoms. With careful optimization, ^{99m}Tc-sestamibi/^{123}I subtraction SPECT/CT is an adequate technique for parathyroid scintigraphy without additional acquisitions. The results of this thesis will provide guidelines for proposing recommendations for parathyroid scintigraphy.

Acknowledgements

This thesis was carried out between 2008-2017 in the Department of Nuclear Medicine of Satakunta Central Hospital in Pori. I would like to thank the staff of the department for all the work during this project. I also would like to thank the head of the department and chief physician Pekka Varjo for supporting this project in addition to our busy clinical work.

My warmest thanks go to Professor Hannu Eskola, who provided me the opportunity to carry out this thesis under his supervision in the Faculty of Biomedical Sciences and Engineering at Tampere University of Technology. Hannu has also guided my postgraduate studies and licentiate thesis and continued with this work. Thank you for your guidance and support during all these years. I also would like to thank my supervisors, PhD, adjunct professor Matti Koskinen and PhD, adjunct professor Tomi Kauppinen for all guidance and valuable discussions during this work. I had the possibility to work as an assistant physicist in Tampere University Hospital between 1999-2000 and feel highly privileged to have had this experience. Matti also guided my licentiate thesis during those years, and some of the first discussions concerning dual-isotope imaging and this thesis go back to those years. Finally, my warmest thanks go to Tomi, with whom we have had hundreds of discussions by email, by phone and by WhatsApp. Thank you for your support, guidance, and friendship.

I wish to thank all my co-authors of the original articles, Pekka Varjo, Matti Koskinen, Aapo Ahonen, Jukka Schildt, Irina Lisinen, Anu Holm, Hannu Eskola, Marko Seppänen, and Tomi Kauppinen for their collaboration and valuable contributions during the preparation of this thesis. Especially I wish to thank Marko Seppänen, who has done most of the image review during this work. It has been a great privilege to work and learn with you. I also wish to express my gratitude to the staff of all departments of nuclear medicine in our country, as they have participated in this project in one way or another.

I wish to express my warmest thanks to the official pre-examiners of this thesis Adjunct Professor Jari Heikkinen and Professor Piotr Slomka, for their valuable comments and careful evaluation of the manuscript. I also wish to express my gratitude to Peter Heath, MA, for his accomplished revision of the English language of this thesis.

I would like to express my gratitude for the financial support of this thesis to Finnish Cultural Foundation / Satakunta Regional Fund, High Technology Foundation of Satakunta, evo-funding of Satakunta Hospital District, Finnish Society of Clinical Physiology and Finnish Society of Nuclear Medicine.

Being a medical physicist in a hospital is somewhat the best job I could imagine. It was 21 years ago when I joined the Department of Nuclear Medicine in Satakunta Central Hospital as a very young physicist. Thank you Pekka for giving me so much freedom in my work and having so much trust in me. Thank you Satu, Tiina and Katja for great work and time together and always-open "*complaint center*". Thank you for the whole staff of our department, it is a pleasure to work with you. In addition to our own de-

partment, being a medical physicist means also being a part of a multidisciplinary medical community and work with many excellent professionals within nuclear medicine and also outside this specialty in Satakunta Central Hospital and also in other hospitals in Finland.

Being a medical physicist means also being a part of a Finnish medical physicists community. Many of my colleagues have also become dear friends during these years. We have travelled together around Europe, visited museums, churches, aquariums (with a family ticket), numerous restaurants and night clubs – and some congress centers as well. At the same time the world (and all hospital stuff) has been put back on tracks. Thank you for team GT (Jussi V, Jussi H, Tomppa, Jarski, Pasi and Mikko) and all dear colleagues and friends who are too numerous to completely list here. However, a special thanks go to Herkko, who reminded me 11 years ago how cool nuclear medicine really was by being a great student! Other special thanks go to Anu with whom I work on a daily basis. Thank you for all valuable comments throughout this process.

I owe my deepest gratitude to my parents, Maija and Pentti Tunninen for great childhood and support for education. As I really wanted to become a horse groom (at the age of 14), my father strongly advised me to go to high school and think of something more reasonable. Even though he had no academic education, he was very interested in science and followed also this work. Unfortunately he passed away before this thesis was finished. I think he would have been the proudest of the whole audience if he could have been with us. While dad and I had thousands of "*lets repair the world*" discussions next to our kitchen table, my mother has been the greatest practical support for my family. She has packed her bags and arrived for help even in the shortest notice. In fact, the final two articles of this thesis wouldn´t have finished if she hadn´t come to keep up the household while I spend the endless nights in the nuclear medicine lab at the beginning of this year. My family also includes my little sister, Suvi. It´s good to have someone with similar sense of (black) humor next to you!

It also requires good friends to keep a PhD student at least partly sane. I won't be able to name you all as this page is going to end soon, but thank you all for friendship! However, a special thought goes to Susanna. Thank you for being there.

The most important ones are saved as last. During the final writing periods of this thesis, my dear family was instructed almost daily "*do not to talk to mum in the next three hours if there is no bleeding, broken bones or fire*". Kari and Anna, you two are my most important people. Thank you for your love and support, thank you for every day with the two of you. Nothing will ever make me more proud than being the mother of this wonderful little girl!

At home, 11th of August, 2017

Contents

Abbreviations

AP	Anterior image
Ca-ion	Ionized calcium
CT	Computed Tomography
EANM	The European Association of Nuclear Medicine
FBP	Filtered back-projection
FWHM	Full width at half maximum
FWTM	Full width at tenth maximum
HPT	Hyperparathyroidism
LEHR	Low-energy high resolution
LEUHR	Low-energy ultra-high resolution
MDR	Multidrug resistance protein
MELP	Medium-energy low penetration
P3	Inferior parathyroid glands originating from third pharyngeal pouches
P4	Superior parathyroid glands originating from fourth pharyngeal pouches
PM tube	Photomultiplier tube
PTH	Parathyroid hormone
ROI	Region of interest
SC-	No scatter correction applied
SC+	Scatter correction applied
SNM	The Society of Nuclear Medicine
SPECT	Single Photon Emission Computed Tomography
TEW	Triple Energy Window
UFOV	Useful field of view
VOI	Volume of interest

List of Original Publications

This thesis is based on the following original publications. They are referred to in the text by Roman numerals I-V.

I Tunninen V, Kauppinen T, Eskola H, Koskinen MO. Parathyroid scintigraphy protocols in Finland in 2010. Results of the query and current status. Nuklearmedizin. 2010;49(5):187-94.

II Virpi Tunninen, Pekka Varjo, Jukka Schildt, et al., "Comparison of Five Parathyroid Scintigraphic Protocols," International Journal of Molecular Imaging, vol. 2013, Article ID 921260, 12 pages, 2013. doi:10.1155/2013/921260

IV Tunninen V., Kauppinen T., Eskola H. (2018) Physical characteristics of collimators for dual-isotope imaging with ^{99m}Tc and ^{123}I. In: Eskola H., Väisänen O., Viik J., Hyttinen J. (eds) EMBEC & NBC 2017. EMBEC 2017, NBC 2017. IFMBE Proceedings, vol 65. Springer, Singapore.

V Tunninen V., Kauppinen T., Eskola H. (2018) Optimization of ^{99m}Tc-sestamibi/^{123}I subtraction SPECT/CT protocol for parathyroid scintigraphy. In: Eskola H., Väisänen O., Viik J., Hyttinen J. (eds) EMBEC & NBC 2017. EMBEC 2017, NBC 2017. IFMBE Proceedings, vol 65. Springer, Singapore.

Unpublished manuscripts

III Virpi Tunninen, Pekka Varjo, Tomi Kauppinen, Anu Holm, Hannu Eskola, Marko Seppänen. Tc-99m-sestamibi/I-123 subtraction SPECT/CT in parathyroid scintigraphy: Is additional pinhole imaging useful?

This thesis also contains some unpublished data

Author´s Contribution

The author was responsible for all parts of Studies I-V, with the exception of the patient image review. The author was responsible for the study design, but valuable comments were received from supervisors and co-authors. The author created all the acquisition and processing protocols used in this thesis, performed all patient image processing and data analysis, and collected patient data from the hospital records. The author prepared all phantoms and performed anthropomorphic phantom measurements and acquisitions and image processing including data analysis. The author had the main responsibility for writing the manuscript, but valuable comments were received from all co-authors

1 Introduction

Hyperparathyroidism (HPT) is a common endocrine disorder caused by one or more hyperfunctioning parathyroid glands that secrete excess amounts of parathyroid hormone and raise the blood calcium level. Surgery is the only curative treatment, and current trends are towards minimally invasive operations. A prerequisite for targeted operation is a sensitive and specific preoperative localization that is capable of identifying ectopic glands and multiple gland disease.

Preoperative localization is performed using nuclear medicine techniques, with ^{99m}Tc-sestamibi being the imaging agent of choice. Unfortunately, ^{99m}Tc-sestamibi is not a specific agent for parathyroid tissue, and it is also taken up by adjacent thyroid tissue. Two methods have evolved to overcome this problem: the dual-phase method and the dual-tracer method. The dual-phase method relies on the fact that thyroid and the parathyroid tissues have different washout kinetics for ^{99m}Tc-sestamibi. By acquiring images immediately after the injection of ^{99m}Tc-sestamibi and then 2 to 3 hours later, the focally increasing uptake will reveal the enlarged parathyroid gland. In the dual-isotope method, ^{99m}Tc-sestamibi is combined with ^{123}I, which is taken up by the thyroid gland only. Subtracting the thyroid image from the ^{99m}Tc-sestamibi image leaves only the enlarged parathyroid glands in the subtraction image.

The dual-phase method is attractive due to its technical simplicity and low cost. Unfortunately, the technique fails to detect parathyroid adenomas with rapid ^{99m}Tc-sestamibi clearance and has low sensitivity for identifying multiple-gland disease. These pitfalls can be avoided by using the technically more difficult dual-isotope method, where thyroid-seeking ^{123}I is acquired simultaneously with ^{99m}Tc-sestamibi, and ^{123}I images are subtracted from the ^{99m}Tc-sestamibi images. In this method, the enlarged parathyroid gland shows up as residual activity in the subtraction images.
Several acquisition techniques with various corrections and adjustable parameters can be used with both methods. Both planar imaging (with parallel hole or pinhole collimators) and three-dimensional (3D) imaging (SPECT and SPECT/CT) are widely used. To increase sensitivity, the techniques are often combined in clinical practice. The imaging protocols are not, however, standardized and a large variety of protocols with variable sensitivity figures are used.

This thesis originated from the question: ”*How should it be done*?” as results of parathyroid scintigraphy were not reliable according to the endocrine surgeon at Satakunta Central Hospital at that time. In this thesis, parathyroid scintigraphic methods and acquisition techniques were evaluated with a group of clinical patients suffering from primary or secondary hyperparathyroidism. The effect of the acquisition and processing techniques and the optimization of the ^{99m}Tc/^{123}I subtraction SPECT/CT protocol were studied using an anthropomorphic phantom.

2 Literature review

2.1 Physics of dual-isotope imaging

2.1.1 Gamma camera

Traditional nuclear medicine has been using the gamma camera based on the scintillation detector "*The Anger Camera*" for more than 50 years (Anger 1958). The basic principles of the gamma camera are invariable, regardless of numerous technical improvements (Brownell et al. 1990, Fahey 1996, O'Connor M et al. 2002, Peterson et al. 2011, Bailey et al. 2013) and are briefly discussed here.

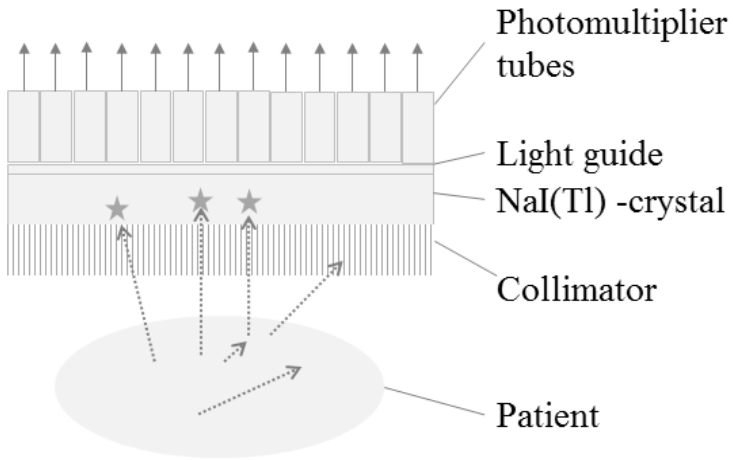

Figure 1. *The basic principle of a gamma camera. The dashed lines represent the gamma photons.*

Gamma photons originating from the patient travel through the collimator holes and reach the NaI(Tl)-crystal, where the photons transfer their energy to crystal electrons in a photoelectric effect, as shown in Figure 1. As a result, visible wavelength photons are detected by photomultiplier (PM) tubes, where light is in turn converted into an electric signal in a series of dynodes. The signal is collected from of all the PM tubes, and the location of the scintillation and the energy of the incoming gamma photon are calculated (Cherry et al. 2003).

The image formation of a gamma camera is not a mathematically exact process. Incoming gamma photons do not experience a photoelectric effect in the crystal with 100% efficiency and there is

some fluctuation in the amount of light produced in the scintillation process. Moreover, the number of photons that interact with the photocathodes (inside PM tube), the number of electrons produced in the photocathodes, and the electrical pulse output of each photomultiplier tube (proportional to the gain of each tube) are also not exactly the same for all identical incoming gamma photons (Cherry et al. 2003). These steps account for the uncertainty in measuring the incoming gamma photon energy, which results in the limited energy resolution of the gamma camera. The typical measure of a modern gamma camera is approximately 9% (Cherry et al. 2003).

The collimator is an essential part of the gamma camera. It is, however, the limiting factor in the performance of the system. Collimators can be classified as parallel-hole, pinhole, and focusing collimators. The characteristics of the parallel-hole collimator are dependent on the collimator thickness, hole diameter and septal thickness, as shown in Figure 2. Together these define the acceptance angle, in which a photon needs to enter the hole in order to pass through without interaction (Cherry et al. 2003). As the acceptance angle increases, the sensitivity of the collimator increases, but at the same time the spatial resolution decreases. Thus, the choice of the collimator is a tradeoff between sensitivity and resolution (Fahey et al. 1992).

Septal penetration is a phenomenon where gamma photons pass through the collimator septa and reach the NaI(Tl) –crystal as shown in Figure 2. This leads to blurring of the images, as all photons are considered to hit the crystal surface perpendicularly. Septal penetration is a significant issue with higher-energy radionuclides and, appears as a streak artifact in an image (McKeighen et al. 1974, Dobbeleir et al. 1999).

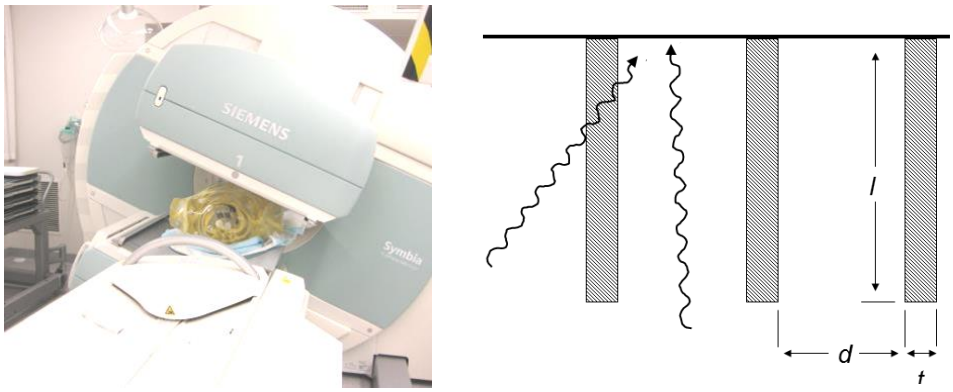

Figure 2. *A gamma camera equipped with a parallel hole collimator (left) and the cross-section of the parallel hole collimator (right) where l = thickness, d = hole diameter, and t = the thickness of the septa.*

The pinhole collimator is a large cone with a single small aperture at the tip of the cone (Figure 3). It creates a magnified image very similar to a traditional *camera obscura*. Nowadays, the use of the pinhole collimator is mainly limited to planar imaging. It is, however, very good in the imaging of small structures due to its superior spatial resolution (Beekman et al. 2007). Due to its design and the thickness of the cone wall, the pinhole collimator does not suffer from the septal penetration phenomenon (McKeighen et al. 1974). There focusing collimators are not applied in parathyroid scintigraphy and are therefore outside the scope of this thesis.

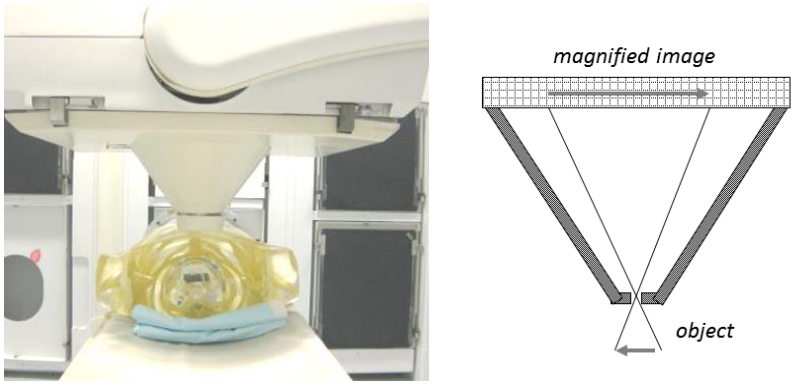

Figure 3. *A gamma camera equipped with a pinhole collimator (left) and the cross-section of the pinhole collimator (right).*

2.1.2 SPECT/CT

Single photon emission computed tomography (SPECT) acquisition with a gamma camera is nowadays part of normal clinical routine. During tomographic acquisition, the gamma camera detectors rotate around the patient and static projection images are acquired between ~2 to 5 degrees over 180 or 360 degrees around the patient (Figure 4). These projection images are reconstructed into transaxial slices using a reconstruction algorithm. The traditional filtered back projection (FBP) algorithm has been replaced by iterative algorithms that give a more detailed image without the typical streak artifact seen in an FBP image (Hudson et al. 1994, Vandenberghe et al. 2001, Cherry et al. 2003).

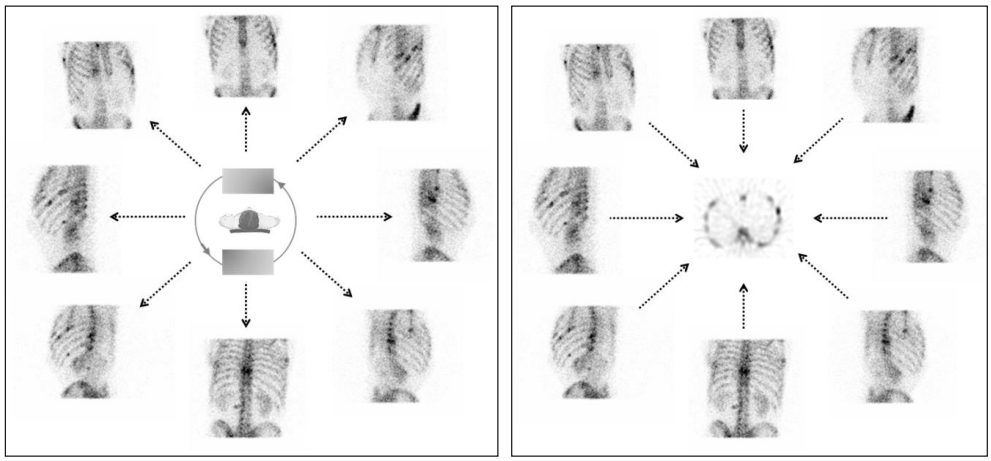

Figure 4. *The principle of SPECT acquisition (left) and reconstruction (right). The gamma camera detectors rotate around the patient and acquire static projection images (left). The projection images are reconstructed into transaxial slices with a reconstruction algorithm (right). One transaxial slice is shown in the middle (right).*

The introduction of the combined SPECT and computed tomography (CT) device enables the exact anatomical localization and attenuation correction of nuclear medicine images. Multimodality, i.e., SPECT/CT imaging, is now playing an increasingly important role in the diagnosis and staging of disease (Buck et al. 2008, Townsend 2008). In Finland, there are 46 gamma cameras (at the end of 2016) and 34 of those are equipped with CT. With newer cameras (less than 5 years), 19 of 20 are equipped with CT.

Figure 5. *A modern SPECT/CT camera.*

2.1.3 SPECT image quality

SPECT images are degraded by several physical phenomena. The primary problems originate from the patient as gamma photons experience both photoelectric effect and Compton scattering in patient. Photon attenuation is corrected using a CT-based attenuation map "*μ-map*", where linear attenuation coefficient values are derived from Hounsfield values in a CT-image. This correction is incorporated in a reconstruction algorithm that has become a clinical standard (Ritt et al. 2011, Seret et al. 2012). Scatter correction, in its simplest form, is a passive method because, the photopeak can be narrowed in order to avoid scattered photons. Correction is usually based on acquiring additional energy windows and by applying subtraction-based correction techniques, such as the triple energy window (TEW) method (Ogawa et al. 1991, Ichihara et al. 1993). In addition, there are also more complex correction methods available, where the scatter is estimated and corrected, for example, based on Monte Carlo simulation (Buvat et al. 1994). However, these methods require additional programs or algorithms and are not applicable in basic clinical work (Hutton et al. 2011).

The limited spatial resolution of the camera gives rise to a third phenomenon, the partial volume effect. The activity of active small regions (smaller than approximately twice the spatial resolution of the imaging system) is spread to the surroundings and underestimated (Cherry et al. 2003, Ritt et al. 2011, Frey et al. 2012). Some correction can be achieved with the use of the resolution recovery that is included in vendor-specific reconstruction algorithms (Seret et al. 2012).

In addition to scatter, attenuation and limited resolution, image quality is affected by other factors, such as patient movement during or between SPECT and CT acquisition, patient organ movement,

radiotracer movement in the patient, and noise in images (statistics are limited due to radiation dose issues).

2.1.4 Simultaneous dual-isotope imaging

The simultaneous acquisition of two radiopharmaceuticals in the same study offers several advantages over two separate acquisitions. For example, simultaneous acquisition offers the possibility to examine two different processes in a single study, thereby reducing total examination time and the probability of patient movement and excludes registration errors. Thus, perfectly registered images for image subtraction or comparison are produced (Links 1996). Simultaneous dual-isotope imaging has been applied in myocardial studies (Bai et al. 2007, Du et al. 2014), in studies of brain perfusion and receptor uptake, (Brinkmann et al. 1999, Dresel et al. 1999) and in parathyroid scintigraphy (Neumann et al. 1997).

There are several physical factors that need to be examined before applying the dual-isotope method in clinical work. These important factors are dependent on the combination of isotopes, but include the cross-contamination of isotopes, the effect of collimator selection, and the effects of energy window selection on uniformity, resolution, and sensitivity (Madsen et al. 1993, Inoue et al. 2003).

2.1.5 Cross-contamination

The major problem with dual-isotope imaging is so-called cross-contamination or "crosstalk", where photons of one radionuclide are detected in the energy window of the other and vice versa. With ^{99m}Tc (140 keV) and ^{123}I (159 keV), there are three types of cross-contamination. First, the primary photons of ^{99m}Tc are detected in the ^{123}I window and the primary photons of ^{123}I are detected in the ^{99m}Tc window due to finite energy resolution. Second, scattered ^{123}I photons are detected in the ^{99m}Tc window and third, the high-energy photons of ^{123}I are detected in both the ^{99m}Tc and ^{123}I energy windows (Devous et al. 1992, Links 1996, Links et al. 1996, Hapdey et al. 2006, Du et al. 2007, Du et al. 2009).

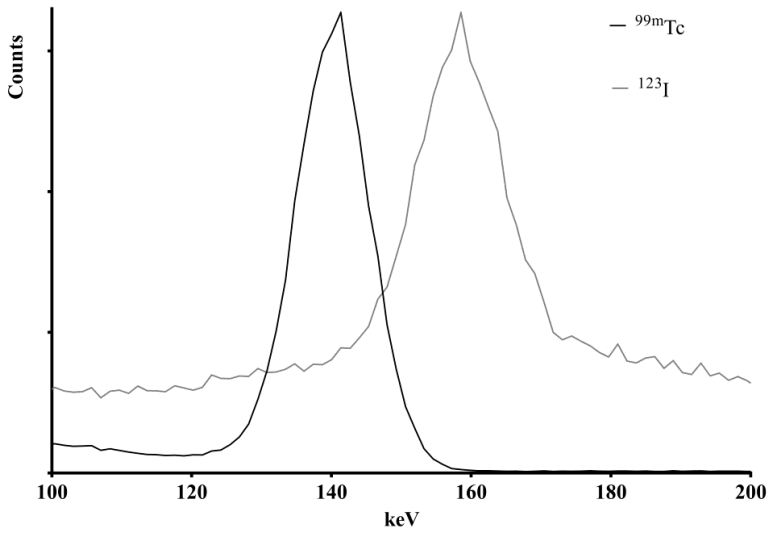

Figure 6. *The spectra of ^{99m}Tc (black) and ^{123}I (grey) acquired with a LEHR collimator at a distance of 20cm from the source in air.*

The amount of cross-contamination depends on the activity of the ^{99m}Tc and ^{123}I used, the local uptake of each isotope, and also on the positioning and width of the energy windows. It has been shown by several authors that there are significant amounts of cross-contamination in both the ^{99m}Tc and ^{123}I energy windows (Hapdey et al. 2006, Du et al. 2007). This can also be seen in Figure 6. Much of the cross-contamination in the ^{99m}Tc window is from primary ^{123}I 159 keV photons, and may contain significant high frequency information. Crosstalk caused by higher-energy photons is low-frequency by nature due to multiple scattering and affects a larger area, resulting in reduced general image contrast (Devous et al. 1992, Links 1996, Du et al. 2009).

2.1.6 Cross-contamination compensation

Cross-contamination of ^{99m}Tc and ^{123}I can severely degrade the image quality and quantitative accuracy, and makes simultaneous dual-isotope imaging with ^{99m}Tc and ^{123}I less clinically useful. Several methods have been suggested to correct the cross-contamination caused by the simultaneous use of ^{99m}Tc and ^{123}I. The use of narrow or asymmetric energy windows is probably the most common approach to avoid cross-contamination. However, results have been somewhat conflicting, as both major limitations and accurate quantitation have been reported (Devous et al. 1992, Ivanovic et al. 1994, Neumann et al. 1997, Brinkmann et al. 1999, Dresel et al. 1999, Dontu et al. 2004, Du et al. 2007, Neumann et al. 2008). Using asymmetric windows is an easy and straightforward method, but large cross-contamination components between ^{123}I and ^{99m}Tc are not eliminated using asymmetric windows. The method also leads to the loss of counting efficiency and large variations in flood field uniformity, as shown in Figure 7, that could cause artifacts in the reconstructed images (Ivanovic et al. 1994).

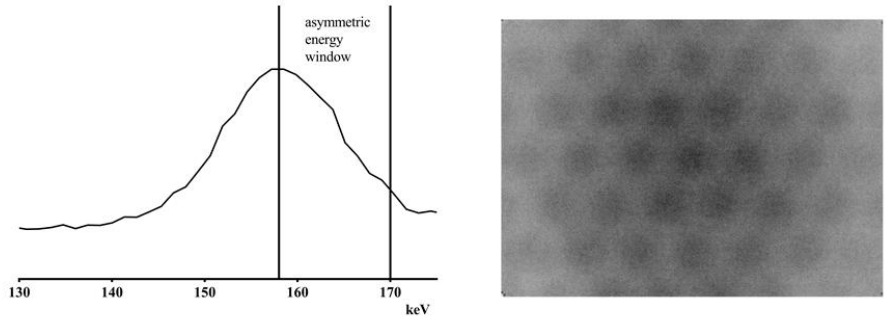

Figure 7. *An asymmetric energy window and the resulting flood field uniformity image with ^{123}I.*

If a narrow energy window is used, more scattered photons are excluded, but at the same time sensitivity is decreased. This in turn decreases the signal-to-noise –ratio. The use of narrow energy windows is not a very efficient method to exclude scattered photons because the loss of photon energy in Compton scattering is not very high. As an example, if a ^{99m}Tc photon is scattered at an angle of 45 degrees, it has lost only 7% of the original energy and is still included in a rather narrow energy window (Cherry et al. 2003).

Subtraction-based methods estimate the cross-contamination component in primary energy windows and subtract the data to yield an uncontaminated result. Different approaches have been proposed, either ^{123}I and ^{99m}Tc images are partially subtracted from each other (Dresel et al. 1999) or a specific scatter image is acquired, and this is then partially subtracted from the ^{123}I image

(Brinkmann et al. 1999). The triple-energy window (TEW) and a modified version of TEW have also been applied (Ichihara et al. 1993, Matsudaira et al. 1997, Ogasawara et al. 1998).

An attempt to correct for cross-contamination using subtractive methods assumes that an image acquired in the ^{99m}Tc window is the sum of the ^{99m}Tc photons and the ^{123}I cross-contamination photons, and that the image recorded in the ^{123}I window is the sum of the ^{123}I photons and the ^{99m}Tc cross-contamination photons. It also assumes that there is no spatial variation in the cross-contamination image. This approach has been shown to be false; the spatial distribution of the photons recorded in the scatter window is not the same as the spatial distribution of the photons recorded in the photopeak window (Ivanovic et al. 1994). This is especially true with ^{123}I cross-contamination in a ^{99m}Tc image; the ^{123}I cross-contamination in the ^{99m}Tc window is dominated by the spatially uncorrelated scatter and the septal penetration of high energy photons (Brinkmann et al. 1999). A major difficulty with a subtraction-based approach is the accurate determination of the cross-contamination fraction, which is greatly dependent on the activity ratios of the radioisotopes used and is also dependent on object (size, shape) and depth (Kadrmas et al. 1999, Hannequin et al. 2000, Hapdey et al. 2006).

More complex methods, such as spectral factor analysis (Hapdey et al. 2006), artificial neural network (El Fakhri et al. 2001, Bai et al. 2007), or model-based methods ((Du et al. 2007, Du et al. 2009, Shcherbinin et al. 2012, Du et al. 2014), have been used. These methods can provide images with less noise than subtraction-based methods. The disadvantage of modeling-based methods lies in the complexity of the models used. Accurately modeling multiple orders of scatter in inhomogeneous media is difficult and implementing such methods in current clinical work is not a very easy task (Kadrmas et al. 1999).

2.1.7 High energy photons of ^{123}I and septal penetration

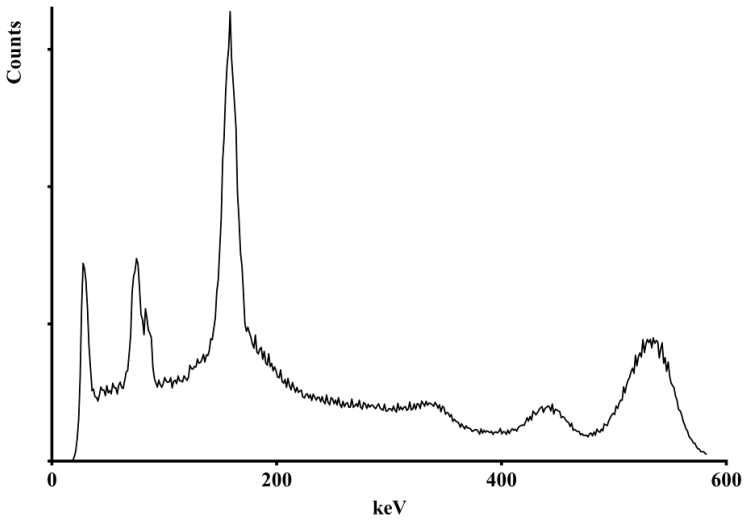

Figure 8. *The spectrum of ^{123}I in air.*

In addition to 159 keV photons, ^{123}I also emits high energy photons of more than 300 keV (Figure 8) that are capable of penetrating the septa of the collimator. This is a potential cause of artifacts when imaging with ^{123}I, as increased scatter decreases the resolution and contrast of the image. At

the same time, the sensitivity of ^{123}I varies as a function of distance as high-energy photons penetrate through the collimator septa into the crystal and behave as a camera would without the collimator (Dobbeleir et al. 1999, Inoue et al. 2003). Thus, the amount of septal penetration varies during SPECT acquisition and distortions in the projection images cause reconstruction artifacts (Macey et al. 1986).

The characteristics of various collimators have been studied for ^{123}I imaging and ^{99m}Tc/^{123}I imaging with a general preference towards medium-energy collimators (Macey et al. 1986, Ivanovic et al. 1994, Geeter et al. 1996, Dobbeleir et al. 1999, Inoue et al. 2003, Verberne et al. 2005, Small et al. 2006).The use of medium-energy collimators reduces the influence of septal penetration of high-energy gamma photons of ^{123}I due to thicker septa. Unfortunately, medium-energy collimators generally provide lower spatial resolution compared to that of low-energy collimators, which may influence the detection of small structures (Dobbeleir et al. 1999, Inoue et al. 2003).

Collimator selection for dual-isotope applications is thus always a compromise in terms of resolution, sensitivity, and the septal penetration of photons. It should be noted that the physical characteristics for ^{123}I imaging and simultaneous dual-isotope imaging with ^{123}I can differ even between low-energy collimators that provide similar sensitivity and spatial resolution (Gilland et al. 1994, Inoue et al. 2003, Kobayashi et al. 2003). It has therefore been suggested that the physical characteristics of each camera-collimator system used for dual-isotope imaging should be investigated before use in clinical studies (Ivanovic et al. 1994, Inoue et al. 2003).

2.2 The parathyroid glands

2.2.1 Anatomy and physiology

The parathyroid glands are small endocrine glands in the neck that are normally located behind the thyroid gland (Figure 9). The weight of a normal parathyroid gland ranges from 20 mg to 45 mg and is smaller than 7 mm in diameter. Approximately 90% of individuals have four parathyroid glands, about 4% have five glands, and about 5% have three glands. Parathyroid glands are derived from the epithelial lining of the third and fourth pharyngeal pouches, with the superior glands (P4) originating from the fourth pouch, and the inferior glands (P3) originating from the higher third pouch (Hindie et al. 2009). Due to the migration of embryological tissues, it is possible that the location of parathyroid glands vary significantly (especially P3 because of the longer route). Parathyroid glands can be found intrathyroidal, within the thyrothymic ligament, within the thymus, in the mediastinum, or remain high in the neck (Kettle et al. 2006, Hindie et al. 2009).

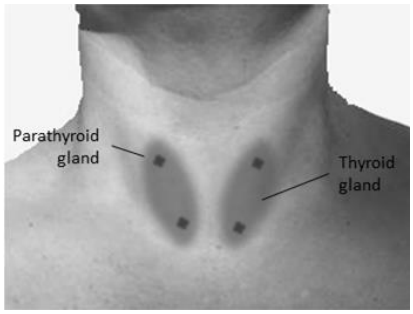

Figure 9. *The parathyroid glands are situated behind the thyroid gland.*

Parathyroid glands control the amount of calcium in the blood and within the bones by producing parathyroid hormone (PTH). PTH keeps the calcium, phosphate and vitamin D levels stable by means of several actions. These actions include stimulating renal tubular calcium reabsorption, urinary phosphate excretion and the activity of the 1α-hydroxylases, the synthesis of calcitriol, increasing calcium absorption from the gastrointestinal tract, and stimulating osteoclastic and osteoblastic activity in the bone that results in the release of calcium and phosphate from the bone (Hindie et al. 2009).

2.2.2 Hyperparathyroidism

Primary hyperparathyroidism is a common endocrine disorder, where hyperactive parathyroid glands cause hypercalcemia and elevated parathyroid hormone levels. About 85% of all primary hyperparathyroidism cases are caused by a single adenoma, a benign tumor of a parathyroid gland. About 15% of cases are caused by parathyroid hyperplasia, a condition where more than one gland is enlarged (Hindie et al. 2009). Secondary hyperparathyroidism results from any medical condition that produces hypocalcaemia, which in turn stimulates the parathyroid glands. The most common cause is renal failure, resulting in hyperplastic changes in the parathyroid glands. Occasionally, one or more of the glands can become autonomous which results in tertiary hyperparathyroidism (Ahmad et al. 2004, Hindie et al. 2009).

The typical clinical signs of hyperparathyroidism are osteoporotic fractures. There are, however, a number of symptoms associated with hyperparathyroidism that involve the kidneys (i.e., impaired renal function), the digestive tract (i.e., constipation), the cardiovascular system (hypertension), and even cognitive impairment and neuropsychiatric symptoms. The diagnosis of hyperparathyroidism is based on laboratory findings, where ionized calcium (Ca-ion) and parathyroid hormone (PTH) levels are elevated. Patients should be referred for parathyroid scintigraphy only when the above-mentioned diagnostic criteria are met. Parathyroid scintigraphy is thus not a diagnostic study, but performed for the localization of the enlarged parathyroid gland (Hindie et al. 2009).

2.2.3 Minimally invasive parathyroidectomy – need for localization

Surgery is the only curative treatment for hyperparathyroidism. The classical surgical approach to primary hyperparathyroidism is based on bilateral neck exploration that involves the identification of at least four parathyroid glands and the removal of the enlarged ones. With an experienced surgeon, bilateral neck exploration has a success rate of 95% (Clark 1995). A famous phrase by Doppman "*The only thing to localize in primary hyperparathyroidism is an experienced surgeon*", which was probably true considering the imaging methods available at that time (Doppman 1968).

The current trend is towards minimally invasive parathyroidectomy. This technique is superior to classical approaches and results in reduced complication rates and operation times, shorter hospital stays, lower total costs, and improved cosmetic results (Johnson et al. 2007, Shindo et al. 2008, Greene et al. 2009, Augustine et al. 2011, Udelsman et al. 2011).

The main reasons for failed surgery are ectopic glands and undetected multiple abnormal glands (Carty 2004, Phitayakorn et al. 2006, Hindie et al. 2009). It is very important that surgical procedures are carried out correctly in the first place because the accuracy of localizing residual hyperactive glands is significantly lower before reoperative parathyroidectomy than before initial surgery (Witteveen et al. 2010). The risk of complications is also increased in the case of reoperation (Taieb et al. 2013, Whitcroft et al. 2014). The introduction of minimally invasive procedures thus underscores the importance of sensitive and accurate imaging methods before operation (Hindie et al. 2009).

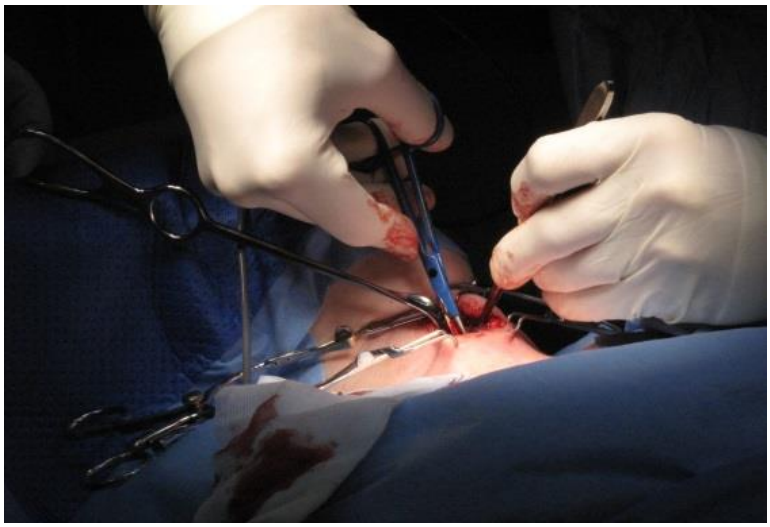

Figure 10. *Minimally invasive parathyroidectomy (image courtesy of endocrine surgeon Jussi Aalto, Satakunta Central Hospital, Pori, Finland).*

2.3 Parathyroid scintigraphy

2.3.1 History

Various radionuclides, i.e., tracers such as ^{67}Ga-citrate ^{75}Se -methionine, ^{57}Co-B12 vitamin, and a combination of ^{131}I-toluidine blue, $^{99m}TcO_4$, and ^{113m}In, and a combination of ^{131}I-toluidine blue and $^{99m}TcO_4$, have been used for parathyroid scintigraphy since the early 1960s (Kang et al. 1968, Skretting et al. 1977, Cann et al. 1980, Zwas et al. 1987).

One of the most widely used techniques was the ^{201}Tl/^{99m}Tc subtraction technique, but with an average sensitivity of only 55% (Ferlin et al. 1983, Young et al. 1983, Doppman et al. 1991). ^{201}Tl had suboptimal imaging properties due to low gamma energy, and the radiation dose to the patient was high mainly due to the long half-life of the radionuclide. Thus, there was a need for better radiotracers for parathyroid scintigraphy.

2.3.2 ^{99m}Tc-sestamibi

^{99m}Tc-sestamibi was first introduced in the late 1980´s as an alternative to ^{201}Tl in myocardial perfusion imaging. It was soon reported that it could also be used for parathyroid imaging (Coakley et al. 1989), and further research confirmed that it was at least as effective as ^{201}Tl in parathyroid localization (O'Doherty et al. 1992, Geatti et al. 1994).

The exact mechanism of sestamibi uptake was not clear, but it was suggested that cellular uptake and the retention of ^{99m}Tc-sestamibi were determined by both mitochondrial and plasma membrane potentials (Chiu et al. 1990). Metabolically active tissues, which are rich in mitochondria, may thus take up sestamibi more avidly than tissues with less (O'Doherty et al. 1992).

Although sestamibi was found to be a superior imaging agent when compared with ^{201}Tl, several factors associated with negative imaging were also discovered. Biological factors, such as the lack of oxyphilic cells and the presence of P-glycoprotein and multidrug resistance protein (MDR) gene products, have been shown to have a negative effect on sestamibi uptake in parathyroid tissue (Pons et al. 2003, Palestro et al. 2005, Mihai et al. 2006, Kannan et al. 2014). Furthermore, low preoperative parathyroid hormone (PTH) and ionized calcium levels (Calva-Cerqueira et al. 2007, Swanson et al. 2010), low serum vitamin D levels (Kannan et al. 2014), the use of calcium channel blockers (Friedman et al. 2004), multiglandular disease, and a small volume of parathyroid glands are also known to have a negative effect on the sensitivity of parathyroid scintigraphy (Chiu et al. 2006). The low radiochemical purity of ^{99m}Tc-sestamibi has also been suggested as an interference in the detection of parathyroid glands (Karam et al. 2005).

2.3.3 Two methods of sestamibi

Similar to ^{201}Tl, ^{99m}Tc-sestamibi is not a specific tracer for parathyroid tissue, it is also taken up by adjacent thyroid tissue. Two methods have been developed to overcome this problem.

In the dual-tracer method, ^{99m}Tc-sestamibi is used together with another tracer that is taken up only by the thyroid gland, with ^{99m}Tc-pertechnetate or with ^{123}I (the latter being usually called the dual-isotope method). When the thyroid image is subtracted from the ^{99m}Tc-sestamibi image, the enlarged parathyroid tissue is shown as residual activity in the subtraction image (Figure 11).

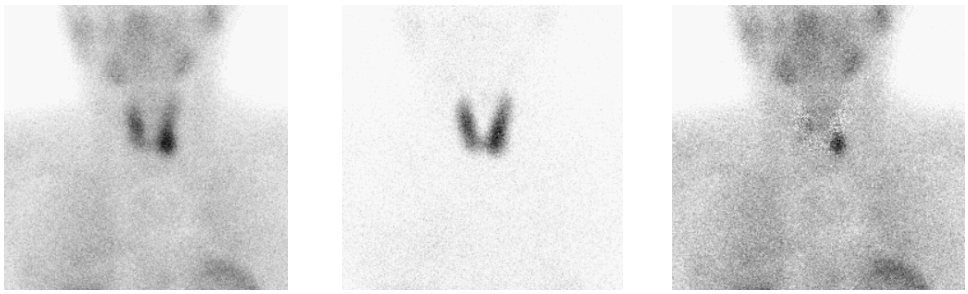

Figure 11. *The dual-isotope method of sestamibi. Anterior planar images were acquired using a parallel-hole collimator. A ^{99m}Tc-sestamibi image is shown on the left, a ^{123}I image is shown in the middle, and a subtracted image revealing the parathyroid adenoma is shown on the right*

First attempts with ^{99m}Tc-sestamibi and ^{123}I were performed in two subsequent acquisitions (Coakley et al. 1989, Wei et al. 1992, Casas et al. 1993, Weber et al. 1993, Halvorson et al. 1994, Hindie et al. 1995). However, this sequential acquisition was prone to motion artifacts and did not gain widespread acceptance. ^{99m}Tc-sestamibi was also combined with ^{99m}Tc-pertechnetate, but it did not gain public acceptance, again due to motion artifacts and high thyroid uptake (Wei et al. 1994, McBiles et al. 1995, Chen et al. 1997, Rubello et al. 2000, Ho Shon et al. 2001, Krausz et al. 2001).

It was soon discovered that ^{99m}Tc-sestamibi could be used with a so-called dual-phase method. The method is based on the different washout kinetics of the tracer between normal thyroid and abnormal parathyroid tissue (Taillefer et al. 1992). When images are acquired in the early and late phases, the focally increasing uptake will reveal hyperfunctioning parathyroid tissue (Figure 12).

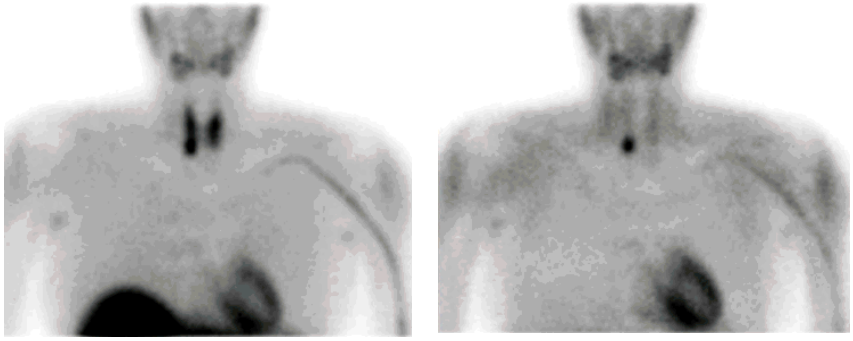

Figure 12. *The dual-phase method of sestamibi. Anterior planar images were acquired using a parallel-hole collimator. The early phase images acquired 10 minutes after the injection of* ^{99m}*Tc-sestamibi are shown on the left and the late phase images acquired 2.5 hours after the injection of* ^{99m}*Tc-sestamibi are shown on the right (images courtesy of Jussi Haanpää, Seinäjoki Central Hospital, Seinäjoki, Finland).*

Although a technically simply and elegant protocol, several authors reported that the difference in washout kinetics may not be accurate even with approximately one third of all patients who may have rapid washout of ^{99m}Tc-sestamibi (Leslie et al. 1995, Rossitch et al. 1995, Chen et al. 1997, Lorberboym et al. 2003, Arveschoug et al. 2007). Small parathyroid adenomas or hyperplastic glands, especially common in multiglandular disease, that blend into the thyroid at an early phase and wash out at the same rate are likely to be missed (Caveny et al. 2012, Taieb et al. 2012).

Several attempts, such as the use of time-activity curves and factor analysis, calculating thyroid count ratios between early and late images, and the use of reduced-time-window scanning, have been suggested as ways to improving the sensitivity and specificity of the dual-phase method (Billotey et al. 1994, Blocklet et al. 1997, Kacker et al. 2000, Gordon et al. 2002). It is hardly a surprise therefore that widely variable sensitivities of the dual-phase method, ranging from 50% to 100%, have been reported (Geatti et al. 1994, Billy et al. 1995, McBiles et al. 1995, Martin et al. 1996, Caixas et al. 1997, Chen et al. 1997, Gordon et al. 2002).

While the dual phase method struggled with the rapid washout phenomenon, Hindié and co-workers switched to the simultaneous dual-isotope method using ^{123}I and ^{99m}Tc-sestamibi to avoid patient movement and achieved excellent total sensitivity results of 92% (Hindie et al. 1997). Several publications from this same group have since been published describing applications for primary hyperparathyroidism, secondary hyperparathyroidism, and patients with multiglandular disease (Hindie et al. 1998, Jeanguillaume et al. 1998, Hindie et al. 1999, Hindie et al. 2000).

To the best of our knowledge, a total of 34 articles using the simultaneous dual-isotope method have been published employing various acquisition techniques (Pubmed 19.3.2017). Interestingly, there has been growing interest recently towards the dual isotope method, as shown in Figure 13.

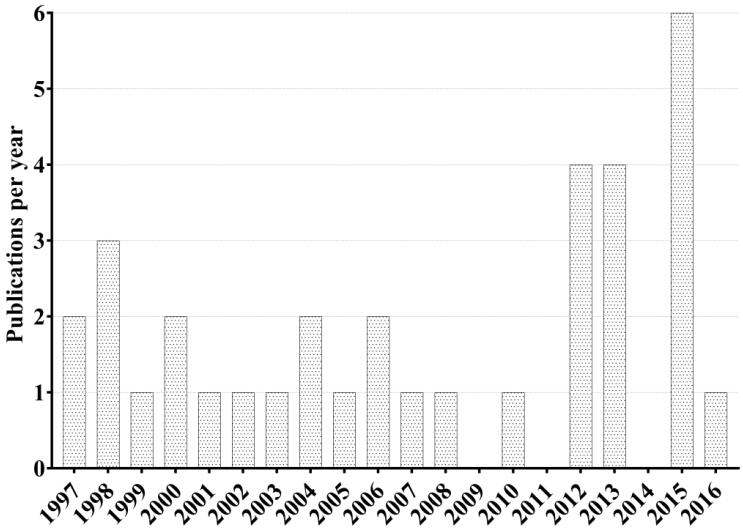

Figure 13. *The annual number of published papers based on dual-isotope parathyroid studies from 1997 to 2016*

The simultaneous dual-isotope and the dual-phase method have been compared using the same patients and the same acquisition session in only 11 publications (Table 1).The results of these comparisons are clear; the dual-isotope method is superior in terms of sensitivity in all studies.

Table 1. Published studies comparing the sensitivity of the dual-isotope method and the dual-phase method using the same group of patients. Pinhole and/or LEHR refers to planar imaging.

		Dual-phase		**Dual-isotope**	
Authors	**n**	**Technique**	**Sensitivity**	**Technique**	**Sensitivity**
(Neumann et al. 1997)	15	SPECT	53%	SPECT	88%
(Hindie et al. 1998)	30	pinhole, LEHR	79%	pinhole, LEHR	94%
(Wakamatsu et al. 2003)	39	LEHR	39%	LEHR	56%
(Taieb et al. 2007)	35	SPECT	78%	pinhole	86%
(Caveny et al. 2012)	37	pinhole, LEHR	66%	pinhole, LEHR	94%
(Tunninen et al. 2013)	24	SPECT	13%	SPECT	77%
(Klingensmith et al. 2013)	33	pinhole	43%	pinhole	66%
(Schalin-Jantti et al. 2013)	21	SPECT/CT	19%*)	LEHR	59%*)
(Krakauer et al. 2015)	91	several	65%	several	93%
(Ryhanen et al. 2015)	269	LEHR	35%*)	LEHR	63%*)
(Lee et al. 2016)	360	SPECT	78%	pinhole	86%

**) accuracy*

The majority of the studies have been performed using various acquisition techniques. Thus, the difference in the sensitivity figures is not only dependent on the method used but also on the acquisition technique. However, if we look at studies performed with similar acquisition techniques, it is clear that the dual-isotope method is significantly more sensitive than the dual-phase method (Figure 14).

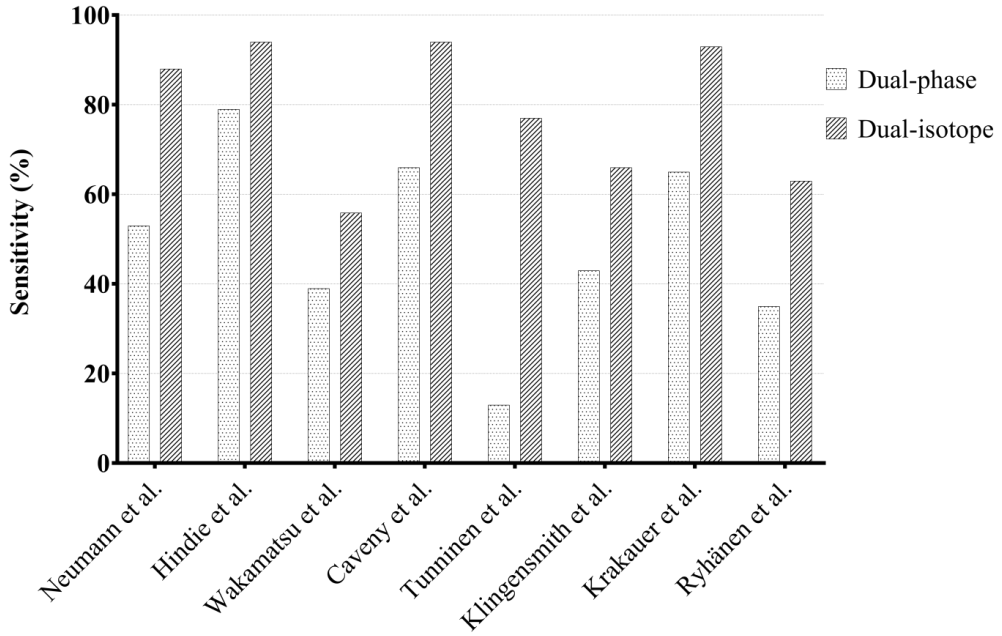

Figure 14. *Published studies comparing the sensitivity of the dual-isotope method (dark grey) and the dual-phase method (light grey). Studies that used the same acquisition technique with both methods within the same group of patients are included. Neumann et al. used SPECT-technique; other comparisons are made with planar techniques.*

2.3.4 Acquisition techniques

During the early years of ^{99m}Tc-sestamibi imaging, planar imaging was the most often applied acquisition technique (using parallel-hole or pinhole collimators), as SPECT was not yet technically highly developed (lack of body-contouring systems, most cameras were equipped with one detector), and the FBP reconstruction algorithm did not produce very high quality images, not to mention the long time required for computation.

If planar imaging is used, there is a general consensus that all planar parathyroid protocols, including pinhole imaging, achieve significantly higher sensitivity compared with those performed with parallel-hole collimator alone (Fujii et al. 1999, Ho Shon et al. 2001, Arveschoug et al. 2002, Tomas et al. 2008, Klingensmith et al. 2013). Planar imaging with pinhole collimator was also recommended as an essential part of the parathyroid scintigraphy in the EANM parathyroid guidelines in 2009 (Hindie et al. 2009). An example of a patient case acquired with both parallel-hole and pinhole collimators is shown in Figure 15.

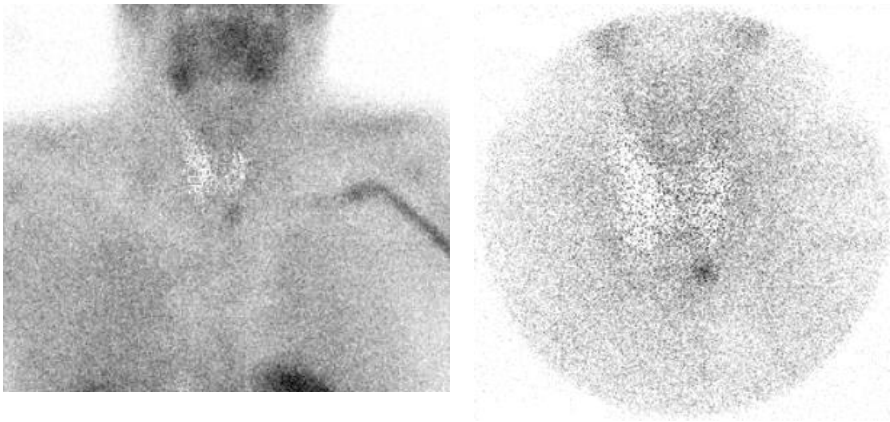

Figure 15. *An example of a planar subtraction image showing a parathyroid adenoma. A planar anterior image acquired using a parallel-hole collimator is shown on the left and a planar anterior image acquired using a pinhole collimator is shown on the right. Both images were acquired from the same patient.*

The high resolution of pinhole collimator also enables the detection of small thyroid nodules. It has been shown that the "iodine-cold" nodules with ^{99m}Tc-sestamibi uptake may indicate thyroid malignancy (Onkendi et al. 2012, Greilsamer et al. 2015). These iodine-cold nodules also create false-positive residual activity in subtraction images that can be easily interpreted as a parathyroid adenoma. Although the pinhole collimator offers the highest resolution possible in nuclear medicine, it has been replaced by SPECT and SPECT/CT have become clinical routine.

Figure 16. *An example of an iodine-cold thyroid nodule. Anterior planar images were acquired using a pinhole collimator. A ^{99m}Tc-sestamibi image is shown on the left, a ^{123}I image is shown in the middle, and a subtracted image revealing the parathyroid adenoma and false-positive residual activity (an arrow) is shown on the right.*

As SPECT became part of normal clinical routine in nuclear medicine, it also became integrated into parathyroid imaging protocols (Figure 17). SPECT, when compared with planar imaging, increases sensitivity and provides more precise localization, especially with patients with previous neck surgery, even when imaging was performed only during the early phase (Moka et al. 2000, Moka et al. 2000, Even-Sapir et al. 2001, Civelek et al. 2002, Schachter et al. 2004, Slater et al.

2005, Ingui et al. 2006, Lavely et al. 2007, Wimmer et al. 2008, Prommegger et al. 2009, Thomas et al. 2009, Taubman et al. 2011).

Simultaneous dual-isotope subtraction SPECT was introduced for parathyroid imaging in 1992, first with ^{123}I and ^{201}Tl. ^{201}Tl, however, was soon replaced by ^{99m}Tc-sestamibi, and the technique was applied in 15 patients with primary HPT with sensitivity of 88% and specificity of 97% (Neumann 1992, Neumann et al. 1997). The same method was used with 19 patients with secondary HPT but with lower sensitivity of 77% (Neumann et al. 1998), and with 14 patients with secondary HPT who had previously undergone parathyroid surgery with sensitivity of 100% (Neumann et al. 2000). A study from the same clinic showed that in a group of 350 patients ^{99m}Tc-sestamibi/^{123}I subtraction SPECT showed a smaller number of false-negative scans compared with all other protocols (Sharma et al. 2006).

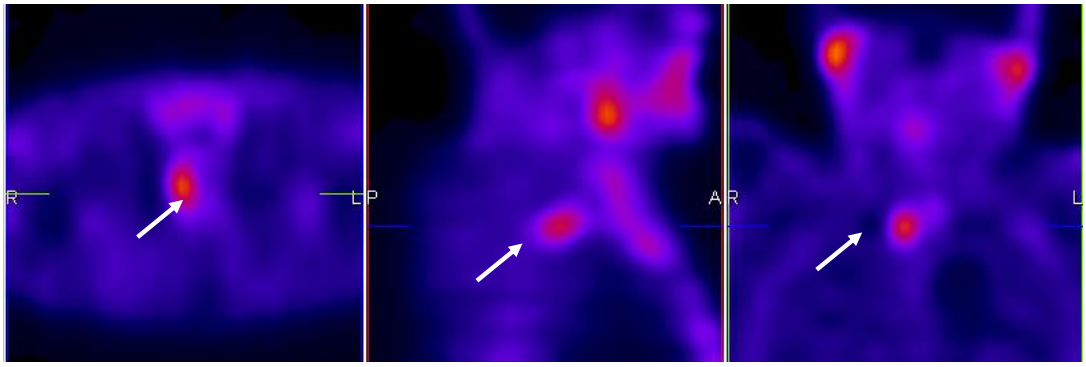

Figure 17. *An example of a ^{99m}Tc-sestamibi/^{123}I subtraction SPECT transaxial image (left), a sagittal image (middle), and a coronal image (right). An adenoma is shown with an arrow.*

As was the case with SPECT, SPECT/CT was also rapidly applied to parathyroid scintigraphy (Figure 18) and was shown to be significantly more specific when compared with SPECT alone with the dual-isotope method (Neumann et al. 2008, Hassler et al. 2013) and also with ^{99m}Tc-sestamibi alone (Wimmer et al. 2009, Pata et al. 2010). SPECT/CT also allows for accurate attenuation correction that improves image contrast and tumor-to-background ratio. Exact anatomical information also assists in the preoperative planning of minimally invasive surgical approaches and results in ever shorter surgical times (Gayed et al. 2005, Ingui et al. 2006, Krausz et al. 2006, Serra et al. 2006, Lavely et al. 2007, Ruf et al. 2007, Harris et al. 2008, Papathanassiou et al. 2008, Prommegger et al. 2009, Thomas et al. 2009, Pata et al. 2011, Taubman et al. 2011, Taieb et al. 2012, Taieb et al. 2013, Wong et al. 2015). SPECT/CT has also been used with ^{99m}Tc-sestamibi alone only in early phase (Martinez-Rodriguez et al. 2011, Mandal et al. 2015).

The main disadvantage of SPECT/CT in addition to increased time and cost is the additional radiation exposure received by the patient (Gayed et al. 2005, Dasgupta et al. 2013). However, the additional dose of approximately 1 mSv may be justified when considering the risks of repeated imaging or the risks associated with repeated general anesthesia and surgical intervention (Levine et al. 2009).

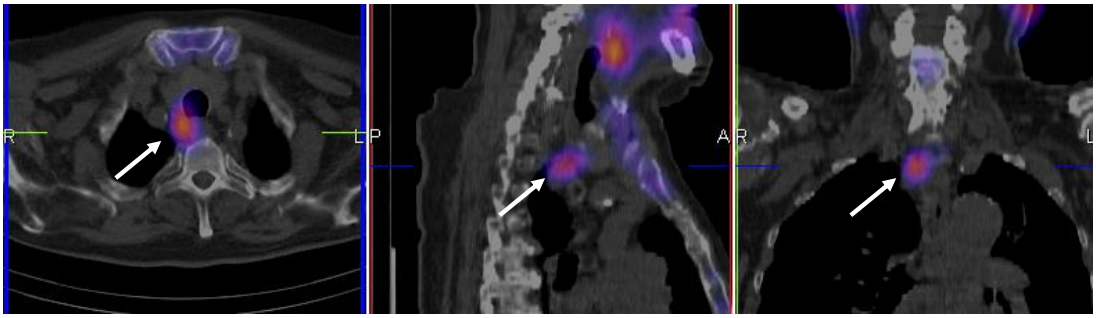

Figure 18. *An example of ^{99m}Tc-sestamibi/^{123}I subtraction SPECT/CT transaxial image (left), a sagittal image (middle), and a coronal image (right). An adenoma is shown with an arrow.*

Controversial studies have also been published. The precise benefit of SPECT/CT has been questioned and several authors have suggested that SPECT/CT should only be used for locating ectopic parathyroid glands (Gayed et al. 2005, Buck et al. 2008).

It is important to note that these early studies of SPECT or SPECT/CT are not quite applicable today because there have been significant improvements in imaging technology and image reconstruction algorithms (Ruf et al. 2007). Some of the studies are also inferior in quality due to the acquisition and processing parameters used (Ali et al. 2011).

2.3.5 Combined protocols

Although superior in term of resolution, the pinhole image lacks the three-dimensional information and accurate anatomical localization that are, offered by a modern SPECT/CT. In order to benefit from both advantages, these techniques are often combined in clinical practice (Lavely et al. 2007, Taieb et al. 2007, Nichols et al. 2008, Bahador et al. 2015, Guerin et al. 2015).

2.3.6 Image processing with dual-isotope imaging

Image processing with planar dual-isotope imaging is a relatively straightforward procedure. A region of interest is usually drawn around the thyroid gland on both the ^{99m}Tc-sestamibi and the ^{123}I images, and a normalization factor is calculated as a ratio of the ^{99m}Tc-sestamibi and ^{123}I maximum pixel counts. The ^{123}I image is then multiplied by this factor and then the scaled ^{123}I image is subtracted from the ^{99m}Tc-sestamibi image. This process is somewhat iterative, as the normalization factor can easily be adjusted in the case of under-subtraction or over-subtraction.

Image processing of ^{99m}Tc-sestamibi/^{123}I subtraction SPECT or SPECT/CT starts with the reconstruction of the ^{99m}Tc-sestamibi and ^{123}I projection images. After reconstruction, the ^{123}I images are multiplied using a normalization factor (a ratio of thyroid maximum voxel counts in ^{99m}Tc-sestamibi images and ^{123}I images) and the scaled ^{123}I images are then subtracted from the ^{99m}Tc-sestamibi images to create subtraction images where the enlarged parathyroid glands are visible.

2.3.7 The protocol of choice

Parathyroid scintigraphy with ^{99m}Tc-sestamibi is the method of choice for the preoperative localization of enlarged parathyroid adenomas, it being superior to ultrasound, magnetic resonance imaging, or CT imaging (Geatti et al. 1994, Peeler et al. 1997, Ishibashi et al. 1998).

Unfortunately, ^{99m}Tc-sestamibi is not a specific agent for parathyroid tissue. As a result, two methods are currently available in addition to several acquisition techniques and numerous adjustable parameters. Several clinical protocols have evolved with varying sensitivities and currently there is no consensus on how the parathyroid scintigraphy should be performed (Mihai et al. 2009). As the official guidelines published by the European Association of Nuclear Medicine (EANM) and the Society of Nuclear Medicine Practice (SNM) do not agree, it is difficult to assemble an optimal protocol for clinical use (Hindie et al. 2009, Greenspan et al. 2012).

3 Aims and objectives of the study

The aim of this thesis was to find out how to best conduct parathyroid scintigraphy using only the clinical tools available. In other words, to answer the question: ”*how to best perform the parathyroid scintigraphy*?”. The main objectives are listed below.

1) To evaluate the national status of the clinical parathyroid scintigraphy protocols used in Finland

2) To compare the sensitivity and specificity of a single-tracer method and a dual-isotope method

3) To evaluate the sensitivity and specificity of the planar and tomographic acquisition techniques used for parathyroid scintigraphy

4) To evaluate the properties of three different collimators for dual-isotope imaging with ^{99m}Tc and ^{123}I

5) To optimize the acquisition and processing parameters of ^{99m}Tc/^{123}I subtraction SPECT/CT

The first objective was realized in Study I, where a complete national status of parathyroid scintigraphy protocols were assessed and updated in a follow-up study (Tunninen et al. 2016). The second objective was realized in Study II, where the single-tracer method and the dual-isotope method were compared on an intrapatient basis. The third objective regarding the acquisition techniques was realized in Study II and Study III, again using an intrapatient comparison. The fourth objective was accomplished in Study IV, where the physical properties of three different collimators used for dual-isotope imaging with ^{99m}Tc and ^{123}I where evaluated. Finally, the last objective was realized in Study V, where the optimal acquisition and processing parameters of ^{99m}Tc/^{123}I subtraction SPECT/CT were examined.

4 Material and Methods

This study comprised five consecutive studies (publications I-V) carried out from 2008 to 2017 at Satakunta Central Hospital, Pori. Additional measurements for Study V were also performed (unpublished) to evaluate the effect of the acquisition arc (360° vs 180°) and matrix size (128 vs 256) on the outcome of ^{99m}Tc/^{123}I subtraction SPECT/CT with LEHR and LEUHR collimators.

4.1 Request for information

All instructions regarding the clinical protocols for parathyroid scintigraphy were requested by e-mail from all the departments of nuclear medicine in Finland (n = 25) in September 2008 and again in January 2010. Instructions concerning the parathyroid scintigraphy, acquisition and image processing parameters and all instructions targeted at patients were received from all the departments performing parathyroid scintigraphy. A follow-up study was also conducted in April 2016(Tunninen et al. 2016).

4.2 Patients

In total, the studies comprised 226 patients (51 patients in Study II and 175 patients in Study III). All patients were clinical patients referred for parathyroid scintigraphy at Satakunta Central Hospital, Finland. Patients for Study II were studied between June 2010 and February 2011, and patients for Study III between March 2011 and June 2016. Institutional approval for the use of patient acquisition data and other information concerning hyperparathyroidism was granted by the Medical Director of Satakunta Hospital District on 5th April 2011. Both Study II and Study III were exempt from institutional ethical committee approval according to Finnish legislation. Informed consent was waived.

All patients had biochemical evidence of hyperparathyroidism (elevated total serum calcium (Ca-ion) and parathyroid hormone level (PTH)). From this original cohort, patient data were included for this retrospective study if the patient proceeded to surgery, and if post-operative Ca-ion and PTH results were available. The final study group comprised 118 patients (24 patients in Study II and 94 patients in Study III).

4.3 Phantoms

Various phantoms were used in Studies IV and V. An overview of phantoms is shown in Table 2. Detailed information on all phantoms and sources used are presented in Study IV and V. The setup of the anthropomorphic phantom is presented in Figure 19.

Table 2. An overview of the phantoms used in Studies IV and V

Study	Phantom	Isotope	Activity	Concentration
IV	The Jaszczak phantom[1] with hot spot insert	^{99m}Tc	1500 MBq	~250kBq/ml
IV	Two identical 1000 ml bottles	^{123}I ^{99m}Tc	40MBq 40MBq	40kBq/ml 40kBq/ml
V	The Thorax phantom[2]	^{99m}Tc	350 MBq	~180kBq/ml
V	A thyroid gland phantom[3]	^{123}I ^{99m}Tc	7MBq 7MBq	500 kBq/ml 500 kBq/ml
V	A spherical phantom[4]	^{99m}Tc	75kBq	300kBq/ml

[1]*Data Spectrum Corporation, Durham, NC, USA (http://www.spect.com/pub/Flanged_Jaszczak_Phantoms.pdf)*
[2]*Radiology Support Devices, Long Beach, CA, USA (http://www.rsdphantoms.com/pages/heartthoraxcardiac.html) volume of ~8200ml*
[3]*Radiology Support Devices, Long Beach, CA, USA (http://www.rsdphantoms.com/pages/fissionproductphantom.html) volume of ~14 ml.*
[4]*Data Spectrum Corporation, Durham, NC, USA (http://www.spect.com/pub/Hollow_Sphere_Sets.pdf), inner diameter of ~8mm, volume of ~0,25ml) representing an adenoma (later referred as adenoma)*

Figure 19. *The anthropomorphic phantom (left), the thyroid gland phantom and the spherical phantom representing an adenoma (middle) and the thyroid and an adenoma attached inside the anthropomorphic phantom for Study V (right).*

Additional measurements for Study V were also performed with the same phantom. The measurements were, however, performed in a separate session because they could not be performed during Study V due to radionuclide decay in the phantom (unpublished). In the additional study, the thyroid gland phantom was filled with ^{123}I and ^{99m}Tc (concentration of 600 kBq/ml, total activity of). The adenoma was filled with ^{99m}Tc at a concentration of 700 kBq/ml and attached behind the thy-

roid gland. The thyroid and adenoma were then inserted into the thorax phantom, which was then filled with 350 MBq of ^{99m}Tc. The activities were measured in a similar manner as in Study V.

4.4 Patient imaging, image processing and review

All patient acquisitions were performed in the Department of Nuclear Medicine of Satakunta Central Hospital, Pori, Finland. Three different gamma cameras were used. A Siemens Symbia Intevo T2 SPECT/CT and a Siemens Symbia T SPECT/CT (Siemens, Erlangen, Germany) were used for all SPECT/CT imaging with a Low Energy High-Resolution (LEHR) collimator. A Philips Skylight (Philips, Milpitas, CA, USA) was used for planar pinhole imaging in Study II and Study III. All cameras are used in clinical work and subjected to strict quality control measures.

The acquisition protocols used in Study II are outlined together with the resulting images for review in Figure 20. The parameters used for the acquisition and reconstruction and for the processing steps are described in detail in Study II.

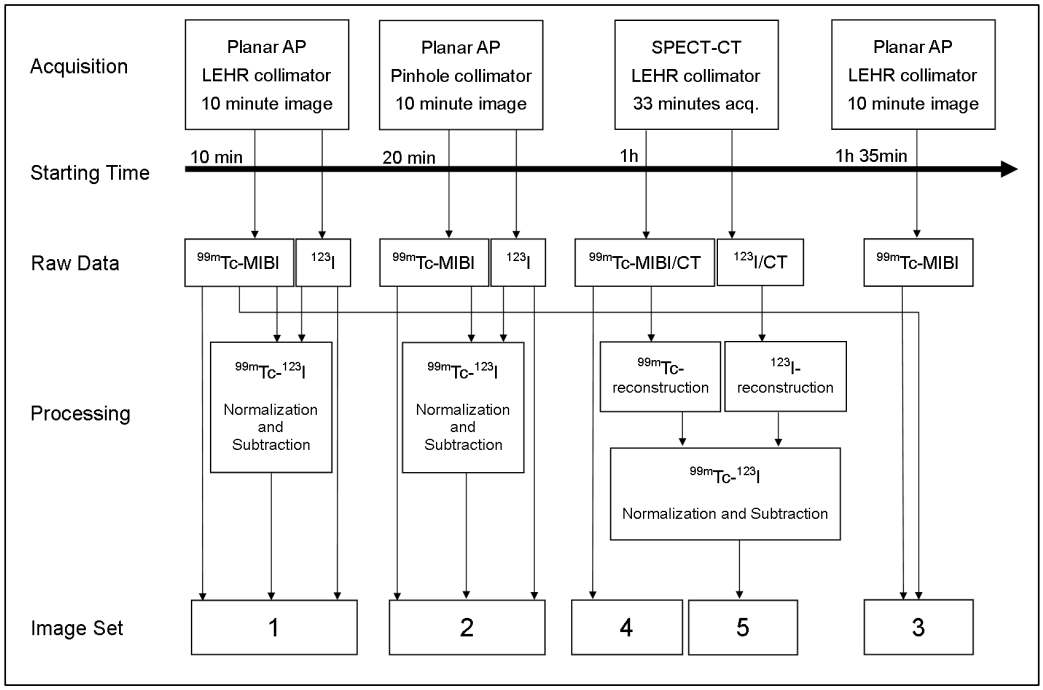

Figure 20. *Acquisitions and processing steps for producing images 1-5 in Study II.*

In Study II, all patient images were anonymized and the images were reviewed by four experienced nuclear medicine physicians (PV, MS, AA, JS) from three different hospitals. All findings were finally classified as true positive, false positive, true negative, or false negative using surgical and histopathological findings with post-operative Ca-ion and PTH levels as the reference standard.

The acquisitions used in the Study III are outlined together with the resulting images for review in Table 3. The parameters for the acquisition and reconstruction and the processing steps are described in detail in Study III.

Table 3. Acquisitions and resulting images in Study III.

Acquisition	Collimator	Resulting images for review
SPECT/CT	LEHR	^{99m}Tc-sestamibi, ^{123}I and subtraction SPECT/CT images
Planar	Pinhole	^{99m}Tc-sestamibi, ^{123}I and subtraction pinhole images

All patient images were anonymized and the images were reviewed by one experienced nuclear medicine physician (MS) in Study III. All findings were finally classified as true positive, false positive, true negative, or false negative with surgical and histopathological findings with postoperative Ca-ion and PTH levels as the reference standard.

4.5 Phantom imaging and image processing

All phantom acquisitions were performed in the Department of Nuclear Medicine of Satakunta Central Hospital, Pori, Finland. A Siemens Symbia Intevo T2 SPECT/CT was used for all acquisitions and measurements. LEHR, Low Energy Ultra High-Resolution (LEUHR) and Medium Energy Low-Penetration (MELP) collimators were used for the acquisitions.

The acquisitions and measurements performed in Study IV are outlined in Table 4. Comprehensive information on the acquisition and processing parameters are presented in Study IV. SPECT spatial resolution was also measured using the acquisition matrix 256×256 (unpublished) using otherwise identical acquisition and processing parameters as with the acquisition matrix 128×128.

Table 4. Measurements performed in Study IV.

Number	Measurement	Parameter (unit)
1	Intrinsic uniformity	Intrinsic uniformity in the UFOV (%)
2	System sensitivity	Sensitivity (cpm/μCi)
3	System spatial resolution at various distances	FWHM (mm), FWTM (mm)
4	SPECT spatial resolution	Visibility of channels
5	SPECT uniformity	Reconstructed uniformity (%rms)
6	Spectrum at various distances without scatter	Spectrum (-)
7	Spectrum at various distances with scatter	Spectrum (-)
8	Scatter-to-photopeak –ratio without scatter	Ratio (%)
9	Scatter-to-photopeak –ratio with scatter	Ratio (%)
10	Cross-contamination	Ratio (%)

Abbreviations used in table: Useful Field of View (UFOV), Full width at half maximum (FWHM), Full width at tenth maximum (FWTM).

Scatter-to-photopeak –ratio is defined as: acquired counts in lower scatter window as a percentage of counts acquired in the main window with equal window widths. The cross-contamination is defined as: acquired counts in ^{99m}Tc window as a percentage of counts acquired in ^{123}I window while acquiring ^{123}I source or acquired counts in ^{123}I window as a percentage of counts acquired in ^{99m}Tc window while acquiring ^{99m}Tc source. Parameters presented in Table 4 were measured or calculated using clinical tools on Siemens Syngo and Hermes workstations.

For the purpose of study V, a total of six SPECT/CT acquisitions were performed with the anthropomorphic phantom. LEHR, LEUHR, and MELP collimators were used with clinical (asymmetric ^{123}I energy window) and test energy windows (symmetric ^{123}I energy window). Eight reconstructions were performed for each (Number of iterations (6, 8, 16, or 32) and scatter correction on/off) resulting in a total of 48 image sets. Comprehensive information on the acquisition and processing parameters are presented in Study V. All images were anonymized and scored from 0 to 5 based on visual appearance. For quantitative analysis, the mean values for the contrast and visual scores were calculated for each combination of collimator, energy window, and processing parameters. Detailed information is presented in publication V.

For quantitative analysis, a volume of interest (VOI) was drawn around the adenoma using the fused CT image as a reference (with corresponding background VOI). An image contrast C for sphere was calculated using the equation (1):

$$C = \frac{C_{adenoma} - C_{background}}{C_{background}} \times 100\% \quad [1]$$

where $C_{adenoma}$ is the number of counts in the sphere, and $C_{background}$ is the number of counts in the background area

A total of four SPECT/CT scans were performed with LEHR and LEUHR collimators in addition to the original acquisitions in Study V (unpublished). The SPECT/CT acquisitions were performed with detectors configured at a 180° angle (H-mode) and a 90° angle (L-mode) as shown in Figure 21. With H-mode, 180° degrees of rotation were acquired (projection data over 360°), with L-mode 90° degrees of rotation were acquired (projection data over 180°, the anterior arc). The acquisition parameters are presented in Table 5. In addition, the phantom was acquired using the clinical pinhole protocol in Study III.

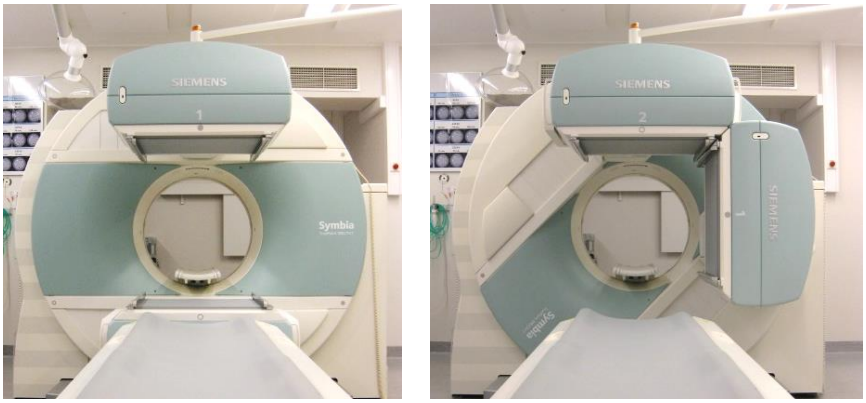

Figure 21. *Detectors set in H-mode (left) and in L-mode (right).*

Table 5. Acquisition parameters for SPECT/CT in additional measures to Study V

Acquisition Parameter	SPECT/CT 360°	SPECT/CT 180°
Detector configuration	180° (H-mode)	90° (L-mode)
Acquisition arc (total)	360°	anterior 180°
Orbit	Body-contour	Body-contour
Collimators	LEHR, LEUHR	LEHR, LEUHR
Matrix	256×256	256×256
Zoom	1	1
Pixel size	4.8 mm, 2,4mm	4.8 mm, 2,4mm
Acquisition mode	Step-and-Shoot	Step-and-Shoot
Views	96 (3,75° per projection)	48 (3,75° per projection)
Time per projection	33 s	66s
Energy windows	Test energy windows	Test energy windows
Voltage	130kVp	130kVp
Collimation	2×2.5 mm	2×2.5 mm
Rotation time	0.8 s,	0.8 s,
Pitch	1,5	1,5
Dose modulation	CARE Dose AEC+DOM	CARE Dose AEC+DOM
Reference exposure	80 mAs	80 mAs

^{99m}Tc-sestamibi and ^{123}I SPECT images (with attenuation correction) were reconstructed on a Siemens Syngo workstation using the FLASH 3D-algorithm with six parameter settings (8, 16, or 32 iterations, 8 subsets, Gaussian 9.00 filter, with and without TEW scatter correction). All SPECT/CT datasets were also converted to the matrix size 128×128 and reconstructed in a similar manner.

^{123}I SPECT images were multiplied by a normalization factor (as the ratio of the thyroid maximum voxel counts in the ^{99m}Tc and ^{123}I SPECT images to create normalized ^{123}I SPECT images, which were then subtracted from the ^{99m}Tc SPECT images. In total, eight group of images were reconstructed (48 image sets in total) for the purpose of data analysis.

All images were subjected to visual evaluation and classified into two groups according to the presence of artifacts in the image. The images classified in the better group (no obvious artifacts) were further evaluated quantitatively. For quantitative analysis, a VOI was drawn around the adenoma using the fused CT image as a reference (with corresponding background VOI). An image contrast C for sphere was calculated using the equation (1).

5 Results

5.1 Parathyroid scintigraphy protocols

The status of clinical parathyroid scintigraphy protocols in Finland was assessed in Study I. In total, 769 parathyroid scintigraphy studies were performed in 19 hospitals, ranging from 7 to 209 studies per year (40,2±39,9). Both dual-phase and dual-tracer methods (with ^{123}I or $^{99m}TcO_4$) were in use with a large variety in the activities used, especially with ^{99m}Tc-sestamibi/^{123}I (Table 6).

Table 6. Parathyroid scintigraphy methods, radionuclides and the activities used with parathyroid scintigraphy in Finland in 2010.

Method	**% of hospitals**	**A (^{99m}Tc)**	**A (^{123}I)**	**A ($^{99m}TcO_4$)**
Dual-tracer, ^{99m}Tc- sestamibi/^{123}I	58	150-800 MBq	10-30 MBq	-
Dual phase, ^{99m}Tc-sestamibi	37	740 MBq	-	-
Dual-tracer, ^{99m}Tc- sestamibi/$^{99m}TcO_4$	5	740 MBq	-	50 MBq

All acquisition techniques (planar imaging with parallel-hole and pinhole collimator, SPECT and SPECT/CT) were used with an emphasis on classic anterior imaging with parallel-hole collimator (Figure 22). SPECT/CT was used in only eight hospitals (42%).

Imaging methods and techniques were combined in most hospitals, and result in 1 to 4 acquisitions per patient study. There was also heterogeneity in the timing of the acquisitions. All early-phase acquisitions were started 5 to 15 minutes after the ^{99m}Tc-sestamibi injection, but the starting time of the late-phase acquisition varied from 1.5 to 4 hours after the ^{99m}Tc-sestamibi injection.

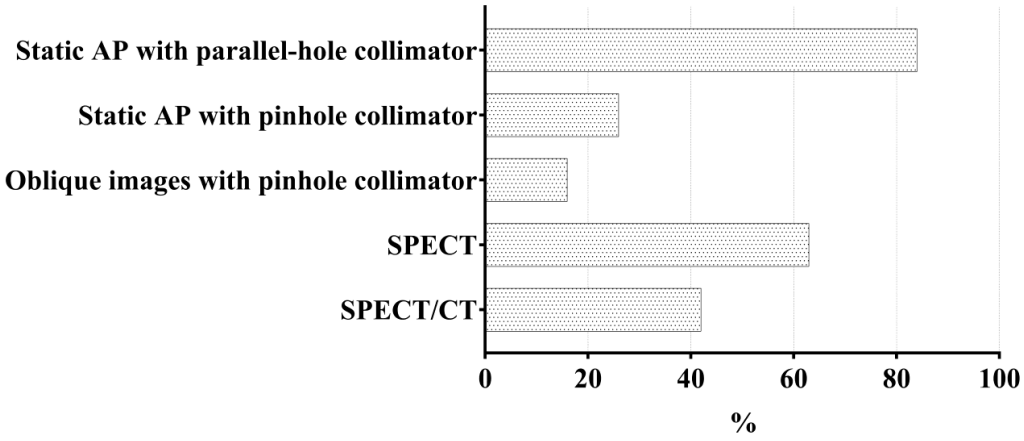

Figure 22. *The acquisition techniques used with parathyroid scintigraphy (all methods combined) in Finland in 2010.*

In addition to a variation in methods and imaging techniques, there was also variation in acquisition protocol parameters. This resulted in 18 protocols being used in 19 hospitals. The imaging methods and acquisition techniques for each hospital are summarized in Table 7.

Table 7. Parathyroid scintigraphy methods and acquisition techniques with parathyroid scintigraphy in Finland in 2010. Each hospital is represented in a column.

Hospital number		**1**	**2**	**3**	**4**	**5**	**6**	**7**	**8**	**9**	**10**	**11**	**12**	**13**	**14**	**15**	**16**	**17**	**18**	**19**
Method	Dual-Phase	x	x	x	x	x	x	x												
	Dual-Tracer								x	x	x	x	x	x	x	x	x	x	x	x
Early phase	LEHR	x	x		x	x		x	x	x	x	x	x	x	x	x		x	x	x
	Pinhole										x					x	x	x	x	
	Pinhole/oblique															x		x	x	
	SPECT		x	x			x			x		x	x		x		x			
	CT									x		x	x				x	x		
Late phase	LEHR	x	x		x	x		x	x	x			x	x						
	Pinhole										x									
	Pinhole/oblique																			
	SPECT		x	x	x	x	x		x					x						
	CT				x	x			x											

5.2 Comparison of the single-tracer and the dual-isotope methods

Five different imaging protocols were compared in Study II. All image sets generated with the dual-isotope method (^{99m}Tc-sestamibi/^{123}I) were more sensitive than any image set acquired with ^{99m}Tc-sestamibi alone, as shown in Table 8. Statistical comparison is presented in Study II.

Table 8. Sensitivity, specificity and accuracy for the dual phase method and the dual-isotope method (average values for physicians and for acquisition techniques).

Method	Sensitivity (%)	Specificity (%)	Accuracy (%)
Dual-isotope	72%	95%	88%
Single tracer	17%	99%	75%

5.3 Comparison of acquisition techniques with the dual-isotope method

Planar imaging protocols with LEHR and pinhole collimator, SPECT/CT, and SPECT/CT combined with the planar pinhole protocol were studied in Study II and Study III. No difference in the sensitivity, specificity, or accuracy between the acquisition techniques using the dual-isotope method was found in Study II (results in Study II, Table 2) (Table 9).

As Study III was conducted for a longer period from 2011 to 2016, more experience with dual-isotope SPECT/CT had been gained, and the sensitivity of SPECT/CT was now much higher at 94%. In addition, when SPECT/CT was combined with pinhole imaging, the sensitivity and specificity were slightly higher than with SPECT/CT alone, but the difference was not significant (results in Study III, Table 2 with statistical comparison). However, additional pinhole imaging resulted in a changed diagnosis in eight patients (8.5% of patients). The results are presented in Table 9.

Table 9. Sensitivity and specificity for the dual-isotope method with planar and tomographic acquisition techniques.

Study	Acquisition Technique	Sensitivity (%)	Specificity (%)
II	Planar AP with LEHR	69	96
II	Planar AP with pinhole	78	94
II	SPECT/CT	68	96
III	SPECT/CT	94	98
III	SPECT/CT + pinhole	97	99

5.4 Collimator properties for ^{99m}Tc/^{123}I subtraction SPECT/CT

The physical characteristics of the LEHR, LEUHR, and MELP collimators for dual-isotope imaging with ^{99m}Tc and ^{123}I were examined with phantoms in Study IV. System sensitivity with ^{99m}Tc was well in line with the specifications given by Siemens. Sensitivity with the ^{123}I symmetric energy window was higher with the low-energy collimators when compared with the sensitivity of ^{99m}Tc, which is caused by the septal penetration of high-energy gamma photons of ^{123}I. The use of an asymmetric energy window with ^{123}I reduced sensitivity compared with the symmetric energy window. With MELP collimators, reduction was approximately 43%, but with low-energy collimators only 15%. This was also due to the septal penetration of high-energy gamma photons of ^{123}I. It was also noticed that with the asymmetric ^{123}I energy window, the uniformity was only 11.9%, whereas intrinsic uniformity was very good for both the ^{99m}Tc and ^{123}I symmetric energy windows.

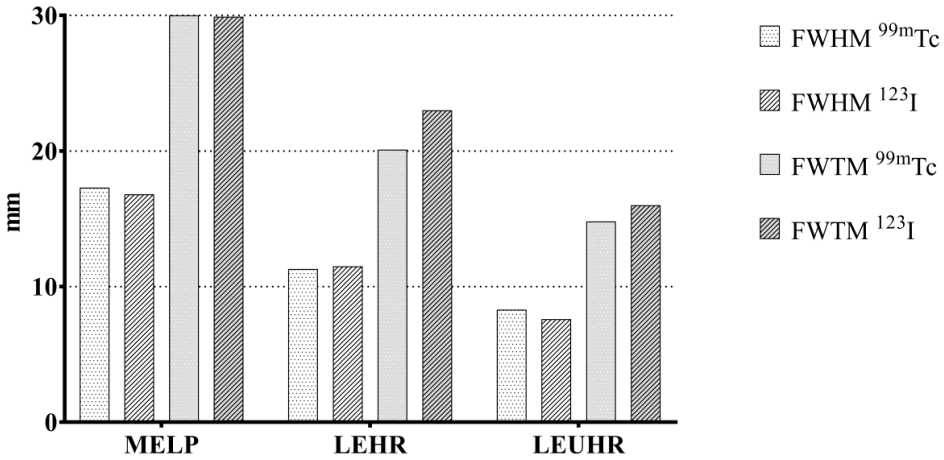

Figure 23. *System spatial resolution for MELP, LEHR, and LEUHR collimators. The spatial resolution values are presented for each collimator. FWHM for ^{99m}Tc (mm) is shown in the first column, FWHM for ^{123}I (mm) is shown in the second column, FWTM for ^{99m}Tc (mm) is shown in the third column, and FWTM for ^{123}I (mm) is shown in the fourth column.*

As expected, system resolution was best for the LEUHR collimator and lowest for the MELP collimator, as shown in Figure 23. There was no difference in resolution for ^{99m}Tc and ^{123}I in terms of FWHM values for the collimators. Septal penetration was again noticed, as was the case for LE collimators, and FWTM was larger with ^{123}I than that with ^{99m}Tc. There was no difference with symmetric and asymmetric energy windows for ^{123}I.

SPECT spatial resolution with the MELP collimators was inadequate for the acquisition of small structures. Hence, only the two largest hollow channels (volume filled with radioactive solution) could be identified. The LEHR and LEUHR collimators performed better, as channels in sectors 3 and 4 could be identified, respectively. In addition to Study IV, SPECT spatial resolution was also measured using the acquisition matrix 256×256 (unpublished). The acquisition matrix with smaller pixel size did not increase resolution (based on visual analysis) for the MELP collimators. For the LEHR collimators, a sharpening of the details could be seen. For the LEUHR collimators, channels in sector 2 could also be identified in addition to a similar sharpening as that seen with the LEHR collimator. An example is shown in Figure 24.

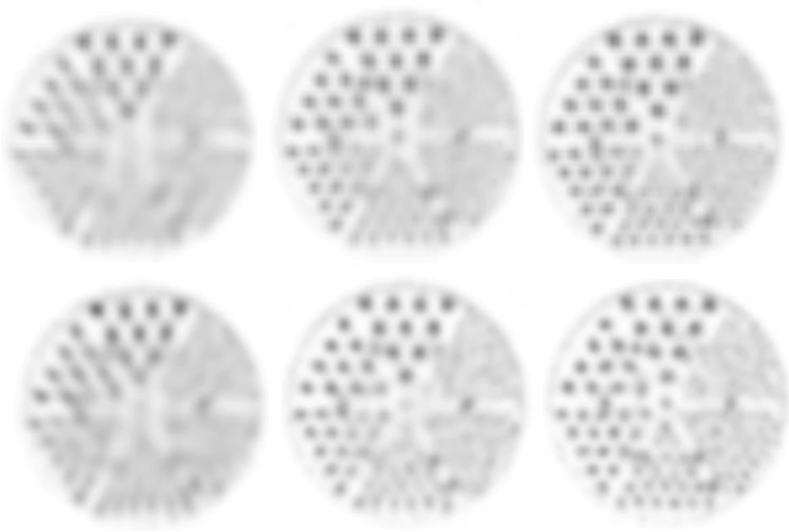

Figure 24. *An example of SPECT resolution for MELP (left), LEHR (middle), and LEUHR (right) collimators with a 128×128 acquisition matrix (upper row) and with a 256×256 acquisition matrix (lower row). SPECT spatial resolution with the MELP collimators was poor compared to those of LEHR and LEUHR collimators. The acquisition matrix with smaller pixel size did not increase resolution for the MELP collimators. For the LEHR and LEUHR collimators, a sharpening of the details could be seen.*

The spectrum of ^{99m}Tc in air was similar for all collimators and the distances between the source and the collimator. Scattering material increased the amount of scatter, but there was no change in the shape as a function of distance or between collimators. There was no difference in scatter-to-photopeak -ratio between the collimators or as a function of distance for ^{99m}Tc (scatter-to-photopeak -ratio was 13.0% to 14.7%).

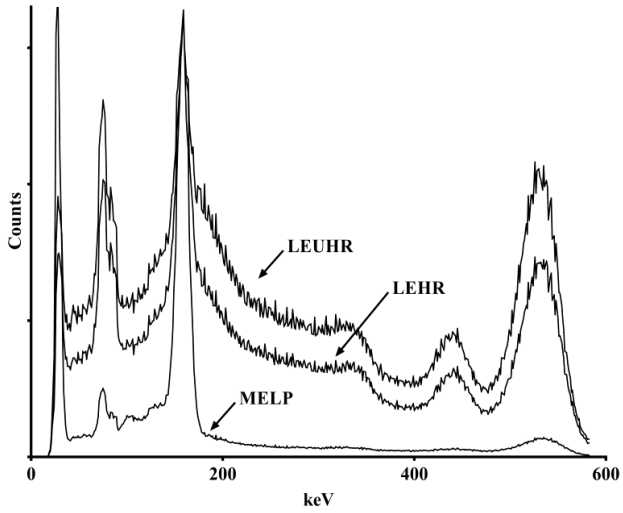

Figure 25. *Spectrum of ^{123}I at 5 cm from the detector in air for MELP, LEHR, and LEUHR collimators.*

The spectrum of ^{123}I was very different for the LEHR, LEUHR, and MELP collimators. The effect of ^{123}I high-energy gamma photons was perceptible (Figure 25). The scatter-to-photopeak -ratio for ^{123}I was highest for the LEUHR-collimator. The scatter-to-photopeak -ratio was not constant, but changed as a function of distance for the low-energy collimators and also for the MELP collimator, as shown in Figure 26.

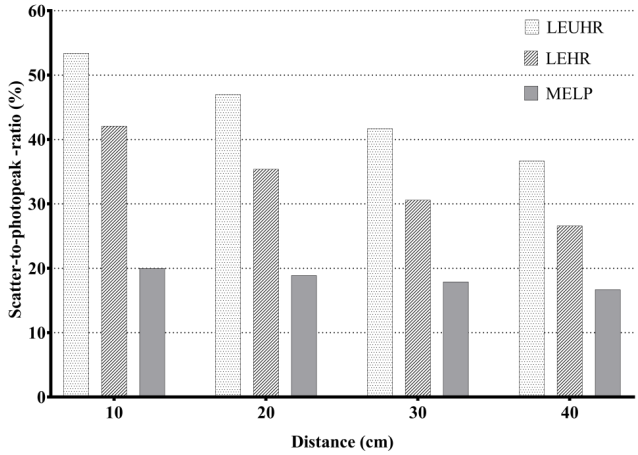

Figure 26. *Scatter- to-photopeak –ratio (%) in air with ^{123}I for LEUHR (dotted), LEHR (lined), and MELP (grey) collimators at a distance of 10 cm, 20 cm, 30 cm, and 40 cm between the collimator and the source.*

Cross-contamination measurements showed similar contamination of the ^{99m}Tc in the ^{123}I window for all collimators (4.7 to 5.1%). The asymmetric energy window for ^{123}I reduced the ^{99m}Tc-contamination approximately to half (1.8 to 2.6%). ^{123}I contamination in the ^{99m}Tc window was significantly higher for all collimators being 28.3 to 50.6%, as shown in Figure 27.

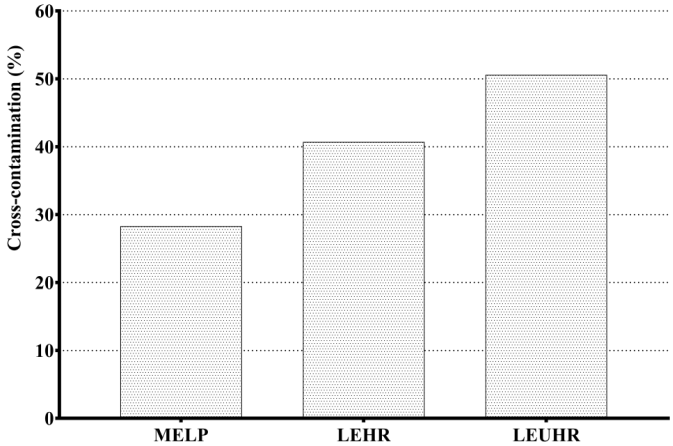

Figure 27. *^{123}I contamination in the ^{99m}Tc energy window for MELP (left), LEHR (middle), and LEUHR (right) collimators. The contamination is expressed as a percentage of ^{123}I counts in the ^{99m}Tc energy window vs ^{123}I counts in the ^{123}I energy window.*

5.5 Optimization of ^{99m}Tc-sestamibi/^{123}I subtraction SPECT/CT

The anthropomorphic parathyroid phantom was set up to mimic a small, low intensity adenoma or hyperplasia in Study V. Thus, it was expected that it would be difficult to visualize. The visual appearance of the images varied from a nonvisible adenoma to a clear image, and visual scores were between 0 and 5. This was in correlation with the calculated contrast for the adenoma that was between 0.4% and 80.9% (Figure 28).

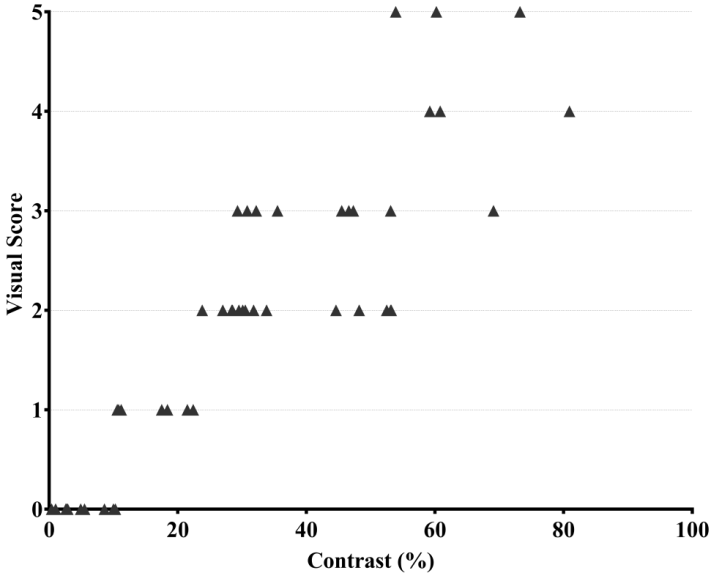

Figure 28. *Visual score of an image as a function of contrast of an adenoma. The visual scoring is based on the clinical appearance of the images (the intensity of adenoma, the presence of artefacts) and scored by a single reviewer.*

The collimator and energy window had the highest effect on the visual scores, as shown in Figure 29. The LEUHR collimator in combination with the symmetric energy window for ^{123}I (test energy window) yielded the best visual scores. The effect of scatter correction was low.

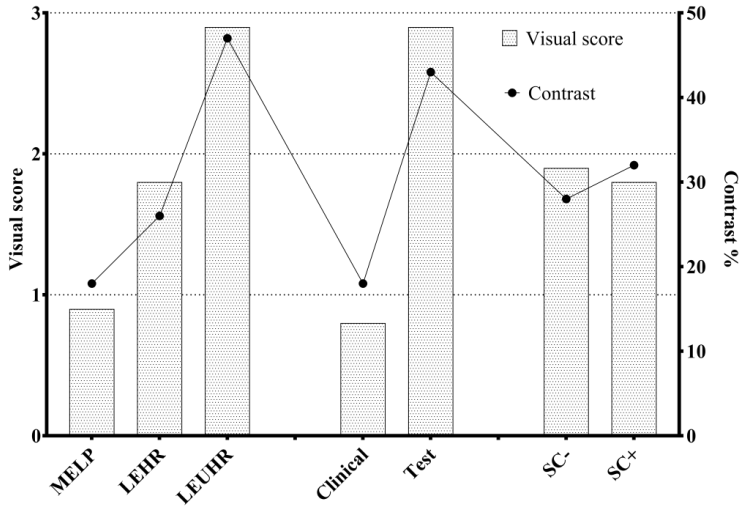

Figure 29. *The mean visual score (columns, axis on the left) and contrast (line, axis on the right) for MELP, LEHR, and LEUHR collimators (mean calculated for all energy windows and processing parameters) is shown on the left, for clinical (asymmetric ^{123}I window) and test (symmetric ^{123}I window) energy windows (mean calculated for collimators and processing parameters) is shown in the middle, and for scatter correction on or off (mean calculated for all collimators and energy windows) on the right.*

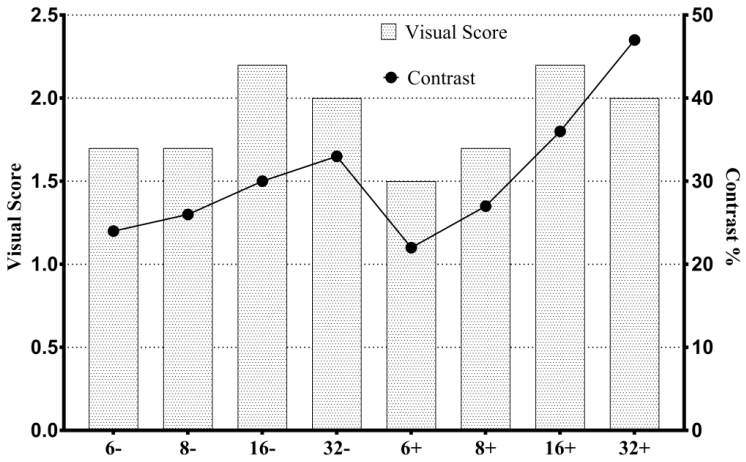

Figure 30. *The mean visual score (columns, axis on the left) and contrast (line, axis on the right) of an adenoma with processing parameters (combined for all collimators and energy windows). "6-" indicates six iterations and scatter correction off, "6+" indicates six iterations and scatter correction on.*

The mean values for contrast for the reconstruction parameters were higher with an increasing number of iterations (mean for all collimators and energy window settings). However, the visual scores were highest with 16 iterations. When the iterations were increased to 32, the visual appearance of the images decreased due to increased noise in the images.

Phantom images with the highest visual scores and with the current clinical protocol are presented in Figure 31.

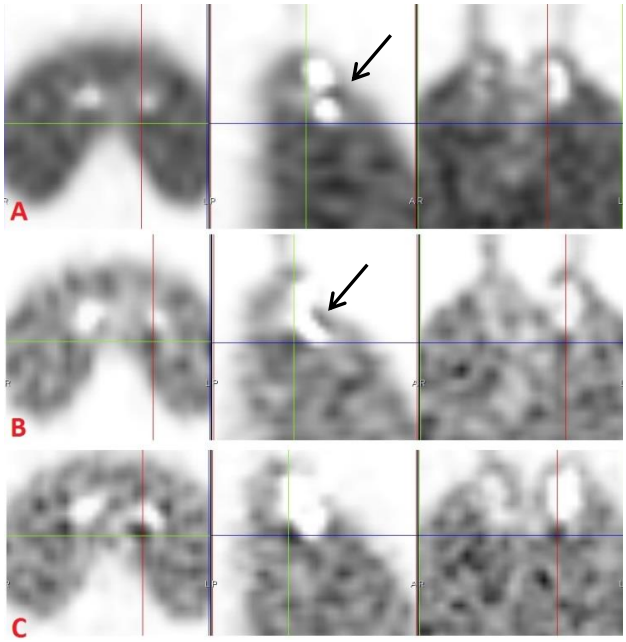

Figure 31. *Transverse (left), sagittal (middle), and coronal (right) images of the phantom and an adenoma situated in the crosshair. The upper row shows images acquired with clinical protocol (LEHR collimators, asymmetric ^{123}I energy window, 8 iterations, 8 subsets, no scatter correction). The middle row shows images acquired with LEHR collimators and a symmetric ^{123}I window (8 iterations, 8 subsets, with scatter correction). The lower row shows images acquired with LEUHR collimators and a symmetric ^{123}I window (16 iterations, 8 subsets, no scatter correction). An arrow shows "the edge artefact".*

In addition to Study V, the optimization of dual-isotope SPECT/CT was further evaluated (unpublished). A combination of two collimator pairs (LEHR, LEUHR), two acquisition arcs (180° and 360°), and two acquisition matrix sizes 128×128 and 256×256 were assessed. All reconstructed images were subjected to visual evaluation. The adenoma was clearly visible in all phantom images, but there was a difference in the presence of artifacts in the image. In the first classification, it was noticed that all images acquired with detectors in L-mode were faintly blurred with more subtraction artifacts present. These images were not subjected to quantitative evaluation. An example of an artifact is shown in Figure 32 in comparison with a corresponding image without any artifacts (detectors in H-mode, otherwise the same collimator, matrix size, and processing parameters).

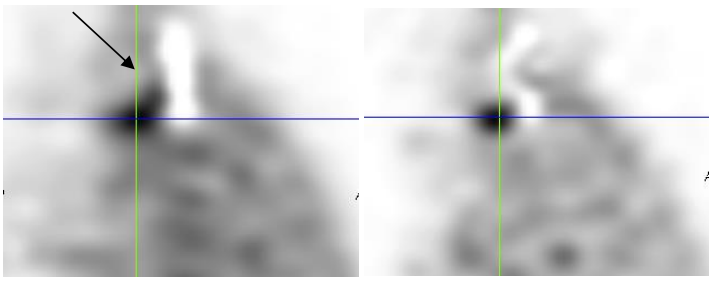

Figure 32. *An example of an artifact (arrow) present in a sagittal image acquired with detectors in L-mode (left) and a flawless image acquired with detectors in H-mode (right). The adenoma is situated in the crosshair.*

Further visual evaluation of the LEHR and LEUHR images with detectors in H-mode showed that all images acquired with the LEHR collimator (both matrix sizes) had more subtraction artifacts present compared with those acquired with the LEUHR collimator. These images were also excluded from quantitative evaluation. An example of an artifact is shown in Figure 33.

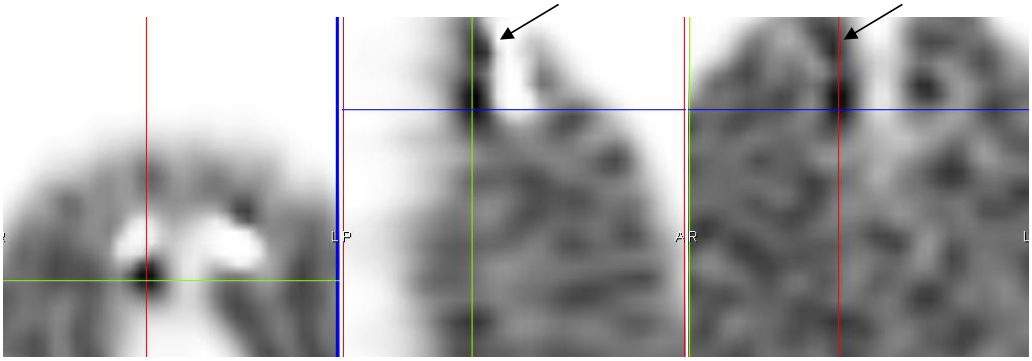

Figure 33. *An example of an artefact (an arrow) present in images acquired with LEHR collimators (transverse (left), sagittal (middle), coronal (right)). The adenoma is situated in the crosshair.*

For quantitative analysis, contrast values were calculated for the adenoma for both matrix sizes and for all processing parameters. The contrast of the adenoma was between 79.4% and 172.6%. The lowest contrast was achieved with 128×128 matrix size and 8 iterations without scatter correction. The highest contrast values were with 256×256 matrix size, 32 iterations, and scatter correction. The results are shown in Figure 34.

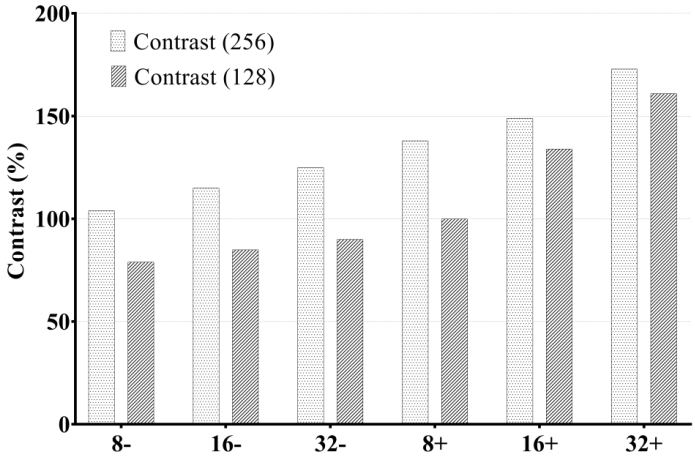

Figure 34. *The mean contrast values of an adenoma acquired with LEUHR collimators in H-mode with a matrix size of 128×128 (lined columns) and 256×256 (dotted columns). "8-" indicates eight iterations and scatter correction off, "8+" indicates eight iterations and scatter correction on.*

The visual appearance of the adenoma was very similar in all images acquired with the LEUHR collimators in H-mode. An example of the highest and the lowest contrast is shown in Figure 35.

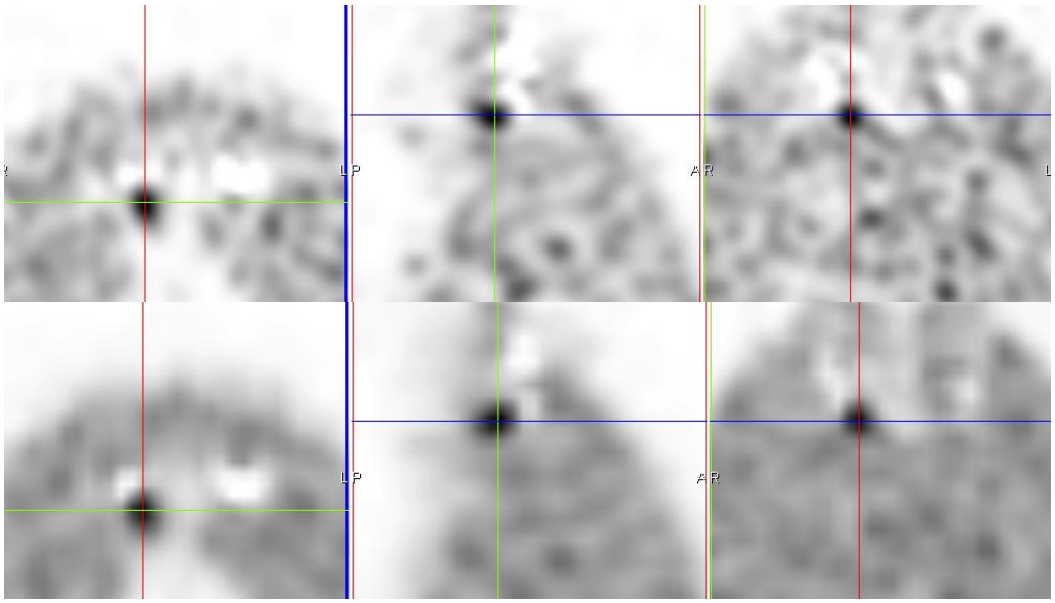

Figure 35. *An example of the highest contrast (upper row) and the lowest contrast (lower row) of images acquired with LEUHR detectors in H-mode. Transverse (left), sagittal (middle), and coronal (right) images are shown. Images in the upper row were processed with the parameters 256×256 matrix size, and 32 iterations with scatter correction. Images in the lower row were processed with the parameters 128×128 matrix size and 8 iterations without scatter correction.*

The phantom was acquired using the clinical pinhole protocol used in Study III. The adenoma could not be visualized in the subtraction pinhole image as shown in Figure 36.

Figure 36. *The pinhole images of the phantom. ^{99m}Tc image on the left, ^{123}I-image in the middle, and a subtraction image on the right. The adenoma cannot be visualized.*

6 Discussion

6.1 The method of choice with ^{99m}Tc-sestamibi

Ten years ago, there was no national consensus on parathyroid scintigraphy protocols in Finland (Study I). As a result, both dual-phase and dual-tracer methods were in use according to the personal preferences in each hospital. The superiority of the dual-tracer method with ^{123}I, i.e., the dual-isotope method, was shown in Study II, where any dual-isotope protocol was significantly more sensitive than any dual-phase protocol. This has been recently acknowledged by several authors (Caveny et al. 2012, Klingensmith et al. 2013, Schalin-Jantti et al. 2013, Krakauer et al. 2015, Ryhanen et al. 2015, Lee et al. 2016).

There has been a considerable change and all Finnish nuclear medicine departments performing parathyroid scintigraphy now use the dual-isotope method with ^{99m}Tc-sestamibi and ^{123}I as their first method of choice in parathyroid scintigraphy (Tunninen et al. 2016). The dual-isotope method is also recommended by the European Association of Nuclear Medicine (EANM) guideline (Hindie et al. 2009). However, this is not the case worldwide as dual-isotope protocols are considered relatively complex and time-consuming. In addition, ^{123}I is regarded as relatively expensive and it may not be readily available in some countries (Caveny et al. 2012). Dual-isotope protocols are also not recommended by the Society of Nuclear Medicine Practice (SNM) Guideline for Parathyroid Scintigraphy 4.0 (Greenspan et al. 2012).

Considering the superior sensitivity of the dual-isotope method shown in this thesis, the additional cost of ^{123}I (approximately 200 € per patient) and the additional radiation dose (with a 35% thyroid uptake, the patient gets an estimated 4.4 mSv effective dose with a 20 MBq injection of ^{123}I compared to a 6.7 mSv dose from 750 MBq of ^{99m}Tc-sestamibi)) can be considered acceptable (Hindie et al. 2009).

6.2 Acquisition techniques in comparison

Planar imaging with parallel-hole collimator has been the traditional clinical method with most nuclear medicine studies. Planar imaging with LEHR collimator was also the most common acquisition technique with parathyroid imaging in Finland as shown in Study I. The pinhole collimator was rarely used, which was surprising considering the superiority of pinhole imaging shown by several authors (Arveschoug et al. 2002, Ho Shon et al. 2008, Tomas et al. 2008, Hindie et al. 2009, Ali et al. 2011, Klingensmith et al. 2013). Those findings are in line with Study II, where anterior planar imaging with pinhole collimator had the highest sensitivity of 78%.

At the time of Study I, SPECT and SPECT/CT were only used in 63% and 42% of the hospitals, respectively. There has been a notable change, as according to our recent survey, 89% of the hospitals are now using SPECT/CT with parathyroid scintigraphy (Tunninen et al. 2016).

In Study II, we could not demonstrate the increased sensitivity of ^{99m}Tc-sestamibi/^{123}I subtraction SPECT/CT when compared with ^{99m}Tc-sestamibi/^{123}I subtraction pinhole imaging. This finding was in line with Hassler and co-workers who showed an equal sensitivity of ^{99m}Tc-sestamibi/^{123}I subtraction SPECT/CT and ^{99m}Tc-sestamibi/^{123}I subtraction pinhole protocols (Hassler et al. 2013). The average sensitivity of ^{99m}Tc-sestamibi/^{123}I subtraction SPECT/CT in Study II was 68%. This study was performed at the early stage of adopting the ^{99m}Tc-sestamibi/^{123}I subtraction SPECT/CT protocol. As Study III was conducted during a longer period of five years, more experience had been gained and the sensitivity of ^{99m}Tc-sestamibi/^{123}I subtraction SPECT/CT was now much higher at 94%.

The use of ^{99m}Tc-sestamibi/^{123}I subtraction pinhole imaging alone was not addressed in Study III, as the pinhole image lacks the three-dimensional information as well as the accurate anatomical localization offered by SPECT/CT. Based on the findings in Study III, the combined protocol of ^{99m}Tc-sestamibi/^{123}I subtraction SPECT/CT and ^{99m}Tc-sestamibi/^{123}I subtraction planar pinhole offers higher sensitivity and specificity of ^{99m}Tc-sestamibi/^{123}I subtraction parathyroid scintigraphy compared to SPECT/CT alone, although the difference was not significant.

This finding is in sharp contrast with those of Bhatt and co-workers who achieved lower sensitivity with combined SPECT/CT and pinhole compared with pinhole imaging alone (Bhatt et al. 2015). A partial reason for this result might be the rapid washout phenomenon, as Bhatt and co-workers started SPECT/CT 45 minutes after the ^{99m}Tc-sestamibi injection. Another explanation could be the acquisition and processing parameters used as, based on the figures shown in the publication, image acquisition and/or processing may not have been optimal. The study of Bhatt and co-workers was conducted right after the installation of SPECT/CT, so it is likely that the inferior results of ^{99m}Tc-sestamibi/^{123}I subtraction SPECT/CT compared with those of pinhole imaging are the consequence of a lack of experience.

The combination of ^{99m}Tc-sestamibi/^{123}I subtraction SPECT/CT and anterior planar pinhole was tested with additional measures in Study V. The adenoma was clearly visible in optimized ^{99m}Tc-sestamibi/^{123}I subtraction SPECT/CT but could not be visualized in the pinhole image, which is line with the findings of Dontu and co-workers (Dontu et al. 2004). Thus, it is suggested that carefully optimized SPECT/CT does not benefit from additional planar pinhole images. On the other hand, the ultimate resolution of the pinhole collimator is highly useful in recognizing thyroid nodules.

6.3 The choice of the collimator

Parathyroid localization places high requirements on the spatial resolution of the imaging system due to the small size of the parathyroid gland. At the same time, the dual-isotope method with ^{99m}Tc-sestamibi and ^{123}I addresses the challenges posed by the cross-contamination of isotopes and the septal penetration of the high energy iodine gamma photons. Collimators optimized for ^{99m}Tc have problems with the septal penetration of ^{123}I high energy gamma photons. Several authors have suggested the use of medium-energy collimators for ^{123}I imaging and also for dual-isotope imaging (Macey et al. 1986, Geeter et al. 1996, Inoue et al. 2003, Small et al. 2006). However, the resolution of medium-energy collimators is inadequate for detecting small structures, as shown in Study IV and V.

Although the LEUHR collimator was inferior to the LEHR and MELP collimators in terms of septal penetration and cross-contamination, as shown in Study IV, the ultra-high resolution of the LEUHR collimator yielded the best results, as shown in Study IV and V. Our finding of the preference of LEUHR collimators over LEHR collimators is in line with the findings of Fahey and co-workers (Fahey et al. 1992).

It should be kept in mind that the most important information in parathyroid scintigraphy is in the ^{99m}Tc-sestamibi image. The ^{123}I image is mainly used for removal of the thyroid gland. Although ^{99m}Tc image is contaminated with ^{123}I photons, their spatial distribution is different because parathyroid glands are separated from thyroid glands (excluding rare cases of intrathyroidal parathyroid glands). Therefore, the selection of the collimator should be based on ^{99m}Tc-sestamibi image optimization.

6.4 Cross-contamination

Dedicated cross-contamination correction methods were not used in any hospital using the dual-isotope method in Study I, but the amount of cross-contamination was minimized with narrow and/or asymmetric energy windows. This approach has also been used by other authors as the only option for correcting cross-contamination in clinical work, with the exception of some early attempts using cross-contamination factors (Hindie et al. 1997, Hindie et al. 1998, Jeanguillaume et al. 1998, Neumann et al. 1998, Hindie et al. 1999, Hindie et al. 2000, Dontu et al. 2004, Neumann et al. 2008).

Although shifting the ^{123}I window to the right to minimizes ^{99m}Tc-contamination in the ^{123}I window, uniformity is decreased, as shown in Study IV, and this in turn creates subtraction artifacts in ^{99m}Tc-sestamibi/^{123}I subtraction SPECT/CT, as shown in Study V. The use of the asymmetric ^{123}I window is thus not recommended.

By contrast, the contamination of ^{123}I in the ^{99m}Tc energy window is much higher regardless of the collimator used. Shifting the ^{99m}Tc window to the left has been shown to be ineffective in reducing ^{123}I crosstalk (Ivanovic et al. 1994) and was therefore not tested here. The use of the scatter correction method did not improve visual scores in Study V with an adenoma of very low activity. The adenoma of higher activity had higher contrast in additional measures to Study V, but there was very little difference in the visual appearance of images.

It was expected that the efficacy of the TEW method is limited with ^{99m}Tc and ^{123}I due to the close proximity of the photopeaks (Yang et al. 1997). However, applying the scatter correction to clinical practice (acquisition of additional scatter windows) has no drawbacks, as it is easy to produce images with and without scatter correction being applied.

6.5 Acquisition parameters

The slight distortion detected in the SPECT images acquired with detectors in L-mode in Study V was not noticed with patient images in a preliminary test of our earlier studies. However, this slight distortion was seen as there was no motion or breathing artifacts with a stationary phantom. This phenomenon results from variable spatial resolution and has been reported by several authors (Knesaurek 1987, Knesaurek et al. 1989, Groch et al. 2000, Notghi et al. 2010). To the best of our knowledge, L-mode has not been applied with dual-isotope parathyroid subtraction SPECT by any other author and, according to our results, it is not recommended.

The use of the 256×256 matrix size (voxel size of 2,3×2,3×2,3 mm) improved the contrast of the adenoma with LEUHR collimators when compared with the 128×128 matrix size (voxel size of 4.6×4,6×4.6 mm). The improved contrast is associated with improved reconstructed resolution due to the smaller voxel size and the partial-volume effect, as shown in the results of Kappadath (Kappadath 2011). Changing the matrix size from 128×128 to 256×256 of course decreases the counts per voxel to 1/8 compared to counts per voxel in the 128×128 matrix, and thus decreases the signal-to-noise ratio. However, it is also beneficial to use a higher acquisition matrix, as it is possible to rebin the imaging matrix of 256×256 to a lower size if counts per voxel are too low in a patient study.

6.6 Image reconstruction and processing

The effect of various reconstruction algorithms was not tested in this study as only vendor-specific Flash 3D was available. However, a significant impact on image quality was noticed in Study V as the parameters of the reconstruction algorithm were adjusted, which is in line with previously published results (Nichols et al. 2007, Bar et al. 2011, van Hoorn et al. 2013, Ekjeen et al. 2015). The effect of improving the resolution as a function of the increasing number of iterations has been shown by van Hoorn and co-workers, but only with a reconstruction algorithm that included resolution recovery (as Flash 3D) (Kappadath 2011, van Hoorn et al. 2013). Kappadath showed that the reconstructed resolution improved in a power-law fashion with the product of iterations and subsets. To reach the highest possible resolution, the product of iterations and subsets needs to be high enough in order to reach the plateau in the resolution curve (i.e., reconstructed resolution as a function of the product of iterations and subsets) (Kappadath 2011). It is also well known that image noise increases with the product of iterations and subsets and was also shown in Study IV. The range for the product of iterations and subsets needs to be carefully selected for optimal trade-off between image noise and spatial resolution with clinical studies, which is also an important topic for further studies.

The first ^{99m}Tc-sestamibi/^{123}I subtraction SPECT/CT study by Neumann and co-workers had a quite low sensitivity of 70% (Neumann et al. 2008), although they used high activity ^{99m}Tc-sestamibi and had many years of experience with subtraction SPECT (Neumann et al. 1997, Neumann et al. 1998,

Neumann et al. 2000). In their study, they used Siemens T6 SPECT/CT with very similar acquisition parameters to those we used in Study III. However, they only used four iterations and eight subsets in reconstruction in comparison to our eight iterations and eight subsets in Study III and an even higher number in Study V. According to the results of Study V, this is one possible explanation behind the low sensitivity reported by Neumann and co-workers (Neumann et al. 2008).

The subtraction step is performed after the reconstruction of the ^{99m}Tc and ^{123}I images and is performed to remove the thyroid gland from the image. If there is no difference in the spatial distribution of the ^{99m}Tc and ^{123}I images, the subtraction of a ^{123}I image should produce an image containing only noise and reconstruction artifacts (Brinkmann et al. 1999).

It was shown in Study IV that there is a small difference in the resolution of the ^{99m}Tc and ^{123}I images, especially in the FWTM values. There was also variation as a function of distance in the sensitivity of ^{123}I, the scatter-to-photopeak ratio of ^{123}I, and the cross-contamination of ^{123}I in the ^{99m}Tc window caused by the septal penetration of high-energy gamma photons of ^{123}I. These results are in line of those of Brinkmann and Ivanovic(Ivanovic et al. 1994, Brinkmann et al. 1999).

As a result, even optimal processing of identical ^{99m}Tc and ^{123}I images does not give a flawless subtraction image. Typical subtraction artifacts are "blobs" surrounding the thyroid gland, the so-called "edge artifacts". To the best of our knowledge, this artifact has not been described earlier in connection with parathyroid scintigraphy. This was also the main cause of artifacts in Study II and in Study III. A careful optimization of the protocol, as shown in Study V, should be able to minimize this artifact.

Although the previously mentioned effects degrade the quantitative precision, the parathyroid scintigraphy analysis does not benefit from a quantitative approach (Nichols et al. 2007). In Study V, a quantitative approach was used to compare various acquisition and processing parameters. However, clinical work is based solely on the visual appearance of the subtraction image and the corresponding anatomical reference in the CT image. Thus, accurate quantitation is not obligatory, as is the case, for example, in neurologic applications (Brinkmann et al. 1999).

6.7 The optimal protocol

^{99m}Tc-sestamibi/^{123}I subtraction imaging with pinhole collimators has been the protocol of choice for several authors. Although the sensitivity figures have been high (Hindie et al. 1998), pinhole imaging lacks the 3D anatomical information offered by modern SPECT/CT (Taieb et al. 2012, Taieb et al. 2013, Wong et al. 2015). However, the sensitivity figures of the first ^{99m}Tc-sestamibi/^{123}I subtraction SPECT/CT were not as high as with planar pinhole imaging (Neumann et al. 2008, Bhatt et al. 2015). This might explain why ^{99m}Tc-sestamibi/^{123}I subtraction SPECT/CT is not very extensively applied worldwide. To date, only three clinical studies (Tunninen et al. 2013 (Hassler et al. 2013, Bhatt et al. 2015) have been published on the ^{99m}Tc-sestamibi/^{123}I subtraction SPECT/CT protocol in addition to that of Neumann and co-workers (Neumann et al. 2008).

We were able to reach the sensitivity of 94% with ^{99m}Tc-sestamibi/^{123}I subtraction SPECT/CT in Study III, and it was even further improved with the additional use of a pinhole imaging. Although the combined use of acquisition techniques is favored by many authors, it increases the acquisition time and thus increases the cost of the study and the discomfort of the patient. According to our phantom experiments, with the careful optimization of ^{99m}Tc-sestamibi/^{123}I subtraction SPECT/CT protocol, it is possible to exclude the pinhole imaging in the clinical protocol.

It is well known that a large parathyroid adenoma can be easily visualized with all protocols in clinical use. However, the clinical problem involves patients with secondary hyperparathyroidism with relatively inactive hyperplastic glands, and patients with multiglandular disease, where the patient has more than one enlarged parathyroid glands (Hindie et al. 2015). Nichols stated already ten years ago *"any technical innovation that aids in the accuracy of the localization process should be employed"* (Nichols et al. 2007). An *a*lmost identical comment by Minisola was published recently *"The time has come for optimally combining the best that technology has to offer in this scenario with the best surgical expertise, for ensuring maximum benefit to patients"* (Minisola et al. 2016). In this scenario, the benefit of an additional pinhole imaging needs to be carefully evaluated.

The dual-isotope SPECT/CT is a highly sensitive and specific method for localizing an enlarged parathyroid adenoma. However, there are several aspects that have a profound effect on the final outcome of the study. With unoptimized choices, the optimal protocol may turn into a worst case scenario. These aspects are summarized in Figure 37.

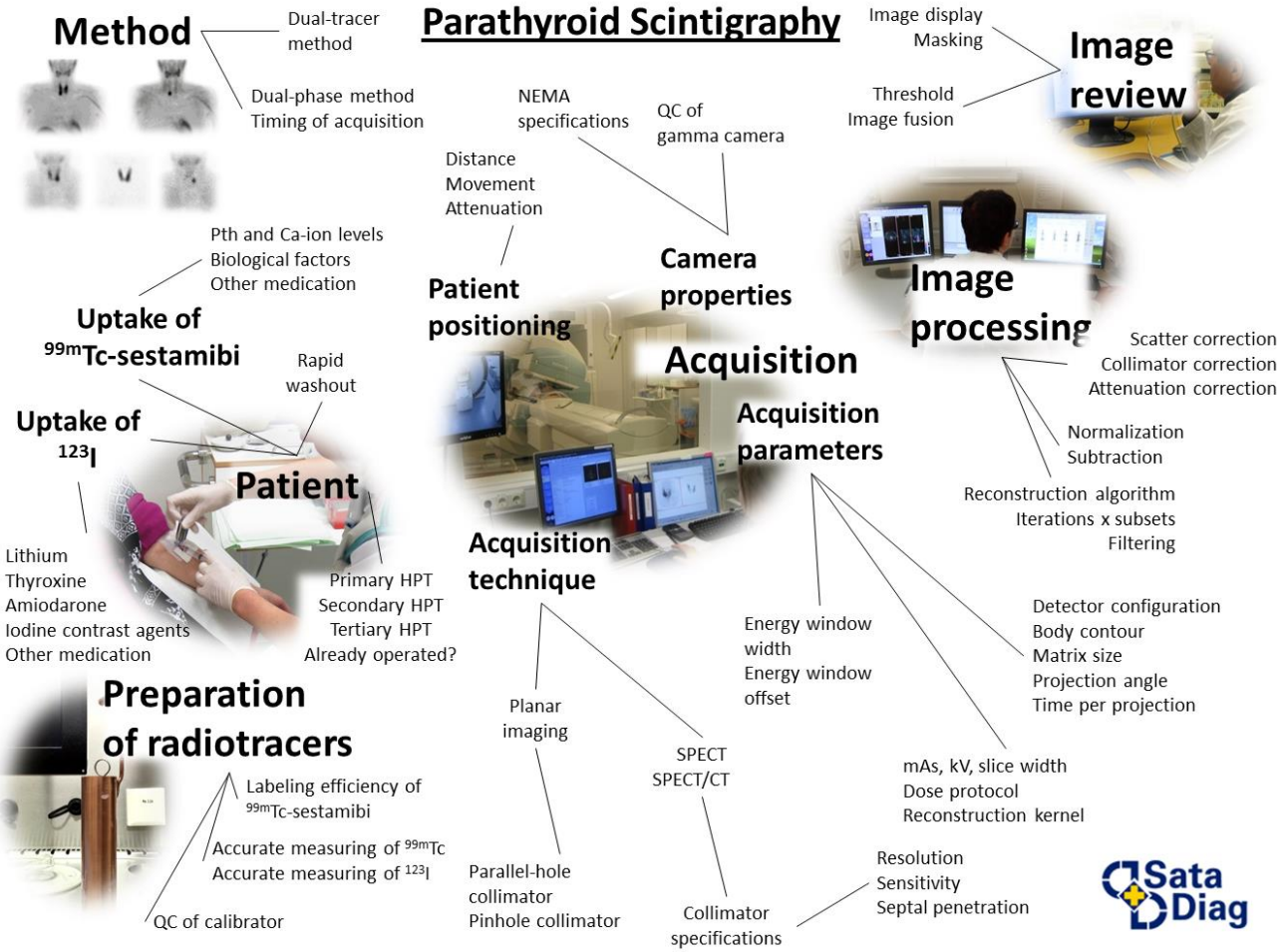

Figure 37. *The technical aspects of ^{99m}Tc-sestamibi/^{123}I subtraction SPECT/CT.*

6.8 Conclusions

All patients referred for parathyroid scintigraphy have already been diagnosed with primary hyperparathyroidism (also with secondary or tertiary hyperparathyroidism), with diagnosis based on laboratory findings. The question is whether the parathyroid scintigraphy protocol is capable of localizing the enlarged glands. Each patient should be studied with the highest accuracy in order to localize all the enlarged parathyroid glands immediately (Taieb et al. 2012, Hindie et al. 2015). Missing an enlarged gland (in multiglandular disease or in the case of double adenoma) will become exposed after surgery causing elevated Ca-ion and PTH levels. For the patient, it means repeated studies with additional radiation doses and repeated surgery with an increased complication rate (Taieb et al. 2013, Whitcroft et al. 2014). In this scenario, all possible efforts should be made to use the parathyroid scintigraphy protocol to yield as accurate results as possible. The combined protocol with pinhole imaging might also give additional information on thyroid nodules, and thus exclude false positive findings and the referring of the patient for further studies in the case of thyroid malignancy(Onkendi et al. 2012, Greilsamer et al. 2015).

The ^{99m}Tc-sestamibi/^{123}I subtraction SPECT/CT protocol is a highly efficient and modern protocol for the localization of enlarged parathyroid glands. A sensitive and specific preoperative localization, also capable of identifying ectopic glands and multiple gland disease, is a prerequisite for minimally invasive surgery, a modern treatment for hyperparathyroidism (Hindie et al. 2009). However, an international debate continues as to whether imaging is best performed using a dual-phase method with ^{99m}Tc-sestamibi alone or using the dual-isotope method with ^{99m}Tc-sestamibi and ^{123}I (O'Doherty et al. 2003, Hindie et al. 2009, Greenspan et al. 2012). Several options for acquisition technique and the selection of parameters have led to a large variety of protocols being used, with a large variety of sensitivity and specificity figures (Mihai et al. 2009). A number of studies have also been published with insufficient information on the acquisition and processing techniques used, and this confuses the field even more as inferior results may also arise from the use of unoptimized technique (Sharma et al. 2006, Ali et al. 2011, Bhatt et al. 2015).

The clinical audit procedure assesses the local practice against the defined good practice (Decree of the Ministry of Social Affairs and Health on the medical use of radiation 423/2000 https://www.stuklex.fi/en/ls/20000423). However, there are still a number of studies within nuclear medicine, including parathyroid scintigraphy, where the good practice has not been well defined. In order to build good practice for parathyroid scintigraphy, a need exists for more research and also for external quality assurance carried out by independent outside observers.

7 Summary and conclusions

This thesis studied the parathyroid scintigraphy protocols. The aim was to find the optimal protocol with the highest sensitivity and specificity possible. We have shown that the dual-isotope method with ^{99m}Tc-sestamibi and ^{123}I is superior to the use of ^{99m}Tc-sestamibi alone. Combining the ^{99m}Tc-sestamibi/^{123}I subtraction method with the SPECT/CT technique is a highly sensitive and specific protocol for parathyroid scintigraphy and should be preferred over planar acquisition techniques due to important anatomical 3D information. On the other hand, ^{99m}Tc-sestamibi/^{123}I subtraction SPECT/CT is a highly technical protocol that requires experience and the thorough testing of each step in the protocol. With careful optimization, superior sensitivity and specificity with accurate anatomical information can be accomplished. The main findings of this study can be summarized as follows:

1) The dual-isotope method with ^{99m}Tc-sestamibi and ^{123}I is superior when compared with a single-tracer method with ^{99m}Tc-sestamibi alone

2) ^{99m}Tc-sestamibi/^{123}I subtraction SPECT/CT is a highly sensitive and specific protocol for parathyroid scintigraphy and should be preferred over planar acquisition techniques due to important anatomical 3D information

3) With careful optimization, ^{99m}Tc-sestamibi/^{123}I subtraction SPECT/CT is an adequate technique for parathyroid scintigraphy without additional acquisitions

4) ^{99m}Tc-sestamibi/^{123}I subtraction SPECT/CT should be optimized with the following aspects:
    a. The SPECT acquisition should be done with the highest resolution achievable in order to minimize subtraction artifacts
    b. The use of symmetrical energy windows is preferred over asymmetrical windows
    c. The use of scatter correction increases the contrast of an adenoma, but may decrease the visual appearance if the number of counts is low
    d. The use of a higher number of iterations in reconstruction increases the contrast and the visual appearance of an adenoma

5) All combinations of collimator and camera together with acquisition and processing parameters should be tested in each center with known phantoms in order to achieve the highest quality possible

8 References

Ahmad, R. and Hammond, J. M. (2004). "Primary, secondary, and tertiary hyperparathyroidism." Otolaryngol Clin North Am **37**(4): 701-713, vii-viii.

Ali, L., Loutfi, I., Biswas, G., Hadi, N. and Girgis, T. (2011). "Improved Delineation of Parathyroid Lesions in Patients with Chronic Renal Failure Using Magnified Pinhole Imaging." Journal of Nuclear Medicine Technology **39**(1): 35-39.

Anger, H. (1958). "Scintillation camera." Rev Sci Instrum **29**: 27-33.

Arveschoug, A. K., Bertelsen, H. and Vammen, B. (2002). "Presurgical localization of abnormal parathyroid glands using a single injection of Tc-99m sestamibi: comparison of high-resolution parallel-hole and pinhole collimators, and interobserver and intraobserver variation." Clin Nucl Med **27**(4): 249-254.

Arveschoug, A. K., Bertelsen, H., Vammen, B. and Brochner-Mortensen, J. (2007). "Preoperative dual-phase parathyroid imaging with tc-99m-sestamibi: accuracy and reproducibility of the pinhole collimator with and without oblique images." Clin Nucl Med **32**(1): 9-12.

Augustine, M. M., Bravo, P. E. and Zeiger, M. A. (2011). "Surgical treatment of primary hyperparathyroidism." Endocr Pract **17 Suppl 1**: 75-82.

Bahador, F. M., Latifi, H. R., Grossman, S. J., Oza, U. D., Xu, H. and Griffeth, L. K. (2015). "Optimal interpretative strategy for preoperative parathyroid scintigraphy." Clin Nucl Med **40**(2): 116-122.

Bai, J., Hashimoto, J., Ogawa, K., Nakahara, T., Suzuki, T. and Kubo, A. (2007). "Scatter correction based on an artificial neural network for 99mTc and 123I dual-isotope SPECT in myocardial and brain imaging." Ann Nucl Med **21**(1): 25-32.

Bailey, D. L. and Willowson, K. P. (2013). "An evidence-based review of quantitative SPECT imaging and potential clinical applications." J Nucl Med **54**(1): 83-89.

Bar, R., Przewloka, K., Karry, R., Frenkel, A., Golz, A. and Keidar, Z. (2011). "Half-Time SPECT Acquisition with Resolution Recovery for Tc-MIBI SPECT Imaging in the Assessment of Hyperparathyroidism." Mol Imaging Biol.

Beekman, F. and van der Have, F. (2007). "The pinhole: gateway to ultra-high-resolution three-dimensional radionuclide imaging." Eur J Nucl Med Mol Imaging **34**(2): 151-161.

Bhatt, P. R., Klingensmith, W. C., 3rd, Bagrosky, B. M., Walter, J. C., McFann, K. K., McIntyre, R. C., Jr., Raeburn, C. D. and Koo, P. J. (2015). "Parathyroid Imaging with Simultaneous Acquisition of 99mTc-Sestamibi and 123I: The Relative Merits of Pinhole Collimation and SPECT/CT." J Nucl Med Technol **43**(4): 275-281.

Billotey, C., Aurengo, A., Najean, Y., Sarfati, E., Moretti, J. L., Toubert, M. E. and Rain, J. D. (1994). "Identifying abnormal parathyroid glands in the thyroid uptake area using technetium-99m-sestamibi and factor analysis of dynamic structures." J Nucl Med **35**(10): 1631-1636.

Billy, H. T., Rimkus, D. R., Hartzman, S. and Latimer, R. G. (1995). "Technetium-99m-sestamibi single agent localization versus high resolution ultrasonography for the preoperative localization of parathyroid glands in patients with primary hyperparathyroidism." Am Surg **61**(10): 882-888.

Blocklet, D., Martin, P., Schoutens, A., Verhas, M., Hooghe, L. and Kinnaert, P. (1997). "Presurgical localization of abnormal parathyroid glands using a single injection of technetium-99m methoxyisobutylisonitrile: comparison of different techniques including factor analysis of dynamic structures." Eur J Nucl Med **24**(1): 46-51.

Brinkmann, B. H., O'Connor, M. K., O'Brien, T. J., Mullan, B. P., So, E. L. and Robb, R. A. (1999). "Dual-isotope SPECT using simultaneous acquisition of 99mTc and 123I radioisotopes: a double-injection technique for peri-ictal functional neuroimaging." J Nucl Med **40**(4): 677-684.

Brownell, A. L., Nikkinen, P. and Liewendahl, K. (1990). "The development of nuclear medicine imaging." Scand J Clin Lab Invest Suppl **201**: 119-125.

Buck, A. K., Nekolla, S., Ziegler, S., Beer, A., Krause, B. J., Herrmann, K., Scheidhauer, K., Wester, H. J., Rummeny, E. J., Schwaiger, M. and Drzezga, A. (2008). "SPECT/CT." J Nucl Med **49**(8): 1305-1319.

Buvat, I., Benali, H., Todd-Pokropek, A. and Di Paola, R. (1994). "Scatter correction in scintigraphy: the state of the art." Eur J Nucl Med **21**(7): 675-694.

Caixas, A., Berna, L., Hernandez, A., Tebar, F. J., Madariaga, P., Vegazo, O., Bittini, A. L., Moreno, B., Faure, E., Abos, D., Piera, J., Rodriguez, J. M., Farrerons, J. and Puig-Domingo, M. (1997). "Efficacy of preoperative diagnostic imaging localization of technetium 99m-sestamibi scintigraphy in hyperparathyroidism." Surgery **121**(5): 535-541.

Calva-Cerqueira, D., Smith, B. J., Hostetler, M. L., Lal, G., Menda, Y., O'Dorisio, T. M. and Howe, J. R. (2007). "Minimally invasive parathyroidectomy and preoperative MIBI scans: correlation of gland weight and preoperative PTH." J Am Coll Surg **205**(4 Suppl): S38-44.

Cann, C. E. and Prussin, S. G. (1980). "Possible parathyroid imaging using Ga-67 and other aluminum analogs." J Nucl Med **21**(5): 471-474.

Carty, S. E. (2004). "Prevention and management of complications in parathyroid surgery." Otolaryngol Clin North Am **37**(4): 897-907, xi.

Casas, A. T., Burke, G. J., Sathyanarayana, Mansberger, A. R., Jr. and Wei, J. P. (1993). "Prospective comparison of technetium-99m-sestamibi/iodine-123 radionuclide scan versus high-

resolution ultrasonography for the preoperative localization of abnormal parathyroid glands in patients with previously unoperated primary hyperparathyroidism." Am J Surg **166**(4): 369-373.

Caveny, S. A., Klingensmith, W. C., 3rd, Martin, W. E., Sage-El, A., McIntyre, R. C., Jr., Raeburn, C. and Wolfe, P. (2012). "Parathyroid imaging: the importance of dual-radiopharmaceutical simultaneous acquisition with 99mTc-sestamibi and 123I." J Nucl Med Technol **40**(2): 104-110.

Chen, C. C., Holder, L. E., Scovill, W. A., Tehan, A. M. and Gann, D. S. (1997). "Comparison of parathyroid imaging with technetium-99m-pertechnetate/sestamibi subtraction, double-phase technetium-99m-sestamibi and technetium-99m-sestamibi SPECT." J Nucl Med **38**(6): 834-839.

Chen, E. M. and Mishkin, F. S. (1997). "Parathyroid hyperplasia may be missed by double-phase Tc-99m sestamibi scintigraphy alone." Clin Nucl Med **22**(4): 222-226.

Cherry, S. R., Sorenson, J. A. and Phelps, M. E. (2003). Physics in nuclear medicine, Saunders.

Chiu, B., Sturgeon, C. and Angelos, P. (2006). "What is the link between nonlocalizing sestamibi scans, multigland disease, and persistent hypercalcemia? A study of 401 consecutive patients undergoing parathyroidectomy." Surgery **140**(3): 418-422.

Chiu, M. L., Kronauge, J. F. and Piwnica-Worms, D. (1990). "Effect of mitochondrial and plasma membrane potentials on accumulation of hexakis (2-methoxyisobutylisonitrile) technetium(I) in cultured mouse fibroblasts." J Nucl Med **31**(10): 1646-1653.

Civelek, A. C., Ozalp, E., Donovan, P. and Udelsman, R. (2002). "Prospective evaluation of delayed technetium-99m sestamibi SPECT scintigraphy for preoperative localization of primary hyperparathyroidism." Surgery **131**(2): 149-157.

Clark, O. H. (1995). "Surgical treatment of primary hyperparathyroidism." Adv Endocrinol Metab **6**: 1-16.

Coakley, A. J., Kettle, A. G., Wells, C. P., O'Doherty, M. J. and Collins, R. E. (1989). "99Tcm sestamibi--a new agent for parathyroid imaging." Nucl Med Commun **10**(11): 791-794.

Dasgupta, D. J., Navalkissoor, S., Ganatra, R. and Buscombe, J. (2013). "The role of single-photon emission computed tomography/computed tomography in localizing parathyroid adenoma." Nucl Med Commun **34**(7): 621-626.

Devous, M. D., Sr., Lowe, J. L. and Payne, J. K. (1992). "Dual-isotope brain SPECT imaging with technetium-99m and iodine-123: validation by phantom studies." J Nucl Med **33**(11): 2030-2035.

Dobbeleir, A. A., Hambye, A. S. and Franken, P. R. (1999). "Influence of high-energy photons on the spectrum of iodine-123 with low- and medium-energy collimators: consequences for imaging with 123I-labelled compounds in clinical practice." Eur J Nucl Med **26**(6): 655-658.

Dontu, V. S., Kettle, A. G., O'Doherty, M. J. and Coakley, A. J. (2004). "Optimization of parathyroid imaging by simultaneous dual energy planar and single photon emission tomography." Nucl Med Commun **25**(11): 1089-1093.

Doppman, J. (1968). "Reoperative parathyroid surgery: localization procedures, parathyroid surgery." Prog Surg **18**: 1171.

Doppman, J. L. and Miller, D. L. (1991). "Localization of parathyroid tumors in patients with asymptomatic hyperparathyroidism and no previous surgery." J Bone Miner Res **6 Suppl 2**: S153-158; discussion S159.

Dresel, S. H., Kung, M. P., Huang, X. F., Plossl, K., Hou, C., Meegalla, S. K., Patselas, G., Mu, M., Saffer, J. R. and Kung, H. F. (1999). "Simultaneous SPECT studies of pre- and postsynaptic dopamine binding sites in baboons." J Nucl Med **40**(4): 660-666.

Du, Y., Bhattacharya, M. and Frey, E. C. (2014). "Simultaneous Tc-99m/I-123 dual-radionuclide myocardial perfusion/innervation imaging using Siemens IQ-SPECT with SMARTZOOM collimator." Phys Med Biol **59**(11): 2813-2828.

Du, Y. and Frey, E. C. (2009). "Quantitative evaluation of simultaneous reconstruction with model-based crosstalk compensation for 99mTc/123I dual-isotope simultaneous acquisition brain SPECT." Med Phys **36**(6): 2021-2033.

Du, Y., Tsui, B. M. and Frey, E. C. (2007). "Model-based crosstalk compensation for simultaneous 99mTc/123I dual-isotope brain SPECT imaging." Med Phys **34**(9): 3530-3543.

Ekjeen, T., Tocharoenchai, C., Pusuwan, P., Fung, G. S., Ghaly, M., Du, Y. and Frey, E. C. (2015). "Optimization and evaluation of reconstruction-based compensation methods and reconstruction parameters for Tc-99m MIBI parathyroid SPECT." Phys Med **31**(2): 159-166.

El Fakhri, G., Moore, S. C., Maksud, P., Aurengo, A. and Kijewski, M. F. (2001). "Absolute activity quantitation in simultaneous 123I/99mTc brain SPECT." J Nucl Med **42**(2): 300-308.

Even-Sapir, E., Keidar, Z., Sachs, J., Engel, A., Bettman, L., Gaitini, D., Guralnik, L., Werbin, N., Iosilevsky, G. and Israel, O. (2001). "The new technology of combined transmission and emission tomography in evaluation of endocrine neoplasms." J Nucl Med **42**(7): 998-1004.

Fahey, F. H. (1996). "State of the art in emission tomography equipment." Radiographics **16**(2): 409-420.

Fahey, F. H., Harkness, B. A., Keyes, J. W., Jr., Madsen, M. T., Battisti, C. and Zito, V. (1992). "Sensitivity, resolution and image quality with a multi-head SPECT camera." J Nucl Med **33**(10): 1859-1863.

Ferlin, G., Borsato, N., Camerani, M., Conte, N. and Zotti, D. (1983). "New perspectives in localizing enlarged parathyroids by technetium-thallium subtraction scan." J Nucl Med **24**(5): 438-441.

Frey, E. C., Humm, J. L. and Ljungberg, M. (2012). "Accuracy and precision of radioactivity quantification in nuclear medicine images." Semin Nucl Med **42**(3): 208-218.

Friedman, K., Somervell, H., Patel, P., Melton, G. B., Garrett-Mayer, E., Dackiw, A. P., Civelek, A. C. and Zeiger, M. A. (2004). "Effect of calcium channel blockers on the sensitivity of preoperative 99mTc-MIBI SPECT for hyperparathyroidism." Surgery **136**(6): 1199-1204.

Fujii, H., Iwasaki, R., Ogawa, K., Hashimoto, J., Nakamura, K., Kunieda, E., Sanmiya, T., Kubo, A. and Inagaki, K. (1999). "[Evaluation of parathyroid imaging methods with 99mTc-MIBI--the comparison of planar images obtained using a pinhole collimator and a parallel-hole collimator]." Kaku Igaku **36**(5): 425-433.

Gayed, I. W., Kim, E. E., Broussard, W. F., Evans, D., Lee, J., Broemeling, L. D., Ochoa, B. B., Moxley, D. M., Erwin, W. D. and Podoloff, D. A. (2005). "The value of 99mTc-sestamibi SPECT/CT over conventional SPECT in the evaluation of parathyroid adenomas or hyperplasia." J Nucl Med **46**(2): 248-252.

Geatti, O., Shapiro, B., Orsolon, P. G., Proto, G., Guerra, U. P., Antonucci, F. and Gasparini, D. (1994). "Localization of parathyroid enlargement: experience with technetium-99m methoxyisobutylisonitrile and thallium-201 scintigraphy, ultrasonography and computed tomography." Eur J Nucl Med **21**(1): 17-22.

Geeter, F. D., Franken, P. R., Defrise, M., Andries, H., Saelens, E. and Bossuyt, A. (1996). "Optimal collimator choice for sequential iodine-123 and technetium-99m imaging." Eur J Nucl Med **23**(7): 768-774.

Gilland, D. R., Jaszczak, R. J., Turkington, T. G., Greer, K. L. and Coleman, R. E. (1994). "Volume and activity quantitation with iodine-123 SPECT." J Nucl Med **35**(10): 1707-1713.

Gordon, L., Burkhalter, W. and Mah, E. (2002). "Dual-phase 99mTc-sestamibi imaging: its utility in parathyroid hyperplasia and use of immediate/delayed image ratios to improve diagnosis of hyperparathyroidism." J Nucl Med Technol **30**(4): 179-184.

Greene, A. B., Butler, R. S., McIntyre, S., Barbosa, G. F., Mitchell, J., Berber, E., Siperstein, A. and Milas, M. (2009). "National trends in parathyroid surgery from 1998 to 2008: a decade of change." J Am Coll Surg **209**(3): 332-343.

Greenspan, B. S., Dillehay, G., Intenzo, C., Lavely, W. C., O'Doherty, M., Palestro, C. J., Scheve, W., Stabin, M. G., Sylvestros, D. and Tulchinsky, M. (2012). "SNM Practice Guideline for Parathyroid Scintigraphy 4.0." J Nucl Med Technol.

Greilsamer, T., Blanchard, C., Christou, N., Drui, D., Ansquer, C., Le Bras, M., Cariou, B., Caillard, C., Mourrain-Langlois, E., Delemazure, A. S., Mathonnet, M., Kraeber-Bodere, F. and Mirallie, E. (2015). "Management of thyroid nodules incidentally discovered on MIBI scanning for primary hyperparathyroidism." Langenbecks Arch Surg **400**(3): 313-318.

Groch, M. W. and Erwin, W. D. (2000). "SPECT in the year 2000: basic principles." J Nucl Med Technol **28**(4): 233-244.

Guerin, C., Lowery, A., Gabriel, S., Castinetti, F., Philippon, M., Vaillant-Lombard, J., Loundou, A., Henry, J. F., Sebag, F. and Taieb, D. (2015). "Preoperative imaging for focused parathyroidectomy: making a good strategy even better." Eur J Endocrinol **172**(5): 519-526.

Halvorson, D. J., Burke, G. J., Mansberger, A. R., Jr. and Wei, J. P. (1994). "Use of technetium Tc 99m sestamibi and iodine 123 radionuclide scan for preoperative localization of abnormal parathyroid glands in primary hyperparathyroidism." South Med J **87**(3): 336-339.

Hannequin, P., Mas, J. and Germano, G. (2000). "Photon energy recovery for crosstalk correction in simultaneous 99mTc/201Tl imaging." J Nucl Med **41**(4): 728-736.

Hapdey, S., Soret, M. and Buvat, I. (2006). "Quantification in simultaneous (99m)Tc/(123)I brain SPECT using generalized spectral factor analysis: a Monte Carlo study." Phys Med Biol **51**(23): 6157-6171.

Harris, L., Yoo, J., Driedger, A., Fung, K., Franklin, J., Gray, D. and Holliday, R. (2008). "Accuracy of technetium-99m SPECT-CT hybrid images in predicting the precise intraoperative anatomical location of parathyroid adenomas." Head Neck **30**(4): 509-517.

Hassler, S., Ben-Sellem, D., Hubele, F., Constantinesco, A. and Goetz, C. (2013). "Dual-Isotope 99mTc-MIBI/123I Parathyroid Scintigraphy in Primary Hyperparathyroidism: Comparison of Subtraction SPECT/CT and Pinhole Planar Scan." Clin Nucl Med.

Hindie, E., Melliere, D., Jeanguillaume, C., Perlemuter, L., Chehade, F. and Galle, P. (1998). "Parathyroid imaging using simultaneous double-window recording of technetium-99m-sestamibi and iodine-123." J Nucl Med **39**(6): 1100-1105.

Hindie, E., Melliere, D., Jeanguillaume, C., Urena, P., deLabriolle-Vaylet, C. and Perlemuter, L. (2000). "Unilateral surgery for primary hyperparathyroidism on the basis of technetium Tc 99m sestamibi and iodine 123 subtraction scanning." Arch Surg **135**(12): 1461-1468.

Hindie, E., Melliere, D., Perlemuter, L., Jeanguillaume, C. and Galle, P. (1997). "Primary hyperparathyroidism: higher success rate of first surgery after preoperative Tc-99m sestamibi-I-123 subtraction scanning." Radiology **204**(1): 221-228.

Hindie, E., Melliere, D., Simon, D., Perlemuter, L. and Galle, P. (1995). "Primary hyperparathyroidism: is technetium 99m-Sestamibi/iodine-123 subtraction scanning the best procedure to locate enlarged glands before surgery?" J Clin Endocrinol Metab **80**(1): 302-307.

Hindie, E., Ugur, O., Fuster, D., O'Doherty, M., Grassetto, G., Urena, P., Kettle, A., Gulec, S. A., Pons, F. and Rubello, D. (2009). "2009 EANM parathyroid guidelines." Eur J Nucl Med Mol Imaging **36**(7): 1201-1216.

Hindie, E., Urena, P., Jeanguillaume, C., Melliere, D., Berthelot, J. M., Menoyo-Calonge, V., Chiappini-Briffa, D., Janin, A. and Galle, P. (1999). "Preoperative imaging of parathyroid glands with technetium-99m-labelled sestamibi and iodine-123 subtraction scanning in secondary hyperparathyroidism." Lancet **353**(9171): 2200-2204.

Hindie, E., Zanotti-Fregonara, P., Tabarin, A., Rubello, D., Morelec, I., Wagner, T., Henry, J. F. and Taieb, D. (2015). "The Role of Radionuclide Imaging in the Surgical Management of Primary Hyperparathyroidism." J Nucl Med **56**(5): 737-744.

Ho Shon, I. A., Bernard, E. J., Roach, P. J. and Delbridge, L. W. (2001). "The value of oblique pinhole images in pre-operative localisation with 99mTc-MIBI for primary hyperparathyroidism." Eur J Nucl Med **28**(6): 736-742.

Ho Shon, I. A., Roach, P. J., Bernard, E. J. and Delbridge, L. W. (2001). "Optimal pinhole techniques for preoperative localization with Tc-99m MIBI for primary hyperparathyroidism." Clin Nucl Med **26**(12): 1002-1009.

Ho Shon, I. A., Yan, W., Roach, P. J., Bernard, E. J., Shields, M., Sywak, M., Sidhu, S. and Delbridge, L. W. (2008). "Comparison of pinhole and SPECT 99mTc-MIBI imaging in primary hyperparathyroidism." Nucl Med Commun **29**(11): 949-955.

Hudson, H. M. and Larkin, R. S. (1994). "Accelerated image reconstruction using ordered subsets of projection data." IEEE Trans Med Imaging **13**(4): 601-609.

Hutton, B. F., Buvat, I. and Beekman, F. J. (2011). "Review and current status of SPECT scatter correction." Phys Med Biol **56**(14): R85-112.

Ichihara, T., Ogawa, K., Motomura, N., Kubo, A. and Hashimoto, S. (1993). "Compton scatter compensation using the triple-energy window method for single- and dual-isotope SPECT." J Nucl Med **34**(12): 2216-2221.

Ingui, C. J., Shah, N. P. and Oates, M. E. (2006). "Endocrine neoplasm scintigraphy: added value of fusing SPECT/CT images compared with traditional side-by-side analysis." Clin Nucl Med **31**(11): 665-672.

Inoue, Y., Shirouzu, I., Machida, T., Yoshizawa, Y., Akita, F., Doi, I., Watadani, T., Noda, M., Yoshikawa, K. and Ohtomo, K. (2003). "Physical characteristics of low and medium energy collimators for 123I imaging and simultaneous dual-isotope imaging." Nucl Med Commun **24**(11): 1195-1202.

Ishibashi, M., Nishida, H., Hiromatsu, Y., Kojima, K., Tabuchi, E. and Hayabuchi, N. (1998). "Comparison of technetium-99m-MIBI, technetium-99m-tetrofosmin, ultrasound and MRI for localization of abnormal parathyroid glands." J Nucl Med **39**(2): 320-324.

Ivanovic, M., Weber, D. A., Loncaric, S. and Franceschi, D. (1994). "Feasibility of dual radionuclide brain imaging with I-123 and Tc-99m." Med Phys **21**(5): 667-674.

Jeanguillaume, C., Urena, P., Hindie, E., Prieur, P., Petrover, M., Menoyo-Calonge, V., Janin, A., Chiappini-Briffa, D., Melliere, D., Boulahdour, H. and Galle, P. (1998). "Secondary hyperparathyroidism: detection with I-123-Tc-99m-Sestamibi subtraction scintigraphy versus US." Radiology **207**(1): 207-213.

Johnson, N. A., Tublin, M. E. and Ogilvie, J. B. (2007). "Parathyroid imaging: technique and role in the preoperative evaluation of primary hyperparathyroidism." AJR Am J Roentgenol **188**(6): 1706-1715.

Kacker, A., Scharf, S. and Komisar, A. (2000). "Reduced-time-window sestamibi scanning for nonlocalized primary hyperparathyroidism." Otolaryngol Head Neck Surg **123**(4): 456-458.

Kadrmas, D. J., Frey, E. C. and Tsui, B. M. (1999). "Simultaneous technetium-99m/thallium-201 SPECT imaging with model-based compensation for cross-contaminating effects." Phys Med Biol **44**(7): 1843-1860.

Kang, G. S. and DiGiulio, W. (1968). "Potential value of toluidine blue analogs as parathyroid scanning agents." J Nucl Med **9**(12): 643-644.

Kannan, S., Milas, M., Neumann, D., Parikh, R. T., Siperstein, A. and Licata, A. (2014). "Parathyroid nuclear scan. A focused review on the technical and biological factors affecting its outcome." Clin Cases Miner Bone Metab **11**(1): 25-30.

Kappadath, S. C. (2011). "Effects of voxel size and iterative reconstruction parameters on the spatial resolution of 99mTc SPECT/CT." J Appl Clin Med Phys **12**(4): 3459.

Karam, M., Dansereau, R. N., Dolce, C. J., Feustel, P. J. and Robinson, L. W. (2005). "Increasing the radiochemical purity of 99mTc sestamibi commercial preparations results in improved sensitivity of dual-phase planar parathyroid scintigraphy." Nucl Med Commun **26**(12): 1093-1098.

Kettle, A. G. and O'Doherty, M. J. (2006). "Parathyroid imaging: how good is it and how should it be done?" Semin Nucl Med **36**(3): 206-211.

Klingensmith, W. C., Koo, P. J., Summerlin, A., Fehrenbach, B. W., Karki, R., Shulman, B. C., Raeburn, C. D. and McIntyre, R. C. (2013). "Parathyroid Imaging: The Importance of Pinhole Collimation with Both Single- and Dual-Tracer Acquisition." Journal of Nuclear Medicine Technology.

Knesaurek, K. (1987). "Comparison of 360 degrees and 180 degrees data collection in SPECT imaging." Phys Med Biol **32**(11): 1445-1456.

Knesaurek, K., King, M. A., Glick, S. J. and Penney, B. C. (1989). "Investigation of causes of geometric distortion in 180 degrees and 360 degrees angular sampling in SPECT." J Nucl Med **30**(10): 1666-1675.

Kobayashi, H., Momose, M., Kanaya, S., Kondo, C., Kusakabe, K. and Mitsuhashi, N. (2003). "Scatter correction by two-window method standardizes cardiac I-123 MIBG uptake in various gamma camera systems." Ann Nucl Med **17**(4): 309-313.

Krakauer, M., Wieslander, B., Myschetzky, P. S., Lundstrom, A., Bacher, T., Sorensen, C. H., Trolle, W., Nygaard, B. and Bennedbaek, F. N. (2015). "A Prospective Comparative Study of Parathyroid Dual-Phase Scintigraphy, Dual-Isotope Subtraction Scintigraphy, 4D-CT, and Ultrasonography in Primary Hyperparathyroidism." Clin Nucl Med.

Krausz, Y., Bettman, L., Guralnik, L., Yosilevsky, G., Keidar, Z., Bar-Shalom, R., Even-Sapir, E., Chisin, R. and Israel, O. (2006). "Technetium-99m-MIBI SPECT/CT in primary hyperparathyroidism." World J Surg **30**(1): 76-83.

Krausz, Y., Shiloni, E., Bocher, M., Agranovicz, S., Manos, B. and Chisin, R. (2001). "Diagnostic dilemmas in parathyroid scintigraphy." Clin Nucl Med **26**(12): 997-1001.

Lavely, W. C., Goetze, S., Friedman, K. P., Leal, J. P., Zhang, Z., Garret-Mayer, E., Dackiw, A. P., Tufano, R. P., Zeiger, M. A. and Ziessman, H. A. (2007). "Comparison of SPECT/CT, SPECT, and planar imaging with single- and dual-phase (99m)Tc-sestamibi parathyroid scintigraphy." J Nucl Med **48**(7): 1084-1089.

Lee, G. S., McKenzie, T. J., Mullan, B. P., Farley, D. R., Thompson, G. B. and Richards, M. L. (2016). "A Multimodal Imaging Protocol, (123)I/(99)Tc-Sestamibi, SPECT, and SPECT/CT, in Primary Hyperparathyroidism Adds Limited Benefit for Preoperative Localization." World J Surg **40**(3): 589-594.

Leslie, W. D., Riese, K. T., Dupont, J. O. and Peterdy, A. E. (1995). "Parathyroid adenomas without sestamibi retention." Clin Nucl Med **20**(8): 699-702.

Levine, D. S., Belzberg, A. S. and Wiseman, S. M. (2009). "Hybrid SPECT/CT imaging for primary hyperparathyroidism: case reports and pictorial review." Clin Nucl Med **34**(11): 779-784.

Links, J. M. (1996). "Simultaneous dual-radionuclide imaging: are the images trustworthy?" Eur J Nucl Med **23**(10): 1289-1291.

Links, J. M., Prince, J. L. and Gupta, S. N. (1996). "A vector Wiener filter for dual-radionuclide imaging." IEEE Trans Med Imaging **15**(5): 700-709.

Lorberboym, M., Minski, I., Macadziob, S., Nikolov, G. and Schachter, P. (2003). "Incremental diagnostic value of preoperative 99mTc-MIBI SPECT in patients with a parathyroid adenoma." J Nucl Med **44**(6): 904-908.

Macey, D. J., DeNardo, G. L., DeNardo, S. J. and Hines, H. H. (1986). "Comparison of low- and medium-energy collimators for SPECT imaging with iodine-123-labeled antibodies." J Nucl Med **27**(9): 1467-1474.

Madsen, M. T., O'Leary, D. S., Andreasen, N. C. and Kirchner, P. T. (1993). "Dual isotope brain SPECT imaging for monitoring cognitive activation: physical considerations." Nucl Med Commun **14**(5): 391-396.

Mandal, R., Muthukrishnan, A., Ferris, R. L., de Almeida, J. R. and Duvvuri, U. (2015). "Accuracy of early-phase versus dual-phase single-photon emission computed tomography/computed tomography (SPECT/CT) in the localization of Parathyroid disease." Laryngoscope.

Martin, D., Rosen, I. B. and Ichise, M. (1996). "Evaluation of single isotope technetium 99M-sestamibi in localization efficiency for hyperparathyroidism." Am J Surg **172**(6): 633-636.

Martinez-Rodriguez, I., Banzo, I., Quirce, R., Jimenez-Bonilla, J., Portilla-Quattrociocchi, H., Medina-Quiroz, P., De Arcocha, M. and Carril, J. M. (2011). "Early Planar and Early SPECT Tc-99m Sestamibi Imaging: Can It Replace the Dual-Phase Technique for the Localization of Parathyroid Adenomas by Omitting the Delayed Phase?" Clin Nucl Med **36**(9): 749-753.

Matsudaira, M., Nakajima, K., Tonami, N. and Hisada, K. (1997). "[Dual isotope SPECT with 99mTc and 123I using four-energy-window (FEW) method]." Kaku Igaku **34**(11): 1013-1020.

McBiles, M., Lambert, A. T., Cote, M. G. and Kim, S. Y. (1995). "Sestamibi parathyroid imaging." Semin Nucl Med **25**(3): 221-234.

McKeighen, R. E., Muehllehner, G. and Moyer, R. A. (1974). "Gamma camera collimator considerations for imaging 123I." J Nucl Med **15**(5): 328-331.

Mihai, R., Gleeson, F., Buley, I. D., Roskell, D. E. and Sadler, G. P. (2006). "Negative imaging studies for primary hyperparathyroidism are unavoidable: correlation of sestamibi and high-resolution ultrasound scanning with histological analysis in 150 patients." World J Surg **30**(5): 697-704.

Mihai, R., Simon, D. and Hellman, P. (2009). "Imaging for primary hyperparathyroidism--an evidence-based analysis." Langenbecks Arch Surg **394**(5): 765-784.

Minisola, S., Cipriani, C., Diacinti, D., Tartaglia, F., Scillitani, A., Pepe, J. and Scott-Coombes, D. (2016). "Imaging of the parathyroid glands in primary hyperparathyroidism." Eur J Endocrinol **174**(1): D1-8.

Moka, D., Eschner, W., Voth, E., Dietlein, M., Larena-Avellaneda, A. and Schicha, H. (2000). "Iterative reconstruction: an improvement of technetium-99m MIBI SPET for the detection of parathyroid adenomas?" Eur J Nucl Med **27**(5): 485-489.

Moka, D., Voth, E., Dietlein, M., Larena-Avellaneda, A. and Schicha, H. (2000). "Technetium 99m-MIBI-SPECT: A highly sensitive diagnostic tool for localization of parathyroid adenomas." Surgery **128**(1): 29-35.

Neumann, D. R. (1992). "Simultaneous dual-isotope SPECT imaging for the detection and characterization of parathyroid pathology." J Nucl Med **33**(1): 131-134.

Neumann, D. R., Esselstyn, C. B., Jr., Go, R. T., Wong, C. O., Rice, T. W. and Obuchowski, N. A. (1997). "Comparison of double-phase 99mTc-sestamibi with 123I-99mTc-sestamibi subtraction SPECT in hyperparathyroidism." AJR Am J Roentgenol **169**(6): 1671-1674.

Neumann, D. R., Esselstyn, C. B., Jr., Madera, A., Wong, C. O. and Lieber, M. (1998). "Parathyroid detection in secondary hyperparathyroidism with 123I/99mTc-sestamibi subtraction single photon emission computed tomography." J Clin Endocrinol Metab **83**(11): 3867-3871.

Neumann, D. R., Esselstyn, C. B., Jr. and Madera, A. M. (2000). "Sestamibi/iodine subtraction single photon emission computed tomography in reoperative secondary hyperparathyroidism." Surgery **128**(1): 22-28.

Neumann, D. R., Obuchowski, N. A. and Difilippo, F. P. (2008). "Preoperative 123I/99mTc-Sestamibi Subtraction SPECT and SPECT/CT in Primary Hyperparathyroidism." J Nucl Med **49**(12): 2012-2017.

Nichols, K. J., Tomas, M. B., Tronco, G. G., Rini, J. N., Kunjummen, B. D., Heller, K. S., Sznyter, L. A. and Palestro, C. J. (2008). "Preoperative parathyroid scintigraphic lesion localization: accuracy of various types of readings." Radiology **248**(1): 221-232.

Nichols, K. J., Tronco, G. G., Tomas, M. B., Kunjummen, B. D., Siripun, L., Rini, J. N. and Palestro, C. J. (2007). "Phantom experiments to improve parathyroid lesion detection." Med Phys **34**(12): 4792-4797.

Notghi, A., O'Brien, J., Clarke, E. A. and Thomson, W. H. (2010). "Acquiring diagnostic DaTSCAN images in claustrophobic or difficult patients using a 180 degrees configuration." Nucl Med Commun **31**(3): 217-226.

O'Connor M, K., Kemp, B., Anstett, F., Christian, P., Ficaro, E. P., Frey, E., Jacobs, M., Kritzman, J. N., Pooley, R. A. and Wilk, M. (2002). "A multicenter evaluation of commercial attenuation compensation techniques in cardiac SPECT using phantom models." J Nucl Cardiol **9**(4): 361-376.

O'Doherty, M. J. and Kettle, A. G. (2003). "Parathyroid imaging: preoperative localization." Nucl Med Commun **24**(2): 125-131.

O'Doherty, M. J., Kettle, A. G., Wells, P., Collins, R. E. and Coakley, A. J. (1992). "Parathyroid imaging with technetium-99m-sestamibi: preoperative localization and tissue uptake studies." J Nucl Med **33**(3): 313-318.

Ogasawara, K., Hashimoto, J., Ogawa, K., Kubo, A., Motomura, N., Hasegawa, H. and Ichihara, T. (1998). "Simultaneous acquisition of iodine-123 emission and technetium-99m transmission data for quantitative brain single-photon emission tomographic imaging." Eur J Nucl Med **25**(11): 1537-1544.

Ogawa, K., Harata, Y., Ichihara, T., Kubo, A. and Hashimoto, S. (1991). "A practical method for position-dependent Compton-scatter correction in single photon emission CT." IEEE Trans Med Imaging **10**(3): 408-412.

Onkendi, E. O., Richards, M. L., Thompson, G. B., Farley, D. R., Peller, P. J. and Grant, C. S. (2012). "Thyroid cancer detection with dual-isotope parathyroid scintigraphy in primary hyperparathyroidism." Ann Surg Oncol **19**(5): 1446-1452.

Palestro, C. J., Tomas, M. B. and Tronco, G. G. (2005). "Radionuclide imaging of the parathyroid glands." Semin Nucl Med **35**(4): 266-276.

Papathanassiou, D., Flament, J. B., Pochart, J. M., Patey, M., Marty, H., Liehn, J. C. and Schvartz, C. (2008). "SPECT/CT in localization of parathyroid adenoma or hyperplasia in patients with previous neck surgery." Clin Nucl Med **33**(6): 394-397.

Pata, G., Casella, C., Besuzio, S., Mittempergher, F. and Salerni, B. (2010). "Clinical appraisal of 99m technetium-sestamibi SPECT/CT compared to conventional SPECT in patients with primary hyperparathyroidism and concomitant nodular goiter." Thyroid **20**(10): 1121-1127.

Pata, G., Casella, C., Magri, G. C., Lucchini, S., Panarotto, M. B., Crea, N., Giubbini, R. and Salerni, B. (2011). "Financial and clinical implications of low-energy CT combined with 99m Technetium-sestamibi SPECT for primary hyperparathyroidism." Ann Surg Oncol **18**(9): 2555-2563.

Peeler, B. B., Martin, W. H., Sandler, M. P. and Goldstein, R. E. (1997). "Sestamibi parathyroid scanning and preoperative localization studies for patients with recurrent/persistent hyperparathyroidism or significant comorbid conditions: development of an optimal localization strategy." Am Surg **63**(1): 37-46.

Peterson, T. E. and Furenlid, L. R. (2011). "SPECT detectors: the Anger Camera and beyond." Phys Med Biol **56**(17): R145-182.

Phitayakorn, R. and McHenry, C. R. (2006). "Incidence and location of ectopic abnormal parathyroid glands." Am J Surg **191**(3): 418-423.

Pons, F., Torregrosa, J. V. and Fuster, D. (2003). "Biological factors influencing parathyroid localization." Nucl Med Commun **24**(2): 121-124.

Prommegger, R., Wimmer, G., Profanter, C., Sauper, T., Sieb, M., Kovacs, P., Bale, R., Putzer, D., Gabriel, M. and Margreiter, R. (2009). "Virtual neck exploration: a new method for localizing abnormal parathyroid glands." Ann Surg **250**(5): 761-765.

Ritt, P., Vija, H., Hornegger, J. and Kuwert, T. (2011). "Absolute quantification in SPECT." Eur J Nucl Med Mol Imaging **38 Suppl 1**: S69-77.

Rossitch, J. C., Cowan, R. J., Ellis, M. B. and Griffith, R. F. (1995). "Tc-99m sestamibi for detection of parathyroid adenoma. Comparison of single and dual tracer imaging." Clin Nucl Med **20**(3): 220-221.

Rubello, D., Saladini, G., Casara, D., Borsato, N., Toniato, A., Piotto, A., Bernante, P. and Pelizzo, M. R. (2000). "Parathyroid imaging with pertechnetate plus perchlorate/MIBI subtraction scintigraphy: a fast and effective technique." Clin Nucl Med **25**(7): 527-531.

Ruf, J., Seehofer, D., Denecke, T., Stelter, L., Rayes, N., Felix, R. and Amthauer, H. (2007). "Impact of image fusion and attenuation correction by SPECT-CT on the scintigraphic detection of parathyroid adenomas." Nuklearmedizin **46**(1): 15-21.

Ryhanen, E. M., Schildt, J., Heiskanen, I., Vaisanen, M., Ahonen, A., Loyttyniemi, E., Schalin-Jantti, C. and Valimaki, M. J. (2015). "(99m)Technetium Sestamibi-(123)Iodine Scintigraphy Is More Accurate Than (99m)Technetium Sestamibi Alone before Surgery for Primary Hyperparathyroidism." Int J Mol Imaging **2015**: 391625.

Schachter, P. P., Issa, N., Shimonov, M., Czerniak, A. and Lorberboym, M. (2004). "Early, postinjection MIBI-SPECT as the only preoperative localizing study for minimally invasive parathyroidectomy." Arch Surg **139**(4): 433-437.

Schalin-Jantti, C., Ryhanen, E., Heiskanen, I., Seppanen, M., Arola, J., Schildt, J., Vaisanen, M., Nelimarkka, L., Lisinen, I., Aalto, V., Nuutila, P. and Valimaki, M. J. (2013). "Planar scintigraphy with 123I/99mTc-sestamibi, 99mTc-sestamibi SPECT/CT, 11C-methionine PET/CT, or selective venous sampling before reoperation of primary hyperparathyroidism?" J Nucl Med **54**(5): 739-747.

Seret, A., Nguyen, D. and Bernard, C. (2012). "Quantitative capabilities of four state-of-the-art SPECT-CT cameras." EJNMMI Res **2**(1): 45.

Serra, A., Bolasco, P., Satta, L., Nicolosi, A., Uccheddu, A. and Piga, M. (2006). "Role of SPECT/CT in the preoperative assessment of hyperparathyroid patients." Radiol Med (Torino) **111**(7): 999-1008.

Sharma, J., Mazzaglia, P., Milas, M., Berber, E., Schuster, D. M., Halkar, R., Siperstein, A. and Weber, C. J. (2006). "Radionuclide imaging for hyperparathyroidism (HPT): which is the best technetium-99m sestamibi modality?" Surgery **140**(6): 856-863; discussion 863-855.

Shcherbinin, S., Chamoiseau, S. and Celler, A. (2012). "Quantitative image reconstruction for dual-isotope parathyroid SPECT/CT: phantom experiments and sample patient studies." Phys Med Biol **57**(15): 4755-4769.

Shindo, M. L., Rosenthal, J. M. and Lee, T. (2008). "Minimally invasive parathyroidectomy using local anesthesia with intravenous sedation and targeted approaches." Otolaryngol Head Neck Surg **138**(3): 381-387.

Skretting, A. and Aas, M. (1977). "A computer algorithm for triple radionuclide subtraction studies applied for preoperative localization of enlarged parathyroid glands." Eur J Nucl Med **2**(4): 239-245.

Slater, A. and Gleeson, F. V. (2005). "Increased sensitivity and confidence of SPECT over planar imaging in dual-phase sestamibi for parathyroid adenoma detection." Clin Nucl Med **30**(1): 1-3.

Small, A. D., Prosser, J., Motherwell, D. W., McCurrach, G. M., Fletcher, A. M. and Martin, W. (2006). "Downscatter correction and choice of collimator in 123I imaging." Phys Med Biol **51**(17): N307-311.

Swanson, T. W., Chan, S. K., Jones, S. J., Bugis, S., Irvine, R., Belzberg, A., Levine, D. and Wiseman, S. M. (2010). "Determinants of Tc-99m sestamibi SPECT scan sensitivity in primary hyperparathyroidism." Am J Surg **199**(5): 614-620.

Taieb, D., Hassad, R., Sebag, F., Colavolpe, C., Guedj, E., Hindie, E., Henry, J. F. and Mundler, O. (2007). "Tomoscintigraphy improves the determination of the embryologic origin of parathyroid adenomas, especially in apparently inferior glands: imaging features and surgical implications." J Nucl Med Technol **35**(3): 135-139.

Taieb, D., Hindie, E., Grassetto, G., Colletti, P. M. and Rubello, D. (2012). "Parathyroid scintigraphy: when, how, and why? A concise systematic review." Clin Nucl Med **37**(6): 568-574.

Taieb, D., Urena-Torres, P., Zanotti-Fregonara, P., Rubello, D., Ferretti, A., Henter, I., Henry, J. F., Schiavi, F., Opocher, G., Blickman, J. G., Colletti, P. M. and Hindie, E. (2013). "Parathyroid Scintigraphy in Renal Hyperparathyroidism: The Added Diagnostic Value of SPECT and SPECT/CT." Clin Nucl Med **38**(8): 630-635.

Taillefer, R., Boucher, Y., Potvin, C. and Lambert, R. (1992). "Detection and localization of parathyroid adenomas in patients with hyperparathyroidism using a single radionuclide imaging procedure with technetium-99m-sestamibi (double-phase study)." J Nucl Med **33**(10): 1801-1807.

Taubman, M. L., Goldfarb, M. and Lew, J. I. (2011). "Role of SPECT and SPECT/CT in the Surgical Treatment of Primary Hyperparathyroidism." Int J Mol Imaging **2011**: 141593.

Thomas, D. L., Bartel, T., Menda, Y., Howe, J., Graham, M. M. and Juweid, M. E. (2009). "Single photon emission computed tomography (SPECT) should be routinely performed for the detection of parathyroid abnormalities utilizing technetium-99m sestamibi parathyroid scintigraphy." Clin Nucl Med **34**(10): 651-655.

Tomas, M. B., Pugliese, P. V., Tronco, G. G., Love, C., Palestro, C. J. and Nichols, K. J. (2008). "Pinhole versus parallel-hole collimators for parathyroid imaging: an intraindividual comparison." J Nucl Med Technol **36**(4): 189-194.

Townsend, D. W. (2008). "Multimodality imaging of structure and function." Phys Med Biol **53**(4): R1-R39.

Tunninen, V., Varjo, P. and Kauppinen, T. (2016). "Towards harmonization in parathyroid scintigraphy in Finland – A seven year follow-up study." EJNMMI **43**(Suppl 2).

Udelsman, R., Lin, Z. and Donovan, P. (2011). "The superiority of minimally invasive parathyroidectomy based on 1650 consecutive patients with primary hyperparathyroidism." Ann Surg **253**(3): 585-591.

Wakamatsu, H., Noguchi, S., Yamashita, H., Tamura, S., Jinnouchi, S., Nagamachi, S. and Futami, S. (2003). "Parathyroid scintigraphy with 99mTc-MIBI and 123I subtraction: a comparison with magnetic resonance imaging and ultrasonography." Nucl Med Commun **24**(7): 755-762.

van Hoorn, R. A., Vriens, D., Postema, J. W., Arens, A. I., Pfestroff, A., Oyen, W. J. and Gotthardt, M. (2013). "The influence of SPECT reconstruction algorithms on image quality and diagnostic accuracy in phantom measurements and 99mTc-sestamibi parathyroid scintigraphy." Nucl Med Commun.

Vandenberghe, S., D'Asseler, Y., Van de Walle, R., Kauppinen, T., Koole, M., Bouwens, L., Van Laere, K., Lemahieu, I. and Dierckx, R. A. (2001). "Iterative reconstruction algorithms in nuclear medicine." Comput Med Imaging Graph **25**(2): 105-111.

Weber, C. J., Vansant, J., Alazraki, N., Christy, J., Watts, N., Phillips, L. S., Mansour, K., Sewell, W. and McGarity, W. C. (1993). "Value of technetium 99m sestamibi iodine 123 imaging in reoperative parathyroid surgery." Surgery **114**(6): 1011-1018.

Wei, J. P., Burke, G. J. and Mansberger, A. R., Jr. (1992). "Prospective evaluation of the efficacy of technetium 99m sestamibi and iodine 123 radionuclide imaging of abnormal parathyroid glands." Surgery **112**(6): 1111-1116; discussion 1116-1117.

Wei, J. P., Burke, G. J. and Mansberger, A. R., Jr. (1994). "Preoperative imaging of abnormal parathyroid glands in patients with hyperparathyroid disease using combination Tc-99m-pertechnetate and Tc-99m-sestamibi radionuclide scans." Ann Surg **219**(5): 568-572; discussion 572-563.

Verberne, H. J., Feenstra, C., de Jong, W. M., Somsen, G. A., van Eck-Smit, B. L. and Busemann Sokole, E. (2005). "Influence of collimator choice and simulated clinical conditions on 123I-MIBG heart/mediastinum ratios: a phantom study." Eur J Nucl Med Mol Imaging **32**(9): 1100-1107.

Whitcroft, K. L. and Sharma, A. (2014). "Sestamibi scintigraphy for parathyroid localisation: a reminder of the dangers of false positives." BMJ Case Rep **2014**.

Wimmer, G., Bale, R., Kovacs, P., Gabriel, M., Putzer, D., Sauper, T., Sieb, M., Profanter, C., Margreiter, R. and Prommegger, R. (2008). "Virtual neck exploration in patients with hyperparathyroidism and former cervical operations." Langenbecks Arch Surg **393**(5): 687-692.

Wimmer, G., Profanter, C., Kovacs, P., Sieb, M., Gabriel, M., Putzer, D., Bale, R., Margreiter, R. and Prommegger, R. (2009). "CT-MIBI-SPECT image fusion predicts multiglandular disease in hyperparathyroidism." Langenbecks Arch Surg.

Witteveen, J. E., Kievit, J., Stokkel, M. P., Morreau, H., Romijn, J. A. and Hamdy, N. A. (2010). "Limitations of Tc99m-MIBI-SPECT imaging scans in persistent primary hyperparathyroidism." World J Surg **35**(1): 128-139.

Wong, K. K., Fig, L. M., Gross, M. D. and Dwamena, B. A. (2015). "Parathyroid adenoma localization with 99mTc-sestamibi SPECT/CT: a meta-analysis." Nucl Med Commun **36**(4): 363-375.

Yang, J. T., Yamamoto, K., Sadato, N., Tsuchida, T., Takahashi, N., Hayashi, N., Yonekura, Y. and Ishii, Y. (1997). "Clinical value of triple-energy window scatter correction in simultaneous dual-isotope single-photon emission tomography with 123I-BMIPP and 201Tl." Eur J Nucl Med **24**(9): 1099-1106.

Young, A. E., Gaunt, J. I., Croft, D. N., Collins, R. E., Wells, C. P. and Coakley, A. J. (1983). "Location of parathyroid adenomas by thallium-201 and technetium-99m subtraction scanning." Br Med J (Clin Res Ed) **286**(6375): 1384-1386.

Zwas, S. T., Czerniak, A., Boruchowsky, S., Avigad, I. and Wolfstein, I. (1987). "Preoperative parathyroid localization by superimposed iodine-131 toluidine blue and technetium-99m pertechnetate imaging." J Nucl Med **28**(3): 298-307.

Original Publications

Publication I

Tunninen V, Kauppinen T, Eskola H, Koskinen MO. Parathyroid scintigraphy protocols in Finland in 2010. Results of the query and current status. Nuklearmedizin. 2010;49(5):187-94.

Parathyroid scintigraphy protocols in Finland in 2010

Results of the query and current status

V. Tunninen[1]; T. Kauppinen[2]; H. Eskola[3]; M.O. Koskinen[4]
[1]The Department of Nuclear Medicine, Satakunta Central Hospital, Pori, Finland; [2]HUS Helsinki Medical Imaging Centre, Helsinki University Hospital, Finland; [3]The Department of Biomedical Engineering, Tampere University of Technology, Finland; [4]Medical Imaging Centre, Tampere University Hospital, Finland

Keywords
Hyperparathyroidism, parathyroid scintigraphy, ^{99m}Tc-sestamibi, iodine-123, numerical data

Summary
The goal of this study was to describe current clinical parathyroid scintigraphy (PS) protocols in Finland. Methods: All departments of nuclear medicine in Finland were contacted, and instructions regarding PS were requested. Results: Instructions regarding PS were received from all of the departments that perform PS (n = 19). Seven hundred and sixty-nine PS studies were performed in 2009 (between 7 and 209 per hospital). Three methods of PS were used. The dual-phase method with ^{99m}Tc-sestamibi is used in seven hospitals, the dual-tracer method with ^{123}I/^{99m}Tc-sestamibi in eleven, and $^{99m}TcO_4$/^{99m}Tc-sestamibi in one hospital. The activities of ^{99m}Tc-sestamibi, ^{123}I and $^{99m}TcO_4$ were 150–800 MBq, 10–30 MBq and 50 MBq, respectively. The anterior image with parallel-hole collimators, the anterior image with pinhole collimator, the oblique angles with pinhole collimator, SPECT and hybrid CT with SPECT were acquired in 84%, 26%, 16%, 63%, and 42% of the hospitals, respectively. Because the imaging techniques were combined, one to four acquisitions were performed per patient. Scatter and attenuation correction were used in five protocols. A correction for crosstalk of ^{123}I and ^{99m}Tc gamma energies was not used, but the amount of crosstalk was decreased by using narrow or asymmetric energy windows in all dual isotope protocols. Conclusion: 19 hospitals used 18 different study protocols. Thus, significant variability exists in the current practice of PS in Finland. The protocols should be tested with known phantoms to determine any differences in sensitivities for detecting small active structures. Further studies with phantoms are needed to determine the optimal imaging techniques. The results of these phantom studies will provide guidelines for proposing national recommendations for PS.

Schlüsselwörter
Hyperparathyroidismus, Nebenschilddrüsen-Szintigraphie, ^{99m}Tc-Sestamibi, Iod-123, numerische Daten

Zusammenfassung
Das Ziel dieser Studie war die Beschreibung aktueller klinischer Protokolle für die Nebenschilddrüsen (NSD)-Szintigraphie in Finnland. Methoden: Alle nuklearmedizinischen Abteilungen in Finnland wurden angeschrieben und um die Vorschriften für die NSD-Szintigraphie gebeten. Ergebnisse: Wir erhielten die Vorschriften aller Abteilungen, die NSD-Szintigraphien durchführen (n = 19). Im Jahr 2009 erfolgten 769 szintigraphische NSD-Untersuchungen (7 bis 209 je Krankenhaus). Drei Methoden wurden für die NSD-Szintigraphie verwendet. Die Dual-Phasen-Methode mit ^{99m}Tc-Sestamibi wird in sieben Krankenhäusern eingesetzt, die Doppelnuklid-Methode mit ^{123}I/^{99m}Tc-Sestamibi in elf und mit $^{99m}TcO_4$/^{99m}Tc-Sestamibi wird in einer Klinik gearbeitet. Die Aktivitäten von ^{99m}Tc-Sestamibi, ^{123}I bzw. $^{99m}TcO_4$ betrugen 150–800 MBq, 10–30 MBq und 50 MBq. Aufnahmen von vorne mit Parallelloch-Kollimatoren oder mit dem Pinhole-Kollimator, Schrägaufnahmen mit dem Pinhole-Kollimator, Aufnahmen mit SPECT und CT/SPECT-Hybridscanner wurden in 84%, 26%, 16%, 63% bzw. 42% der Kliniken akquiriert. Da die Methoden kombiniert wurden, erfolgten je Patient ein bis vier Datenakquisitionen. In fünf Protokollen wurde nach Streuung und Abschwächung korrigiert. Eine Korrektur der Überlagerung von ^{123}I- und ^{99m}Tc-Gammastrahlungen fand nicht statt, jedoch wurde das Ausmaß der Überlagerungen dadurch reduziert, dass man bei allen Doppelnuklid-Protokollen enge oder asymmetrische Energiefenster verwendete. Schlussfolgerung: In 19 Krankenhäusern kamen 18 verschiedene Studienprotokolle zum Einsatz. In der aktuellen Praxis der NSD-Szintigraphie besteht daher in Finnland eine signifikante Variabilität. Die Protokolle sollten an bekannten Phantomen getestet werden, um alle Sensitivitätsunterschiede bei der Darstellung kleiner aktiver Strukturen aufzudecken. Weitere Studien an Phantomen sind erforderlich, um die optimale Bildtechnik zu definieren. Die Ergebnisse dieser Phantomstudien ermöglichen es, Richtlinien für nationale Empfehlungen für die NSD-Szintigraphie zu erstellen.

Correspondence to:
Virpi Tunninen, medical physicist
The department of nuclear medicine
Satakunta Central Hospital, Pori, Finland
Tel. +358/(0)2/627 73 66; +358/(0)2/627 73 70
E-mail: virpi.tunninen@satshp.fi

Parathyreoidale Szintigraphieprotokolle in Finnland im Jahr 2010 – Ergebnisse einer Umfrage und aktueller Stand
Nuklearmedizin 2010; 49: 187–194
doi:10.3413/Nukmed-0311-10-04
received: April 28, 2010
accepted in revised form: July 23, 2010
prepublished online: August 25, 2010

^{99m}Tc-sestamibi was first introduced as a parathyroid imaging agent in 1989 (9). It is least as effective as ^{201}Tl in parathyroid localisation and quickly replaced ^{201}Tl because of its

- higher target-to-background ratio,
- better imaging characteristics with ^{99m}Tc and
- favourable dosimetry (29).

The problem with ^{99m}Tc-sestamibi is that it is a non-specific tracer for parathyroid tissues and is taken up by adjacent thyroid tissue. Two methods have been used to overcome this problem:

- the dual-phase method and
- the dual-tracer method.

The dual-phase method is based on the different washout kinetics of the tracer between the normal thyroid and the abnormal parathyroid tissue (37). It requires only a single radionuclide and a comparison of the two images acquired ~15 and 150 minutes after the injection. However, any interference with the assumed difference in kinetics, such as the rapid washout of the abnormal parathyroid tissue, limits the efficacy of detection of parathyroid disease with dual-phase ^{99m}Tc-sestamibi scintigraphy (25). Other limiting factors such as vitamin D deficiency have also been proposed (34).

In the dual-tracer method, ^{123}I or ^{99m}Tc-pertechnetate is used simultaneously with ^{99m}Tc-MIBI. The ^{123}I or ^{99m}Tc-pertechnetate is taken up by the thyroid gland only. The thyroid image is subtracted from the ^{99m}Tc-sestamibi image. This process helps to visualise the parathyroid tissue.

With ^{99m}Tc-pertechnetate, the thyroid image must be acquired before the ^{99m}Tc-sestamibi is injected and without moving the patient. Sequential imaging has the risk of motion artefacts and thus problems with alignment. With ^{123}I, simultaneous imaging is possible, but using two isotopes brings new problems such as the cross-over of two photopeaks.

Whichever method is used, several techniques can be selected for the acquisition (e. g., planar acquisitions with parallel-hole or pinhole collimators, single photon emission computed tomography (SPECT) or computed tomography (CT)). Within each acquisition technique, several choices must be made. The timing of the acquisition, the acquisition length, the collimators used, the energy window placements, the various corrections and the processing protocols are examples of these choices.

Few direct comparisons exist between the different imaging techniques, and little evidence supports the superiority of one over another. Thus, the optimal protocol for parathyroid scintigraphy PS with ^{99m}Tc-MIBI is still not clear. As a result, many different protocols are in clinical use today, and these protocols have variable sensitivities ranging from 34% to 100% (26).

Because no national guidelines or recommendations exist for PS, variable protocols have presumably also been used in clinical practice in Finland. Variability has raised some concerns among nuclear medicine professionals, who have discussed the standardisation of the PS protocols. The first priority is the sensitivity of the study because large differences should not exist between hospitals nationally. Other important aspects are the time required for the study, the patient discomfort and the total cost of the study.

The goal of this study was to determine which methods are in current clinical use for PS in Finland and how imaging and image processing are performed in daily clinical practice. To our knowledge, this information has not previously been published for any country.

Tab. 1 Parathyroid scintigraphy protocols in Finland in 2010

method	%
dual-tracer with ^{123}I/^{99m}Tc-sestamibi	58
dual phase ^{99m}Tc-sestamibi	37
dual-tracer with $^{99m}TcO_4$/^{99m}Tc-sestamibi	5

Methods

All departments of nuclear medicine in Finland (n = 25) were contacted in September 2008, and instructions regarding clinical protocols for PS were requested. If instructions were unclear or some information was missing, the department was contacted by telephone or by email. All departments were contacted again in January 2010, and the information was updated. The results presented here were extracted from these documents. All departments in Finland performing PS took part in this survey. Therefore, we have very realistic results on the current clinical status of PS in Finland.

Results

Response

Instructions were received from all of the departments performing PS (n=19). These instructions included details regarding patient preparation, acquisition and data processing.

Methods in use

Three methods of PS are being used in Finland in 2010 (▶Tab. 1). The dual-phase method with ^{99m}Tc-sestamibi is used in 7 hospitals. The dual-tracer method with ^{123}I and ^{99m}Tc-sestamibi is used in 11 hospitals, and $^{99m}TcO_4$/^{99m}Tc-sestamibi is used in 1 hospital.

Six hospitals using dual-tracer method with ^{123}I and ^{99m}Tc-sestamibi combine this method with the dual-phase method and repeat acquisitions 2–3 hours after the ^{99m}Tc sestamibi injection.

Alternative methods have been used in two hospitals (e. g., when iodine was unavailable or if the patient had not followed instructions for medication). However, the number of alternative studies is low, and thus they are excluded from this study.

Number of studies

Seven hundred and sixty-nine parathyroid studies were performed in 2009. The number of studies varied from 7 to 209 per hospital (▶Fig. 1).

Radionuclides and activities

In the dual-phase method, the ^{99m}Tc-sestamibi activity was 740 MBq in all hospitals. In the dual-tracer method with ^{123}I/^{99m}Tc-sestamibi, the ^{99m}Tc-activity was 150–800 MBq, and the ^{123}I activity was 10–30 MBq. (Iodine was given as a capsule in 4 hospitals and as an injection in 7 hospitals). In the dual-tracer method with $^{99m}TcO_4$/^{99m}Tc-sestamibi, the ^{99m}Tc-pertechnetate activity was 50 MBq, and the ^{99m}Tc-sestamibi activity was 740 MBq.

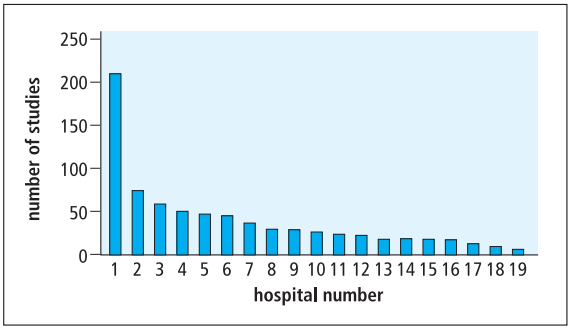

Fig. 1 The number of parathyroid scintigraphy studies in Finnish hospitals in 2009

Imaging techniques

Dual-phase method

In the dual-phase method, the early phase acquisition starts 7–15 minutes after the ^{99m}Tc-sestamibi injection. The late phase acquisition starts 1,5–4 hours after the ^{99m}Tc-sestamibi injection.

A static anterior (AP) image is acquired with parallel-hole collimator in 71% of the hospitals in both the early and the late phase. A pinhole collimator was not used at all in any hospitals that use the dual-phase protocol. SPECT is used in the early phase in 43% of the hospitals and in the late phase in 71% of the hospitals. All hospitals using SPECT in the early phase also used SPECT in the late phase. A hybrid CT with SPECT is used in 29% of the hospitals during the late phase. Altogether, 2 to 4 acquisitions are performed per patient. Imaging techniques used in hospitals using the dual-phase method are presented in ▶Figure 2a.

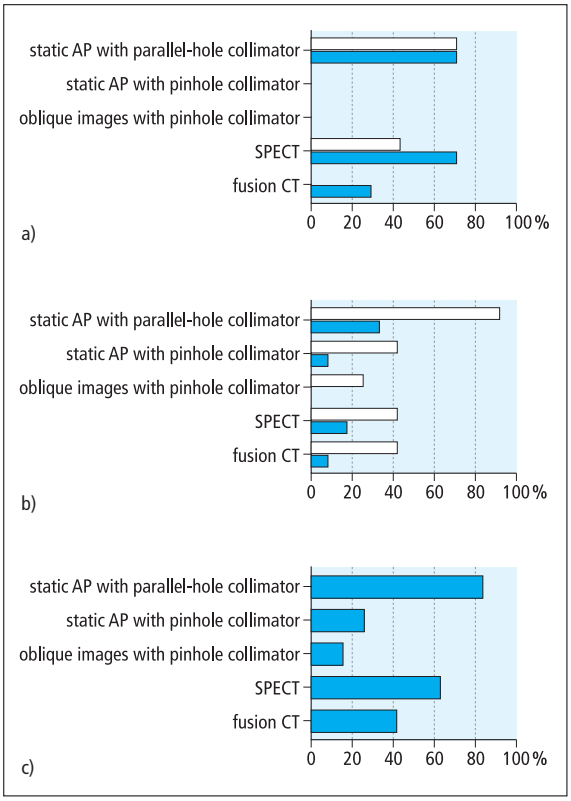

Fig. 2 Imaging techniques in hospitals used for parathyroid scintigraphy (static AP: anterior image with parallel-hole collimator; □ early phase; ■ late phase) **a)** dual-phase method with ^{99m}Tc-sestamibi **b)** dual-tracer methods_ with ^{99m}Tc-sestamibi and ^{123}I or ^{99m}Tc-pertechetate **c)** summarised for all hospitals (■)

Dual-tracer method

In the dual-tracer method, the acquisition begins 5–10 minutes after the ^{99m}Tc-sestamibi injection. The optional late phase acquisition was used in 42% of the hospitals, and it starts 2–3 hours after the ^{99m}Tc-sestamibi injection. A static AP image is acquired with parallel-hole collimator in 92% of the hospitals in the early phase and in 33% of the hospitals in the late phase. A static AP image is acquired with a pinhole collimator in 42% of the hospitals in the early phase and in 8% of the hospitals in the late phase. Oblique angles are acquired in 25% of the hospitals in the early phase and not used at all in the late phase. SPECT is used in 42% of the hospitals in the early phase and in 17% of the hospitals in the late phase. Hybrid CT with SPECT is used in 42% of the hospitals in the early phase and in 8% of the hospitals in the late phase. One to four acquisitions are performed per patient. Imaging techniques used in hospitals using the dual-phase method are presented in ▶Figure 2b.

All methods combined

If all methods are combined, the static AP image is acquired with parallel-hole collimator in 84% of the hospitals (n = 16). A static AP image is acquired with a pinhole

Tab. 2 Imaging techniques used in parathyroid scintigraphy in Finland in 2010: The dots indicate which method is used in each hospital and which acquisition techniques are used in the early and/or late phase. (The hospital numbers are the same as in Figure 1.)

DP: dual phase method; DT: dual tracer method with either iodine or technetium; AP: anterior image with parallel-hole collimator; PIN: anterior image with pinhole collimator; OBL: oblique images with a pinhole collimator; acquisitions: total number of acquisitions per patient

hospital number			11	7	2	3	9	5	17	1	18	14	16	15	12	10	8	13	6	19	4
method		DP	•	•	•	•	•	•	•												
		DT								•	•	•	•	•	•	•	•	•	•	•	•
acquisitions in the	early phase	AP	•	•		•	•		•	•	•	•	•	•	•	•	•		•	•	•
		PIN										•					•	•	•	•	
		OBL															•		•	•	
		SPECT		•	•			•			•		•	•		•		•			
		CT									•		•	•				•	•		
	late phase	AP	•	•		•	•		•	•	•			•	•						
		PIN										•									
		OBL																			
		SPECT		•	•	•	•	•		•					•						
		CT				•	•			•											
acquisitions			2	4	2	4	4	2	2	4	4	3	3	4	3	2	3	3	4	3	1

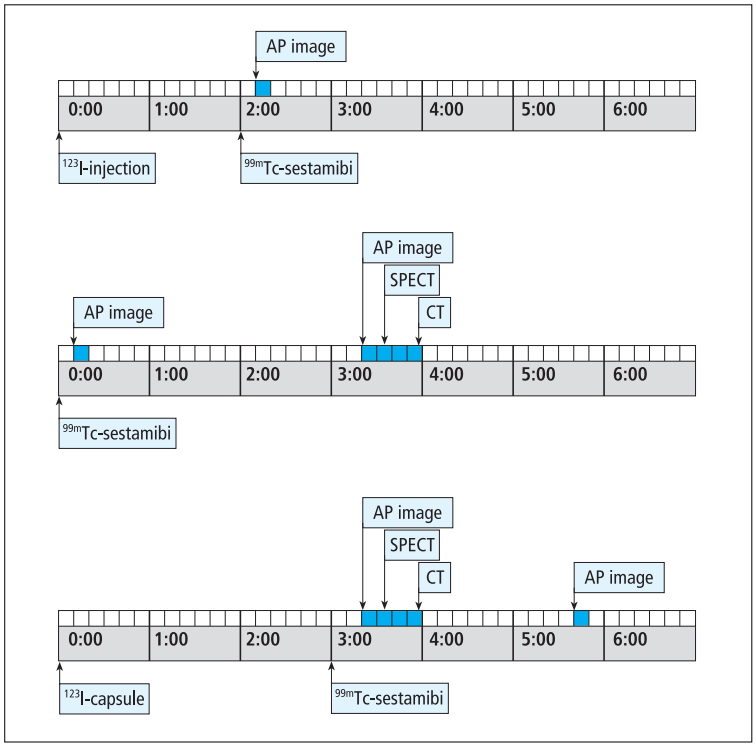

Fig. 3 Three examples of the time requirements of different parathyroid scintigraphy protocols (AP: anterior image with a parallel-hole collimator)

collimator in 26% of the hospitals (n = 5). Oblique angles are acquired in 16% of the hospitals (n = 3). SPECT is used in 63% of the hospitals (n = 12), and hybrid CT with SPECT is used in 42% of the hospitals (n = 8). The imaging techniques are summarised for all methods in ▶Figure 2c.

These imaging techniques are combined in each hospital in a variety of ways (▶Tab. 2). Examples of three different protocols are presented in ▶Figure 3. The timeline represents the time requirements for the different protocols.

Energy windows and corrections

Correction for crosstalk of the ^{123}I and ^{99m}Tc gamma photons is not used in any hospital. The amount of crosstalk to the ^{99m}Tc-window is minimised by using energy window widths of 10–16%. The amount of crosstalk to the ^{123}I-window is minimised by using energy window widths of 10–15% and an asymmetric window setting (the window centre is at 160–167 keV).

Scatter correction is used with SPECT acquisition in four hospitals using the dual-tracer method with ^{123}I and ^{99m}Tc-MIBI. CT-based attenuation correction is used in

five hospitals using the dual-tracer method with ^{123}I and ^{99m}Tc-MIBI. Scatter and/or attenuation correction is not used in the single isotope studies.

Processing protocols

In the dual-phase method, early and late planar images are displayed together. When SPECT imaging is used, SPECT images are reconstructed using iterative reconstruction algorithms, and the early and late images (i. e. transverse, coronal and sagittal slices) are displayed together. Subtraction of the late images from the early images is not used in any of the hospitals using the dual-phase method.

In the dual-tracer method, planar images of the thyroid and parathyroids are subtracted. Subtraction is performed after normalisation of the images. The normalisation is performed according to the total counts or the maximum counts per pixel in the thyroid area. The amount subtracted varies based on the visual appearance of the image, and several subtraction factors are used simultaneously. If SPECT imaging is used, the subtracted SPECT images are reconstructed using an iterative reconstruction algorithms transverse, and the coronal and sagittal slices are displayed. Subtraction of late and early images is not used in any of the hospitals using the dual-tracer method combined with the dual-phase method.

Data processing is performed mainly by medical physicists, but technologists or physicians may also be involved. Several hospitals report that data processing can be performed by any of these professionals.

Discussion

The imaging and processing protocols in Finland were chosen in each department so that a large variety exists in the protocols. We found only two clinical protocols that were identical in all aspects. As a result, 18 protocols are in use in 19 hospitals (alternative protocols are excluded).

The debate continues as to whether PS is best performed using the dual-tracer method or the dual-phase method (30). At the same time, various imaging techniques are in clinical use with both methods, and each of the techniques can be modified in several ways.

All methods (i. e., the dual-phase method or the dual-tracer method with ^{123}I or $^{99m}TcO_4$) presented in the latest European Association of Nuclear Medicine (EANM) Parathyroid Scintigraphy Guideline (18) are being used in Finland. The dual-tracer method with ^{123}I/^{99m}Tc-sestamibi is the method most often used (in 57,9% of the hospitals in Finland). This method is combined with the late phase imaging in a little less than half of

the hospitals using the dual-tracer method. The EANM guideline states that "*delayed images (2 h post-injection) are not useful and do not add to the sensitivity of the subtraction protocol*" (18). However, the opposite opinion has also been presented (35).

A great variation exists in the number of studies per hospital. Because the success rate of the visualisation of parathyroid adenomas is related to the experience of the imaging unit, keeping the standards high with a low number of studies may be challenging (3).

The activity of ^{99m}Tc-sestamibi was similar in all hospitals using the dual-phase method but varied greatly in the hospitals using the dual-tracer method. The smallest activity of ^{99m}Tc-sestamibi was 150 MBq, and other hospitals used activities between 550–800 MBq. The reference level given by the Finnish radiation safety authorities for PS is 800 MBq. Therefore, increasing the activity in some hospitals might be worth considering. The use of small activities might be related to the poor visualisation of small parathyroid nodules.

The starting time of the late phase imaging varied from 1,5 to 4 hours after the injection of the ^{99m}Tc-sestamibi. Because the accuracy of the dual-phase technique is based on the different washout kinetics of the tracer between the normal thyroid and the abnormal parathyroid tissue, timing of the acquisition has great importance on the results. Even with correct timing, using the dual-phase method may result in some abnormal parathyroids being missed because of the rapid washout of the abnormal parathyroid tissue (25).

All imaging techniques presented in the latest EANM Parathyroid Scintigraphy guideline (18) except pinhole SPECT are used in Finland. If all three methods are observed as a whole, the AP image is acquired with a parallel-hole collimator in 84% of the Finnish hospitals (n = 16), The AP image is acquired with a pinhole collimator in 26% of hospitals (n = 5), and oblique images are acquired with a pinhole in 16% of hospitals (n=3). SPECT is acquired in 63% (n = 12), and CT is acquired in 42% (n = 8) of the hospitals performing PS.

Because pinhole collimator has much better spatial resolution than parallel-hole collimator (8), we were surprised to see that pinhole collimator is used so rarely. The use of pinhole collimators increases the sensitivity of PS compared to parallel-hole collimators (2, 39) and is even preferred to SPECT (19). Pinhole-SPECT might be the optimal imaging technique for PS (6), but it is rarely possible with modern gamma cameras. The rare use of the pinhole collimator is partially explained by the instrumentation in the hospitals. Hospitals that have a pinhole collimator but do not use it have several reasons for their behaviour. The time required for the collimator change is too long. The use of the pinhole collimator is awkward, and SPECT is often preferred. Clinical experience with the new generation SPECT-CT results in a preference for planar imaging protocols. To our knowledge, no publications compare imaging protocols with a pinhole collimator and a SPECT-CT.

The use of SPECT is also surprising. Only a little more than half of the hospitals use SPECT, even though all hospitals have gamma cameras that are capable of performing SPECT imaging. In spite of a few controversial reports (7, 40), SPECT has been shown to improve sensitivity significantly compared to planar imaging with parallel-hole collimators (25, 27, 36) because it provides more information about the depth of the parathyroid tumour and its anatomic location. Planar imaging might even be completely unnecessary if SPECT is used (38).

Because SPECT-CT technology was implemented in clinical practice, this methodology was also applied in PS. This method provides precise anatomic localisation of the lesion, resulting in better planning of surgical procedures (11). SPECT-CT is superior to CT or SPECT alone in correctly detecting the exact position of abnormal parathyroid glands. It has also been shown to have significant additional value over conventional SPECT for ectopic parathyroid adenomas or with patients who had distorted neck anatomy due to previous operations (14, 22, 31, 32).

The integrated SPECT-CT also makes CT-based attenuation correction possible. The use of attenuation correction does not necessarily improve traditional SPECT, but the image contrast and the tumour-to-background ratio improve. The sensitivity of the parathyroid SPECT may also be improved (33).

Controversial reports have also been published. One paper recommends that SPECT-CT be used only for locating ectopic parathyroid glands (14). The main disadvantage of SPECT-CT is the patient's additional radiation exposure. However, the additional dose may be justified when considering the risks of repeated imaging or the risks associated with a repeated general anaesthetic and surgical intervention. The use of low-dose CT parameters can retain much of the advantages of SPECT-CT while reducing the associated radiation burden (24).

The popularity of SPECT-CT with PS is increasing as new systems are installed. The precise benefit of SPECT-CT is still a matter of debate, and a definite role for SPECT/CT has not yet been confirmed (5). However, the use of SPECT-CT is increasing in Finland. Currently in Finland, a SPECT-CT is installed in 11 of the 19 hospitals performing PS, and it is used in 8. Of those three not using it, two have had their systems installed recently, so new techniques have not yet been applied to PS.

Although SPECT and SPECT-CT imaging are becoming very helpful, they cannot replace the standard planar and pinhole protocols that are still essential for optimal resolution in the thyroid bed region and for correct diagnoses (18).

When the dual-tracer method with ^{123}I is used, the crosstalk between the two radionuclides and the septal penetration of high-energy photons of ^{123}I should be tested before clinical use (12, 20, 21). Dedicated crosstalk correction methods were not used in any hospital using the dual-tracer method with ^{123}I, but the amount of crosstalk was minimised with narrow and/or asymmetric energy windows. Pinhole collimators are useful in part because they do not suffer from septal penetration problems (8).

Imaging and processing protocols in Finland have been chosen in each department, resulting in a large variety in protocols. One to four acquisitions are performed for each patient with various imaging techniques because building a clinical para-

thyroid study protocol can be very confusing, and conflicting reports are published on sensitivity figures of various methods and imaging techniques. Although the sensitivity of PS may be improved by adopting a variety of imaging strategies (1, 23, 35), implementing various strategies increases the acquisition time and thus increases the cost of the study and the discomfort for the patient. To find the optimal clinical protocol, extensive technical phantom studies are needed.

Surprisingly, the technical details of PS have not been thoroughly studied. To our knowledge, only six published studies exist that use any kind of phantoms in parathyroid imaging optimisation (4, 10, 13, 15, 17, 28). Only two of these use the dual-tracer method using ^{99m}Tc and ^{123}I (10, 17). An adequate comparison of various imaging techniques using phantoms is indispensable for reaching any kind of consensus and harmonisation of protocols.

In the meantime, existing protocols should be tested with known phantoms to find differences in the ability to accurately show and locate adenoma-like structures of various sizes and activities. Thus, a need exists for external quality assurance by independent outside observers (16). We are planning to carry out a national quality assurance project of PS in co-operation with the Finnish Society of Nuclear Medicine. As stated in EU-legislation concerning clinical audit, building a national good practice is the first step to harmonisation.

Conclusion

The optimal technical aspects for ^{99m}Tc-sestamibi parathyroid scintigraphy are still not clear. As a result, many different methodologies are in clinical use today. This study showed that significant variability exists in the methods and imaging techniques of PS in Finland.

The imaging techniques must be optimised to reach the highest sensitivity possible and to minimise the time required for the study, the patient discomfort and the total cost of the study. Further studies with phantoms are needed. The results of the phantom studies will provide guidelines for proposing national recommendations for parathyroid scintigraphy .

Acknowledgement

This study was supported by The Finnish Society of Nuclear Medicine and the Finnish Cultural Foundation/Satakunta Regional Fund.

Conflict of interest

The authors declare, that there is no conflict of interest.

References

1. Ansquer C, Mirallie E, Carlier T et al. Preoperative localization of parathyroid lesions. Value of ^{99m}Tc-MIBI tomography and factors influencing detection. Nuklearmedizin 2008; 47: 158–162.
2. Arveschoug AK, Bertelsen H, Vammen B. Presurgical localization of abnormal parathyroid glands using a single injection of ^{99m}Tc-sestamibi: comparison of high-resolution parallel-hole and pinhole collimators, and interobserver and intraobserver variation. Clin Nucl Med 2002; 27: 249–254.
3. Bilezikian JP, Potts JT Jr, Fuleihan Gel H et al. Summary statement from a workshop on asymptomatic primary hyperparathyroidism: a perspective for the 21st century. J Clin Endocrinol Metab 2002; 87: 5353–5361.
4. Brownless SM, Gimlette TM. Comparison of techniques for thallium-201-technetium-99m parathyroid imaging. Br J Radiol 1989; 62: 532–535.
5. Buck AK, Nekolla S, Ziegler S et al. SPECT/CT. J Nucl Med 2008; 49: 1305–1319.
6. Carlier T, Oudoux A, Mirallie E et al. ^{99m}Tc-MIBI pinhole SPECT in primary hyperparathyroidism: comparison with conventional SPECT, planar scintigraphy and ultrasonography. Eur J Nucl Med Mol Imaging 2008; 35: 637–643.
7. Chen CC, Holder LE, Scovill WA et al. Comparison of parathyroid imaging with technetium-99m-pertechnetate/sestamibi subtraction, double-phase technetium-99m-sestamibi and technetium-99m-sestamibi SPECT. J Nucl Med 1997; 38: 834–839.
8. Cherry SR, Sorenson JA, Phelps ME. Physics in nuclear medicine. 3rd ed. Saunders 2003.
9. Coakley AJ, Kettle AG, Wells CP et al. ^{99m}Tc sestamibi – a new agent for parathyroid imaging. Nucl Med Commun 1989; 10: 791–794.
10. Dontu VS, Kettle AG, O'Doherty MJ, Coakley AJ. Optimization of parathyroid imaging by simultaneous dual energy planar and single photon emission tomography. Nucl Med Commun 2004; 25: 1089–1093.
11. Even-Sapir E, Keidar Z, Sachs J et al. The new technology of combined transmission and emission tomography in evaluation of endocrine neoplasms. J Nucl Med 2001; 42: 998–1004.
12. Fleming JS, Alaamer AS. Influence of collimator characteristics on quantification in SPECT. J Nucl Med 1996; 37: 1832–1836.
13. Fujii H, Iwasaki R, Ogawa K et al. Evaluation of parathyroid imaging methods with ^{99m}Tc-MIBI--the comparison of planar images obtained using a pinhole collimator and a parallel-hole collimator. Kaku Igaku 1999; 36: 425–433.
14. Gayed IW, Kim EE, Broussard WF et al. The value of ^{99m}Tc-sestamibi SPECT/CT over conventional SPECT in the evaluation of parathyroid adenomas or hyperplasia. J Nucl Med 2005; 46: 248–252.
15. Gimlette TM, Brownless SM, Taylor WH et al. Limits to parathyroid imaging with thallium-201 confirmed by tissue uptake and phantom studies. J Nucl Med 1986; 27: 1262–1265.
16. Heikkinen JO, Kuikka JT, Ahonen AK, Rautio PJ. Quality of dynamic radionuclide renal imaging: multicentre evaluation using a functional renal phantom. Nucl Med Commun 2001; 22: 987–995.
17. Hindie E, Melliere D, Jeanguillaume C et al. Parathyroid imaging using simultaneous double-window recording of technetium-99m-sestamibi and iodine-123. J Nucl Med 1998; 39: 1100–1105.
18. Hindie E, Ugur O, Fuster D et al. 2009 EANM parathyroid guidelines. Eur J Nucl Med Mol Imaging 2009; 36: 1201–1216.
19. Ho Shon IA, Yan W, Roach PJ et al. Comparison of pinhole and SPECT 99mTc-MIBI imaging in primary hyperparathyroidism. Nucl Med Commun 2008; 29: 949–955.
20. Inoue Y, Shirouzu I, Machida T et al. Physical characteristics of low and medium energy collimators for 123I imaging and simultaneous dual-isotope imaging. Nucl Med Commun 2003; 24: 1195–1202.
21. Ivanovic M, Weber DA, Loncaric S, Franceschi D. Feasibility of dual radionuclide brain imaging with I-123 and Tc-99m. Med Phys 1994; 21: 667–674.
22. Krausz Y, Bettman L, Guralnik L et al. Technetium-99m-MIBI SPECT/CT in primary hyperparathyroidism. World J Surg 2006; 30: 76–83.
23. Lavely WC, Goetze S, Friedman KP et al. Comparison of SPECT/CT, SPECT, and planar imaging with single- and dual-phase ^{99m}Tc-sestamibi parathyroid scintigraphy. J Nucl Med 2007; 48: 1084–1089.
24. Levine DS, Belzberg AS, Wiseman SM. Hybrid SPECT/CT imaging for primary hyperparathyroidism: case reports and pictorial review. Clin Nucl Med 2009; 34: 779–784.
25. Lorberboym M, Minski I, Macadziob S et al. Incremental diagnostic value of preoperative ^{99m}Tc-MIBI SPECT in patients with a parathyroid adenoma. J Nucl Med 2003; 44: 904–908.
26. Mihai R, Simon D, Hellman P. Imaging for primary hyperparathyroidism--an evidence-based analysis. Langenbecks Arch Surg 2009; 394: 765–784.
27. Moka D, Voth E, Dietlein M et al. Technetium 99m-MIBI-SPECT: A highly sensitive diagnostic tool for localization of parathyroid adenomas. Surgery 2000; 128: 29–35.
28. Nichols KJ, Tronco GG, Tomas MB et al. Phantom experiments to improve parathyroid lesion detection. Med Phys 2007; 34: 4792–4797.
29. O'Doherty MJ, Kettle AG, Wells P et al. Parathyroid imaging with technetium-99m-sestamibi: preoperative localization and tissue uptake studies. J Nucl Med 1992; 33: 313–318.
30. O'Doherty MJ, Kettle AG. Parathyroid imaging: preoperative localization. Nucl Med Commun 2003; 24: 125–131.
31. Papathanassiou D, Flament JB, Pochart JM et al. SPECT/CT in localization of parathyroid adenoma

or hyperplasia in patients with previous neck surgery. Clin Nucl Med 2008; 33: 394–397.
32. Prommegger R, Wimmer G, Profanter C et al. Virtual neck exploration: a new method for localizing abnormal parathyroid glands. Ann Surg 2009; 250: 761–765.
33. Ruf J, Seehofer D, Denecke T et al. Impact of image fusion and attenuation correction by SPECT-CT on the scintigraphic detection of parathyroid adenomas. Nuklearmedizin 2007; 46: 15–21.
34. Schmidt M, Thoma N, Dietlein M et al. ^{99m}Tc-MIBI SPECT in primary hyperparathyroidism. Influence of concomitant vitamin D deficiency for visualization of parathyroid adenomas. Nuklearmedizin 2008; 47: 1–7.
35. Schommartz B, Cupisti K, Antke C et al. Localisation of parathyroid glands using planar ^{99m}Tc-sestamibi scintigraphy. Comparison between subtraction- and dual-phase technique. Nuklearmedizin 2006; 45: 115–121.
36. Slater A, Gleeson FV. Increased sensitivity and confidence of SPECT over planar imaging in dual-phase sestamibi for parathyroid adenoma detection. Clin Nucl Med 2005; 30: 1–3.
37. Taillefer R, Boucher Y, Potvin C, Lambert R. Detection and localization of parathyroid adenomas in patients with hyperparathyroidism using a single radionuclide imaging procedure with technetium-99m-sestamibi (double-phase study). J Nucl Med 1992; 33: 1801–1807.
38. Thomas DL, Bartel T, Menda Y et al. Single photon emission computed tomography (SPECT) should be routinely performed for the detection of parathyroid abnormalities utilizing technetium-99m sestamibi parathyroid scintigraphy. Clin Nucl Med 2009; 34: 651–655.
39. Tomas MB, Pugliese PV, Tronco GG et al. Pinhole versus parallel-hole collimators for parathyroid imaging: an intraindividual comparison. J Nucl Med Technol 2008; 36: 189–194.
40. Weiss M, Beneke F, Schmid R et al. Can supplemental imaging with SPECT technique improve the diagnostic value of preoperative Tc-99m-MIBI scintigraphy in primary hyperparathyroidism? Med Klin (Munich) 2002; 97: 389–395.

Publication II

Virpi Tunninen, Pekka Varjo, Jukka Schildt, et al., “Comparison of Five Parathyroid Scintigraphic Protocols,” International Journal of Molecular Imaging, vol. 2013, Article ID 921260, 12 pages, 2013. doi:10.1155/2013/921260

Hindawi Publishing Corporation
International Journal of Molecular Imaging
Volume 2013, Article ID 921260, 12 pages
http://dx.doi.org/10.1155/2013/921260

Clinical Study

Comparison of Five Parathyroid Scintigraphic Protocols

Virpi Tunninen,[1] Pekka Varjo,[1] Jukka Schildt,[2] Aapo Ahonen,[2] Tomi Kauppinen,[3] Irina Lisinen,[4] Anu Holm,[1] Hannu Eskola,[5] and Marko Seppänen[4,6]

[1] *Department of Nuclear Medicine, Satakunta Central Hospital, Sairaalantie 3, 28500 Pori, Finland*
[2] *Department of Clinical Physiology and Nuclear Medicine, Helsinki University Central Hospital, HUS, P.O. Box 340, 00029 Helsinki, Finland*
[3] *HUS Medical Imaging Center, Helsinki University Central Hospital, P.O. Box 340, 00029 Helsinki, Finland*
[4] *Turku PET Centre, Turku University Hospital, P.O. Box 52, 20521 Turku, Finland*
[5] *Department of Biomedical Engineering, Tampere University of Technology, P.O. Box 527, 33101 Tampere, Finland*
[6] *Department of Clinical Physiology and Nuclear Medicine, Turku University Hospital, P.O. Box 52, 20521 Turku, Finland*

Correspondence should be addressed to Virpi Tunninen; virpi.tunninen@satshp.fi

Received 25 October 2012; Revised 23 December 2012; Accepted 27 December 2012

Academic Editor: Francesca Pons

Objectives. We compared five parathyroid scintigraphy protocols in patients with primary (pHPT) and secondary hyperparathyroidism (sHPT) and studied the interobserver agreement. The dual-tracer method (^{99m}Tc-sestamibi/^{123}I) was used with three acquisition techniques (parallel-hole planar, pinhole planar, and SPECT/CT). The single-tracer method (^{99m}Tc-sestamibi) was used with two acquisition techniques (double-phase parallel-hole planar, and SPECT/CT). Thus five protocols were used, resulting in five sets of images. *Materials and Methods*. Image sets of 51 patients were retrospectively graded by four experienced nuclear medicine physicians. The final study group consisted of 24 patients (21 pHPT, 3 sHPT) who had been operated upon. Surgical and histopathologic findings were used as the standard of comparison. *Results*. Thirty abnormal parathyroid glands were found in 24 patients. The sensitivities of the dual-tracer method (76.7–80.0%) were similar ($P = 1.0$). The sensitivities of the single-tracer method (13.3–31.6%) were similar ($P = 0.625$). All differences in sensitivity between these two methods were statistically significant ($P < 0.012$). The interobserver agreement was good. *Conclusion*. This study indicates that any dual-tracer protocol with ^{99m}Tc-sestamibi and ^{123}I is superior for enlarged parathyroid gland localization when compared with single-tracer protocols using ^{99m}Tc-sestamibi alone. The parathyroid scintigraphy was found to be independent of the reporter.

1. Introduction

^{99m}Tc-methoxyisobutylisonitrile (^{99m}Tc-sestamibi), first introduced by Coakley and coworkers as a parathyroid imaging agent in 1989 [1], is the imaging agent of choice for parathyroid scintigraphy (PS) [2]. Unfortunately, ^{99m}Tc-sestamibi is not a specific tracer for parathyroid tissue but is taken up by adjacent thyroid tissue. This problem can be overcome by using either a single-tracer (double phase) or a dual-tracer method.

In the single tracer method, it is assumed that thyroid and parathyroid tissues have different washout kinetics for ^{99m}Tc-sestamibi [3]. By acquiring images in the early and late phases, the focally increasing uptake will reveal hyperfunctioning parathyroid tissue. In the dual-tracer method, ^{99m}Tc-sestamibi is used combined with ^{123}I or ^{99m}Tc-pertechnetate, which are taken up by the thyroid gland only. Subtracting the thyroid image from the ^{99m}Tc-sestamibi image provides visualization of the parathyroid tissue alone [4].

With both single-tracer and dual-tracer methods, several acquisition techniques can be used (i.e., planar acquisitions with parallel-hole or pinhole collimators and SPECT or SPECT/CT), and several choices can be made about the settings used for each technique (e.g., matrix size, energy

settings, and acquisition time). There are several studies that provide comparisons between the different imaging methods or techniques, although there is little evidence supporting the superiority of one over another, resulting in the use of various study protocols today [5, 6].

We have previously shown that there is significant variability in the current practice of PS in Finland [7]. This is also true in other countries, with reported sensitivities for localizing abnormal parathyroid tissue ranging from 34% to 100% [8].

As a result of our previous study, the clinical protocol of parathyroid scintigraphy in Satakunta central hospital was changed in June 2010. Pinhole and SPECT/CT acquisition techniques were included to increase the sensitivity of the study. Additional late phase imaging was also included to benefit from the double phase method as well.

The goal of this study was to compare the sensitivity and specificity of a single-tracer method and a dual-tracer method with various acquisition techniques. The dual-tracer method (^{99m}Tc-sestamibi/^{123}I) was used with three acquisition techniques (parallel-hole planar, pinhole planar, and SPECT/CT). The single-tracer method (^{99m}Tc-sestamibi) was used with two acquisition techniques (double phase parallel-hole planar, and SPECT/CT). In addition, the agreement between the findings of four experienced nuclear medicine physicians was studied.

2. Methods

2.1. Patients. This was a retrospective single-center study of fifty-one patients referred for PS between June 2010 and February 2011 in Satakunta Central Hospital, Finland. Patient data were included if there was biochemical evidence of hyperparathyroidism, if scintigraphy was requested for preoperative tumor localization, and if the patient proceeded to surgery. Histopathological finding was used as the gold standard. The final study group consisted of 6 men and 18 women with a mean age of 62.3 years (range, 32.1–86.8 years). Twenty-one patients had pHPT. Preoperative plasma intact parathyroid hormone (iPTH) values ranged from 69 ng/L to 277 ng/L (mean 190 ng/L, normal values 10–65 ng/L), and values for preoperative serum calcium (Ca) ranged from 1.37 mmol/L to 1.73 mmol/L (mean 1.48 mmol/L, normal values 1.16–1.3 mmol/L). Three patients had sHPT due to renal failure. Preoperative iPTH values ranged from 210 ng/L to 400 ng/L (mean 380 ng/L), values for preoperative Ca ranged from 1.21 mmol/L to 1.8 mmol/L (mean 1.45 mmol/L). Twenty-seven patients did not proceed to surgery for a variety of reasons (patient condition, death, and other illnesses). This study was exempt from institutional review board approval according to Finnish legislation. Informed consent was waived.

2.2. Imaging: Doses and Acquisition. Patients received 20 MBq of ^{123}I (MAP Medical Technologies) intravenously. Two hours later, 550 MBq of ^{99m}Tc-sestamibi (Mallinckrodt Medical B.V.) was injected intravenously. Ten minutes after the ^{99m}Tc-sestamibi administration, imaging was started. Five different image sets were acquired. The order and the timing (after the injection or ^{99m}Tc-sestamibi) of the acquisitions and the resulting image sets are presented in Figure 1.

First, a static 10-minute anterior image of the neck and chest was acquired using a low-energy, high-resolution, parallel-hole collimator (LEHR) (256 × 256 matrix; 1.85x zoom). Next, a static 10-minute anterior image of the neck was acquired from a distance of 10 cm from the patient's skin using a 5 mm diameter pinhole collimator (256 × 256 matrix; 2.19x zoom). Acquisitions were performed with the same dual-head gamma camera (Skylight; Philips). All data were collected in dual-energy windows. The ^{99m}Tc window was centered at 140 keV and had a 10% width (range, 133–147 keV). The ^{123}I window was centered at 159 keV and had a 10% width (range, 151–167 keV). Narrow windows were used to minimize crosstalk between isotopes.

One hour after the ^{99m}Tc-sestamibi injection, the SPECT/CT acquisition was started (Symbia T; Siemens). SPECT data were acquired in a step-and-shoot sequence with a noncircular orbit (180° detector configuration; low-energy, parallel-hole, high-resolution collimators; 128 × 128 matrix; 4.8 mm pixel size; 48 views for each detector (3,75° per projection); 33 s/projection; total scan time, 32 min). All data were collected in dual-energy windows. The ^{99m}Tc window was centered at 140 keV and had a 15% width (range, 129.5–150.5 keV). The ^{123}I window was placed with a 4% offset above 159 keV and had a 15% width (range, 153.4–177.3 keV). The 4% offset was used to minimize the spillover of the ^{99m}Tc photopeak into the ^{123}I photopeak. After the SPECT acquisition was complete, the patient remained still on the table for the CT acquisition. A topogram scout scan (130 kVp, 30 mA, anterior view) was performed first, and limits for the CT acquisition were set (from the neck to the diaphragm). Then, a helical CT scan was performed (130 kVp, 2 × 2.5 mm collimation, 0.8 s rotation time, 1.5 pitch). The dose was controlled by tube-current modulation (CARE Dose AEC+DOM; Siemens), with the reference exposure set to 30 mAs.

Finally, a static 10-minute anterior image of the neck and chest was acquired using a low-energy, high-resolution collimator with a Siemens Symbia T-gamma camera (256 × 256 matrix; 1.85x zoom (32.2 cm field)). The same energy settings as those in the SPECT acquisition were used. Eleven of the patients did not complete this final image due to limited camera time or patient-related reasons. A ^{99m}Tc intrinsic flood was used for both energy windows in both cameras. It was verified that the image-field uniformity was acceptable for all energy windows used.

2.3. Image Processing. All planar images were analyzed in a Hermes workstation (Hermes Medical Solutions). For dual-tracer images, a normalization factor (NF) was defined as the ratio of the thyroid maximum pixel counts in the ^{123}I and ^{99m}Tc-sestamibi images. Gradient subtraction images were created by multiplying the ^{99m}Tc-sestamibi image with 10 successive NFs (with 20% steps from 20% to 200% of

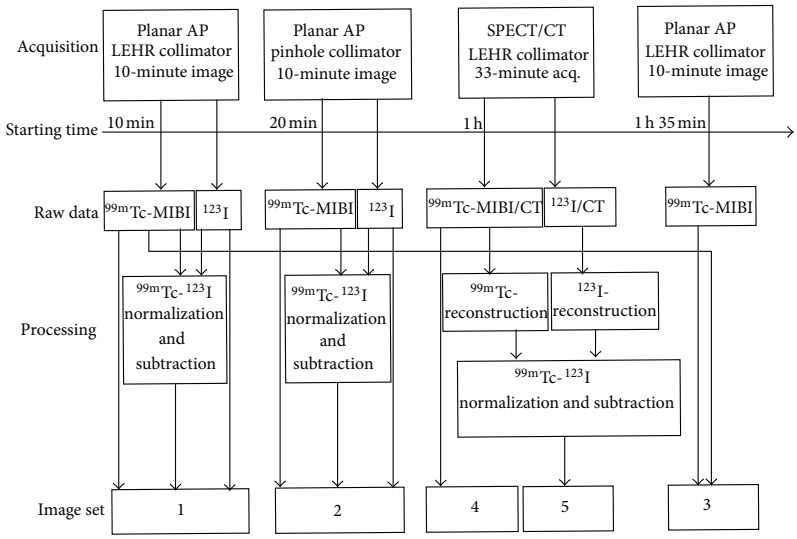

Figure 1: The orders and the timings of the acquisitions and the resulting image sets. Set 1: ^{99m}Tc-sestamibi, ^{123}I, and subtraction images with parallel-hole collimator. Set 2: ^{99m}Tc-sestamibi, ^{123}I, and subtraction images with pinhole collimator. Set 3: ^{99m}Tc-sestamibi double phase images with parallel-hole collimator. Set 4: ^{99m}Tc-sestamibi SPECT/CT. Set 5: ^{99m}Tc-sestamibi, ^{123}I, and subtraction SPECT/CT images.

the original NF), and the ^{123}I image was subtracted from each normalized ^{99m}Tc-sestamibi image, resulting in 10 subtraction images to avoid oversubtraction [9, 10]. The final image sets consisted of ^{99m}Tc-sestamibi and ^{123}I images and gradient subtraction images (image set 1 acquired with LEHR, image set 2 with pinhole). ^{99m}Tc-sestamibi early- and late-phase images were displayed side-by-side on the Hermes workstation (image set 3).

SPECT images were reconstructed on the Siemens Syngo workstation (Siemens) using the FLASH 3D algorithm (8 iterations, 8 subsets, Gaussian 9.00 filter). No scatter correction was used. The initial NF was defined as the ratio of the corresponding thyroid maximum voxel counts in ^{99m}Tc-sestamibi and ^{123}I SPECT data. ^{123}I SPECT data were multiplied by NF to create normalized ^{123}I SPECT data, which were then subtracted from ^{99m}Tc-sestamibi SPECT data to create the subtraction SPECT dataset, as described by Neumann and coworkers [4]. The NF was adjusted until the subtraction SPECT images were subjectively satisfactory. CT data were reconstructed on the Siemens Syngo workstation (Siemens) for attenuation correction using the B08s kernel, and for fusion display purposes with a B40s medium kernel. The CT images were downsampled to match the SPECT image matrix and converted from Hounsfield units into effective attenuation values at 140 keV (^{99m}Tc) and 159 keV (^{123}I). The final image sets consisted of ^{99m}Tc-sestamibi SPECT/CT data (image set 4) and ^{123}I, ^{99m}Tc-sestamibi, and subtraction SPECT/CT data (image set 5). The accuracy of the SPECT/CT data coregistration was checked. All image processing was performed by an experienced medical physicist.

2.4. Image Interpretation. All patient image datasets were anonymized before review by four experienced nuclear medicine physicians, who were blinded to all patient-related information. Five image sets (Figure 1) were reviewed. Datasets 1, 2, and 3 were read in separate reading sessions. Image sets 4 and 5 were reviewed in a single session in this order, with the physician being aware that the datasets belonged to the same patient.

Each quadrant in relation to the thyroid gland (right upper, right lower, left upper, and left lower) was classified on a 3-point scale (0 = negative, 1 = uncertain, and 2 = positive). The image review criteria for positive finding were as follows: (a) for image sets 1 and 2: clear abnormal residual activity on the planar subtraction images, (b) for image set 3: focally increased uptake that persisted or increased in intensity from early to late images, (c) for image set 4: focally increased uptake outside the normal ^{99m}Tc-sestamibi biodistribution that had an anatomic correlation in the CT images, and (d) for image set 5: clear abnormal residual activity on the subtraction SPECT images that had an anatomic correlation in the CT images.

2.5. Surgery and Histologic Analysis. All patients were operated upon by an endocrine surgeon using an open technique. The surgeon was aware of all initial scintigraphic results prior to surgery. All glands were not identified for all patients. Postoperative iPTH and Ca values were reviewed to confirm surgery success. The mean interval between scintigraphy and surgery was 181 days (range, 29–457 days). A histopathological analysis was performed for all excised tissue.

2.6. Data Analysis. To estimate the sensitivity, specificity, and accuracy for the localization for each image set, scores of 0-1 were considered negative and scores of 2 were considered positive. Findings were classified as true positive, false positive, true negative, or false negative with histologic analysis as the reference standard. For each patient, four scores, one for each quadrant, were assigned. The false-positive image rate was defined as the ratio of false positives to the sum of true positives plus false positives [11].

2.7. Statistical Methods. The sensitivity, specificity, and accuracy of each image set were calculated for each physician separately. A McNemar test was performed to compare the sensitivities, specificities, and accuracies between the image sets. The results from physician 1 were chosen when comparing the image sets, as he had the most experience with the imaging methods and techniques used. The Mann-Whitney U nonparametric test was used to compare the size of the visualized and nonvisualized glands. A McNemar test was also used to analyze the accuracy of the different physicians. The differences for each method/technique were analyzed separately. κ coefficients were used to quantify the agreement between the results from the four physicians. Positive kappa values within the ranges of 0.01–0.20, 0.21–0.4, 0.41–0.60, 0.61–0.80, and 0.81–1.00 were interpreted as "very weak," "weak," "medium," "good," and "very good" agreement, respectively [12]. A P value <0.05 was considered statistically significant. Statistical analyses were conducted using SAS 9.2 (SAS Institute Inc., Cary, NC, USA) and SPSS statistical analysis software (SPSS Inc., Chicago, IL, USA).

3. Results

3.1. Histological Findings. Altogether, 30 enlarged glands were found in 24 patients. Twenty patients had a solitary parathyroid adenoma, two patients had double adenomas, and two patients had multiglandular disease. The mean weight of the abnormal parathyroid glands was 677 mg (weight information was not available for four glands).

The postoperative serum Ca values were normalized for all patients. The postoperative iPTH values were normalized for 17 patients. For 7 patients, these values were slightly elevated (ranged from 80 ng/L to 134 ng/L (mean 90 ng/L), but decreased from the preoperative values (ranged from 138 ng/L to 400 ng/L (mean 165 ng/L)). Four glands were visualized in the operation for these patients.

The pathological findings together with the image findings for physician 1 are listed in Table 1.

3.2. ^{99m}Tc-Sestamibi versus ^{123}I/^{99m}Tc-Sestamibi. All image sets with ^{123}I/^{99m}Tc-sestamibi were significantly more sensitive than any image set with ^{99m}Tc-sestamibi, regardless of the acquisition technique (Tables 2 and 3). ^{99m}Tc-sestamibi SPECT/CT (image set 4) had the highest specificity (100%), as there were no false-positive readings (Table 2).

^{99m}Tc-sestamibi SPECT/CT revealed only 4 abnormal glands, while ^{123}I/^{99m}Tc-sestamibi subtraction SPECT/CT revealed 23 abnormal glands (Table 1). A representative patient case is shown in Figure 2.

3.3. Planar AP with LEHR versus Planar AP with Pinhole versus SPECT/CT. There was no difference in the sensitivity, specificity, or accuracy between the acquisition techniques using ^{99m}Tc-sestamibi alone. There was also no difference in the sensitivity, specificity, or accuracy between the acquisition techniques using ^{123}I/^{99m}Tc-sestamibi (Tables 2 and 3).

Although there was no difference in the sensitivity, SPECT/CT may offer invaluable three-dimensional information about the location of the enlarged parathyroid adenomas together with anatomical information (Figure 3).

3.4. False-Positive Findings. Ten patients had 12 different false-positive findings (40 false-positive findings if all physicians and image sets are summed up). The false-positive findings are presented in Table 4.

Four of these were due to cold thyroid nodules in ^{123}I images, causing erroneous interpretation in the subtraction image (Figure 4). Uneven ^{123}I uptake caused thus 55% of all false-positive findings.

One patient had clear uptake in the ^{99m}Tc-sestamibi image below the thyroid as seen in planar images. All physicians interpreted this as a positive finding in the planar images. In the SPECT/CT images, it was revealed that the uptake was in the cervical vertebra (Figure 5). This bone uptake caused 20% of all false-positive findings.

Three false positive findings were due to the "edge effect" in ^{123}I/^{99m}Tc-sestamibi subtraction SPECT/CT images (residual activity around the thyroid lobes after subtraction). This artefact caused 10% of all false-positive findings.

Four positive findings were caused by an error in image interpretation, mainly in double phase ^{99m}Tc-sestamibi images. Difficulty in setting the line between the positive and the negative findings caused 15% of all false-positive findings.

As seen in Table 4, ^{123}I/^{99m}Tc-sestamibi dual-tracer method with various acquisition techniques produced 90% of all false-positive findings. Subtraction SPECT/CT yielded the lowest percentage of false positives when compared to the other subtraction methods. The double phase ^{99m}Tc-sestamibi method produced only 10% of all false-positive findings. The false-positive image rate (%) is presented in Table 5.

3.5. False-Negative Findings. There was only one abnormal parathyroid gland (number 10, Table 1) that was visualized in all image sets and by all of the physicians. Thus 23 patients had 29 different false-negative findings (267 false-negative findings if all physicians and image sets are summed up). ^{99m}Tc-sestamibi/^{123}I subtraction planar images with parallel-hole collimator produced 13.9% of all false-negative findings, ^{99m}Tc-sestamibi/^{123}I subtraction planar images with pinhole collimator produced 9.7% of all false-negative findings, ^{99m}Tc-sestamibi double phase images with parallel-hole collimator produced 22.8% of all false-negative

Table 1: Number of adenomas and hyperplastic glands and image findings for physician 1.

Patient number	Gland number	Weight (mg)	Findings for image set				
			1	2	3	4	5
1	1	170	FN	FN	NA	FN	FN
1	2	570	TP	TP	NA	FN	TP
2	3	980	TP	TP	FN	FN	TP
3	4	830	TP	TP	FN	TP	TP
4	5	1280	TP	TP	FN	FN	TP
4	6	840	TP	FN	FN	FN	TP
4	7	2140	TP	TP	FN	FN	TP
5	8	NA	TP	TP	NA	FN	TP
6	9	1200	TP	TP	NA	FN	TP
7	10	960	TP	TP	TP	TP	TP
8	11	1880	TP	TP	TP	FN	TP
9	12	1160	FN	TP	FN	FN	FN
10	13	299	TP	TP	FN	FN	TP
11	14	200	FN	FN	FN	FN	FN
12	15	260	TP	TP	FN	FN	TP
13	16	570	TP	TP	TP	TP	TP
14	17	370	TP	TP	FN	FN	TP
15	18	300	TP	FN	NA	FN	FN
15	19	400	TP	TP	NA	FN	TP
15	20	NA	TP	TP	NA	FN	TP
16	21	510	TP	TP	NA	FN	TP
17	22	340	TP	TP	FN	FN	TP
18	23	NA	TP	TP	TP	FN	TP
19	24	420	FN	FN	TP	FN	FN
20	25	300	FN	TP	NA	FN	FN
20	26	NA	TP	TP	NA	FN	TP
21	27	520	TP	TP	NA	FN	TP
22	28	400	TP	TP	FN	FN	TP
23	29	550	TP	TP	TP	TP	TP
24	30	160	FN	FN	FN	FN	FN

TP: true positive for abnormal parathyroid gland; FN: false negative for abnormal parathyroid gland; NA: image set not available for patient.

(a) (b)

Figure 2: ^{99m}Tc-sestamibi SPECT (a) and ^{123}I/^{99m}Tc-sestamibi subtraction SPECT (b) coronal images for a 34-year-old man with secondary hyperparathyroidism. Three hyperplastic parathyroid glands not visualized in coronal ^{99m}Tc-sestamibi image are clearly visible in the subtraction SPECT coronal image (b).

Table 2: Sensitivity, specificity, and accuracy for localization of abnormal parathyroid glands.

Image set	Physician	Sensitivity (%)	Specificity (%)	Accuracy (%)
1	1	80.0	93.9	89.6
	2	70.0	95.5	87.5
	3	63.3	97.0	86.5
	4	63.3	97.0	86.5
2	1	80.0	92.4	88.5
	2	80.0	93.9	89.6
	3	76.7	95.5	89.6
	4	76.7	95.5	89.6
3	1	31.6	93.9	76.5
	2	21.1	98.0	76.5
	3	10.5	100.0	75.0
	4	15.8	100.0	76.5
4	1	13.3	100.0	72.9
	2	16.7	100.0	74.0
	3	10.0	100.0	71.9
	4	10.0	100.0	71.9
5	1	76.7	92.4	87.5
	2	76.7	95.5	89.6
	3	56.7	98.5	85.4
	4	63.3	98.5	87.5

Table 3: Statistical significance for differences in sensitivity, specificity, and accuracy for comparisons of image sets for physician 1.

Compared image sets	P for sensitivity	P for specificity	P for accuracy
1 versus 2	NS	NS	NS
1 versus 3	0.0117	NS	0.0352
1 versus 4	$1.907E-06$	0.0455	0.0015
1 versus 5	NS	NS	NS
2 versus 3	0.0117	NS	NS
2 versus 4	$1.907E-06$	0.0253	0.0041
2 versus 5	NS	NS	NS
3 versus 4	NS	NS	NS
3 versus 5	0.0117	NS	NS
4 versus 5	$3.815E-06$	0.0253	0.0066

NS: not significant.

findings, ^{99m}Tc-sestamibi SPECT/CT produced 39.3% of all false-negative findings, and ^{99m}Tc-sestamibi/^{123}I subtraction SPECT/CT produced 14.2% of all false-negative findings (all physicians and all image sets are summed up).

The smallest gland located in this series was 260 mg. There were three smaller abnormal parathyroid glands (160 mg, 170 mg, and 200 mg) that could not be located with any method or imaging technique by any of the physicians. The mean gland size of false-negative and true-positive findings for all physicians and image sets are presented in Table 6 together with the statistical significance.

3.6. Interobserver Variability. The κ coefficient for the agreement of the results between the four physicians for the five study readings are shown in Table 7.

The highest agreement for accuracy was found for ^{99m}Tc-sestamibi SPECT/CT, which did not have any false-positive findings for any physician. The highest agreement for sensitivity was found for the planar subtraction images of ^{123}I/^{99m}Tc-sestamibi with the pinhole collimator.

4. Discussion

Our results clearly show that a dual-tracer method with ^{99m}Tc-sestamibi and ^{123}I is superior to a single-tracer method with ^{99m}Tc-sestamibi for PS, regardless of the acquisition technique used. This has been proposed by other authors as well [4, 9, 13, 14].

To our knowledge, this is the first study comparing planar imaging with parallel-hole and pinhole collimators using the

Table 4: The false-positive findings for all physicians.

Image set	1				2				3				5				Reason for FP	% of FP
Patient number	Physician				Physician				Physician				Physician					
	1	2	3	4	1	2	3	4	1	2	3	4	1	2	3	4		
2					RL								RL					
3	RL	RL	RL	RL	RL		RL	RL					RL		RL	RL	Uneven iodine uptake	55
8					RU	RU												
22	RU	RU			RU	RU	RU	RU					RU	RU				
20	RL	RL	RL	RL	RL	RL	RL	RL									Bone uptake	20
4													LL					
10														LL			Edge effect	10
24													RU	RU				
24									LL									
24	RL					RL			RL								Other	15
13										LU								
19									LL									
% of FP	27.5				37.5				10				25					

FP: false positive, RU: right upper, RL: right lower, LU: left upper, and LL: left lower.

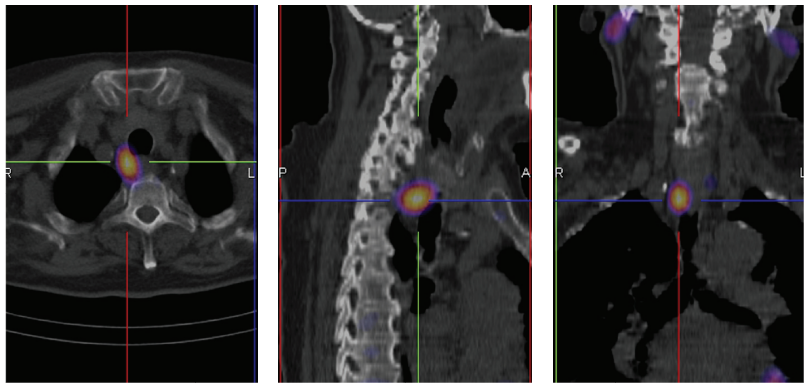

(a) (b) (c)

Figure 3: A ^{99m}Tc-sestamibi uptake in a parathyroid adenoma located behind the trachea. ^{123}I/^{99m}Tc-sestamibi subtraction SPECT/CT images (transversal (a), sagittal (b), and coronal (c)).

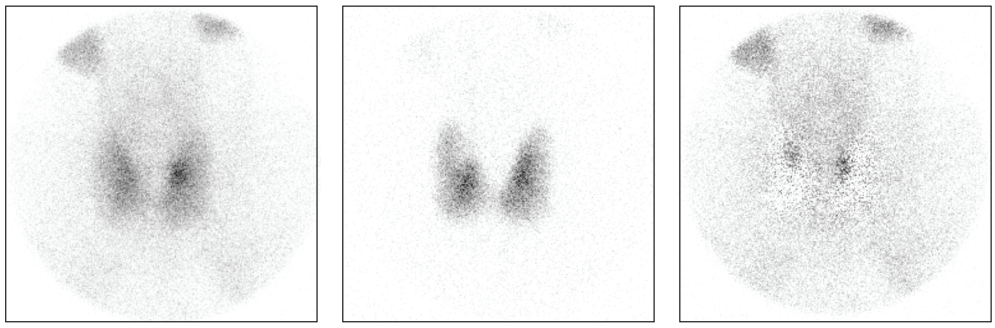

(a) (b) (c)

Figure 4: A cold nodule in the upper quadrant of a right thyroid lobe in the ^{123}I image (b) causing a false-positive finding in the subtraction image (c).

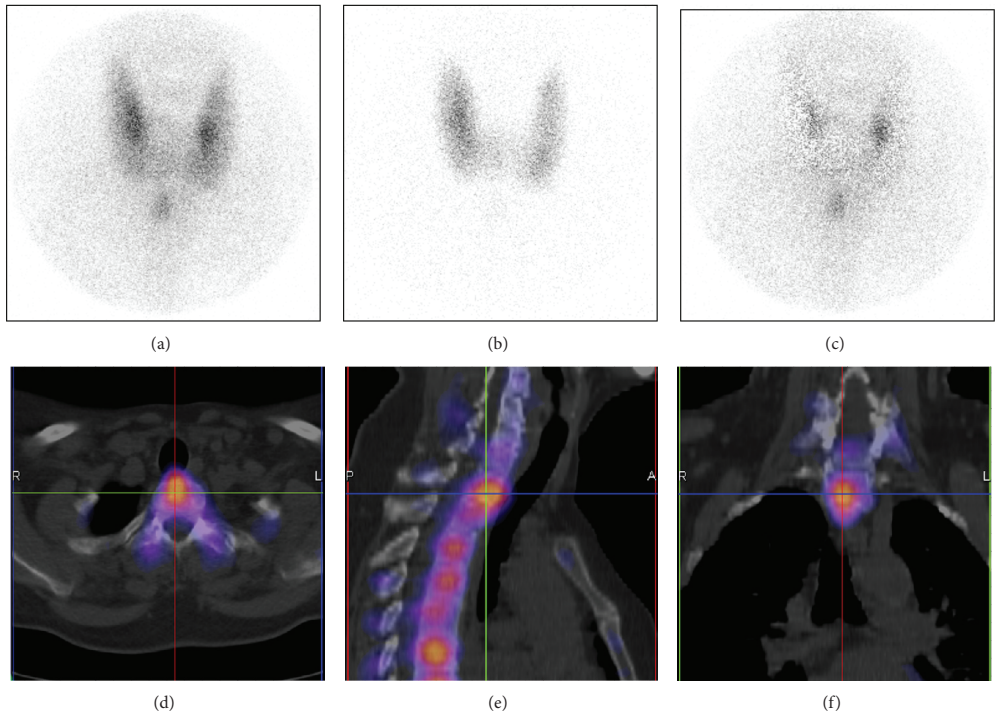

Figure 5: A ^{99m}Tc-sestamibi focal uptake inferior to the thyroid seen in the anterior image acquired with a pinhole collimator. ^{99m}Tc-sestamibi (a), ^{123}I (b), and subtraction image (c). All physicians interpreted this uptake as an abnormal parathyroid gland. The same patient seen in ^{123}I/^{99m}Tc-sestamibi subtraction SPECT/CT images (transversal (d), sagittal (e), and coronal (f)). Focal uptake was due to bone uptake in the cervical vertebra.

Table 5: The false-positive image rate (%) for each image set and each physician.

Physician	False-positive rate (%) for image set				
	1	2	3	4	5
1	14.3	17.2	33.3	0.0	17.9
2	12.5	14.3	20.0	0.0	11.5
3	9.5	11.5	0.0	0.0	5.6
4	2.1	3.1	0.0	0.0	1.0
Average	9.6	11.5	13.3	0.0	9.0

Table 6: The mean gland size of false-negative and true-positive findings for all physicians and all image sets.

	Image set				
	1	2	3	4	5
Smallest gland visualized	260	260	420	550	260
Mean weight of FN (mg)	300	420	485	420	300
Mean weight of TP (mg)	560	570	960	830	560
P (FN versus TP)	0.002	<0.001	0.046	0.026	<0.001

Table 7: The comparison of reader agreement (accuracy and sensitivity) between physicians.

κ coefficient for	Physicians	Image set				
		1	2	3	4	5
Accuracy	1 versus 4	0.56	0.84	0.67	0.97	0.62
	1 versus 3	0.56	0.84	0.72	0.97	0.56
	1 versus 2	0.69	0.84	0.59	0.92	0.69
	4 versus 3	1.00	1.00	0.96	1.00	0.91
	4 versus 2	0.86	0.78	0.84	0.89	0.59
	3 versus 2	0.86	0.78	0.88	0.89	0.53
Sensitivity	1 versus 4	0.44	0.90	0.30	0.84	0.69
	1 versus 3	0.44	0.90	0.41	0.84	0.57
	1 versus 2	0.56	1.00	0.20	0.61	0.81
	4 versus 3	1.00	1.00	0.77	1.00	0.86
	4 versus 2	0.85	0.90	0.48	0.43	0.69
	3 versus 2	0.85	0.90	0.61	0.43	0.57

^{123}I/^{99m}Tc-sestamibi subtraction method with patients. We could not demonstrate the improved sensitivity from the use of the pinhole collimator that has been shown by several authors when using ^{99m}Tc-sestamibi [15–20].

SPECT alone has been shown to improve sensitivity compared with planar imaging with parallel-hole collimators [6, 21–24]. SPECT/CT has been shown to offer precise anatomical localization and an improvement in diagnostic specificity and accuracy over conventional SPECT, especially for patients with previous neck surgery or multiglandular disease [5, 25–32]. The use of SPECT/CT also shortens surgical times (when compared with SPECT alone) and eventually lowers costs [33, 34]. Opposite opinions have also been presented, and the use of SPECT/CT has been found to be important only for locating ectopic parathyroid adenomas [35, 36].

We could not demonstrate an increased sensitivity for ^{123}I/^{99m}Tc-sestamibi subtraction SPECT/CT when compared with planar ^{99m}Tc-sestamibi/^{123}I subtraction image sets. However, the use of ^{123}I/^{99m}Tc-sestamibi SPECT/CT decreased the false-positive rate for three observers when compared with planar ^{123}I/^{99m}Tc-sestamibi image sets.

The low sensitivity of double phase planar ^{99m}Tc-sestamibi or ^{99m}Tc-sestamibi SPECT/CT cannot be explained by the rapid washout of ^{99m}Tc-sestamibi, as 19 enlarged parathyroid glands were visible in ^{123}I/^{99m}Tc-sestamibi SPECT/CT images that could not be visualized with ^{99m}Tc-sestamibi SPECT/CT. A low sensitivity for a single tracer or the double phase protocols has also been reported by other authors [3, 37].

The low sensitivity of the ^{99m}Tc-sestamibi SPECT/CT in this study could not be linked to the timing of the acquisition. SPECT acquisition was started approximately one hour after ^{99m}Tc-sestamibi injection. Lavely and coworkers were able to demonstrate much better sensitivity for early-phase SPECT/CT (62%) and also for early planar/delayed planar imaging (56,5%) [5]. The timing of their early planar and SPECT/CT acquisitions was almost identical to ours.

Our results for the ^{123}I/^{99m}Tc-sestamibi subtraction SPECT/CT are comparable to the results of Neumann and coworkers [26], who demonstrated a sensitivity of 70% and a specificity of 96% in a group of 61 patients with primary hyperparathyroidism. The increase of specificity (when compared with SPECT alone) was explained by reducing the number of false positives.

There were three abnormal parathyroid glands that were visible in ^{123}I/^{99m}Tc-sestamibi subtraction planar images (with a parallel-hole or a pinhole collimator) but not visible in ^{123}I/^{99m}Tc-sestamibi subtraction SPECT/CT. This could be due to rapid washout [38] as SPECT/CT was performed one hour later than the planar images were acquired. Thus, the timing of the various acquisitions should be considered carefully, and SPECT/CT should be performed in the early phase so as not to miss abnormal parathyroid gland(s) with rapid washout [10].

The average false-positive rate was comparable to previous reports [6, 11]. In this retrospective study, the five image sets were not reviewed together, which is normally done in our clinical scenario. With careful observation of the ^{123}I images of the thyroid, it should be possible to decrease the false-positive rate in subtraction images.

It seems that a major factor influencing detection of abnormal parathyroid glands is their size. The difference of mean gland size of false-negative and true-positive findings was statistically significant for all protocols used in this study.

There was lower number of ectopic glands in this patient group than could be expected [39]. There might have been small ectopic glands which were not recognized in scintigraphy or in surgery. This might explain the slightly elevated iPTH values for 7 patients.

Several imaging protocols for PS with ^{99m}Tc-sestamibi are in use, with a wide range of sensitivities (34–100%) reported [8]. No large study exists that compares the accuracy of each [6]. We have shown the superiority of the ^{123}I/^{99m}Tc-sestamibi subtraction method of PS. The high popularity of the single-tracer method with ^{99m}Tc-sestamibi alone can only be explained by its technical simplicity. It

is true that the ^{123}I/^{99m}Tc-sestamibi subtraction method, especially SPECT/CT, is technically demanding. There are several possible sources of artifacts, such as scaling and the subtraction process. In our opinion, the data processing should be performed by an experienced medical physicist.

Even optimal processing of identical ^{99m}Tc and ^{123}I targets does not give flawless subtraction image, some activity is always left around the edges. In this series, it was in few cases interpreted as a positive finding. To our knowledge, this artefact has not been described earlier concerning parathyroid scintigraphy [40].

The overall interobserver agreement in this study was good. The average κ coefficient was 0.79 for accuracy and 0.70 for sensitivity. These results are comparable to previous results [12, 15].

One of the main limitations of this study is the number of patients in the image set 3 (^{99m}Tc-sestamibi double phase images). Another limitation of our study relates to the fact that the delay phase was acquired with another gamma camera. However, quality assurance measurements are routinely performed for both cameras. There are no differences in important parameters regarding image quality.

The clinical PS protocol presented in this study, which included various acquisitions, is quite time consuming. The discomfort for the patient should be decreased by rejecting unnecessary acquisitions. This study indicates that the ^{123}I/^{99m}Tc-sestamibi subtraction method combined with any imaging technique is adequate to locate abnormal parathyroid glands. However, ^{123}I/^{99m}Tc-sestamibi subtraction SPECT/CT is recommended because it provides accurate three-dimensional information about the location of enlarged parathyroid adenomas together with anatomical information (Figure 3) and may influence the surgical approach [14]. With SPECT/CT, it is also possible to avoid some false-positive findings resulting from the ^{99m}Tc-sestamibi uptake in bone structures. The additional use of anterior pinhole images may be useful for recognizing cold thyroid nodules and thus further reducing the false-positive rate. Determining the optimal technical aspects (acquisition and processing parameters, various physical corrections) still requires further study.

5. Conclusion

The results of this study show that the ^{123}I/^{99m}Tc-sestamibi subtraction method combined with any imaging technique is superior for enlarged parathyroid gland localization when compared with ^{99m}Tc-sestamibi alone with any acquisition technique. ^{123}I/^{99m}Tc-sestamibi subtraction SPECT/CT is recommended because it provides accurate three-dimensional information about the location of enlarged parathyroid adenomas. The use of anterior pinhole images may be useful for recognizing cold thyroid nodules and thus reducing the false-positive rate. The overall interobserver agreement for accuracy and for sensitivity in this study was good. Thus the parathyroid scintigraphy is independent of the reporter.

There are two limitations that need to be acknowledged regarding this study. The first limitation is the number of patients in the ^{99m}Tc-sestamibi double phase group. Another limitation relates to the fact that the delay phase was acquired with another gamma camera.

Acknowledgments

The authors thank the staff of the Department of Nuclear Medicine at Satakunta Central Hospital. This study was supported by a grant from the Research Funding of Satakunta Central Hospital (Erityisvaltionosuus). No other potential conflict of interests is reported.

References

[1] A. J. Coakley, A. G. Kettle, C. P. Wells, M. J. O'Doherty, and R. E. C. Collins, "99Tcm sestamibi—a new agent for parathyroid imaging," *Nuclear Medicine Communications*, vol. 10, no. 11, pp. 791–794, 1989.

[2] F. Lumachi, M. Ermani, S. Basso, P. Zucchetta, N. Borsato, and G. Favia, "Localization of parathyroid tumours in the minimally invasive era: Which technique should be chosen? Population-based analysis of 253 patients undergoing parathyroidectomy and factors affecting parathyroid gland detection," *Endocrine-Related Cancer*, vol. 8, no. 1, pp. 63–69, 2001.

[3] R. Taillefer, Y. Boucher, C. Potvin, and R. Lambert, "Detection and localization of parathyroid adenomas in patients with hyperparathyroidism using a single radionuclide imaging procedure with technetium-99m-sestamibi (double-phase study)," *Journal of Nuclear Medicine*, vol. 33, no. 10, pp. 1801–1807, 1992.

[4] D. R. Neumann, C. B. Esselstyn Jr., R. T. Go, C. O. Wong, T. W. Rice, and N. A. Obuchowski, "Comparison of double-phase 99mTc-sestamibi with 123I-99mTc-sestamibi subtraction SPECT in hyperparathyroidism," *American Journal of Roentgenology*, vol. 169, no. 6, pp. 1671–1674, 1997.

[5] W. C. Lavely, S. Goetze, K. P. Friedman et al., "Comparison of SPECT/CT, SPECT, and planar imaging with single- and dual-phase 99mTc-sestamibi parathyroid scintigraphy," *Journal of Nuclear Medicine*, vol. 48, no. 7, pp. 1084–1089, 2007.

[6] J. Sharma, P. Mazzaglia, M. Milas et al., "Radionuclide imaging for hyperparathyroidism (HPT): Which is the best technetium-99m sestamibi modality?" *Surgery*, vol. 140, no. 6, pp. 856–865, 2006.

[7] V. Tunninen, T. Kauppinen, H. Eskola, and M. O. Koskinen, "Parathyroid scintigraphy protocols in Finland in 2010: Results of the query and current status," *NuklearMedizin*, vol. 49, no. 5, pp. 187–194, 2010.

[8] R. Mihai, D. Simon, and P. Hellman, "Imaging for primary hyperparathyroidism-an evidence-based analysis," *Langenbeck's Archives of Surgery*, vol. 394, no. 5, pp. 765–784, 2009.

[9] S. Ceyssens and L. Mortelmans, "Parathyroid imaging: basic principles and KU Leuven experience: MIBI-dual phase versus MIBI/I-123," *Acta Oto-Rhino-Laryngologica Belgica*, vol. 55, no. 2, pp. 103–117, 2001.

[10] E. Hindie, O. Ugur, D. Fuster et al., "2009 EANM parathyroid guidelines," *European Journal of Nuclear Medicine and Molecular Imaging*, vol. 36, no. 7, pp. 1201–1216, 2009.

[11] E. Hindié, D. Mellière, C. Jeanguillaume, L. Perlemuter, F. Chéhadé, and P. Galle, "Parathyroid imaging using simultaneous double-window recording of technetium-99m-sestamibi and iodine-123," *Journal of Nuclear Medicine*, vol. 39, no. 6, pp. 1100–1105, 1998.

[12] C. Dalar, O. Ozdogan, M. G. Durak et al., "Inter-observer and intra-observer agreement in parathyroid scintigraphy; what can be done for making parathyroid scintigraphy more reliable?" *Endocrine Practice*, pp. 1–32, 2012.

[13] M. J. O'Doherty and A. G. Kettle, "Parathyroid imaging: preoperative localization," *Nuclear Medicine Communications*, vol. 24, no. 2, pp. 125–131, 2003.

[14] D. Taieb, E. Hindie, G. Grassetto, P. M. Colletti, and D. Rubello, "Parathyroid scintigraphy: when, how, and why? A concise systematic review," *Clinical Nuclear Medicine*, vol. 37, pp. 568–574, 2012.

[15] A. K. Arveschoug, H. Bertelsen, and B. Vammen, "Presurgical localization of abnormal parathyroid glands using a single injection of Tc-99m sestamibi comparison of high-resolution parallel-hole and pinhole collimators, and interobserver and intraobserver variation," *Clinical Nuclear Medicine*, vol. 27, no. 4, pp. 249–254, 2002.

[16] A. K. Arveschoug, H. Bertelsen, B. Vammen, and J. Brøchner-Mortensen, "Preoperative dual-phase parathyroid imaging with Tc-99m-sestamibi: accuracy and reproducibility of the pinhole collimator with and without oblique images," *Clinical Nuclear Medicine*, vol. 32, no. 1, pp. 9–12, 2007.

[17] V. S. Dontu, A. G. Kettle, M. J. O'Doherty, and A. J. Coakley, "Optimization of parathyroid imaging by simultaneous dual energy planar and single photon emission tomography," *Nuclear Medicine Communications*, vol. 25, no. 11, pp. 1089–1093, 2004.

[18] I. A. Ho Shon, W. Yan, P. J. Roach et al., "Comparison of pinhole and SPECT99mTc-MIBI imaging in primary hyperparathyroidism," *Nuclear Medicine Communications*, vol. 29, no. 11, pp. 949–955, 2008.

[19] I. A. Ho Shon, E. J. Bernard, P. J. Roach, and L. W. Delbridge, "The value of oblique pinhole images in pre-operative localisation with 99mTc-MIBI for primary hyperparathyroidism," *European Journal of Nuclear Medicine*, vol. 28, no. 6, pp. 736–742, 2001.

[20] M. B. Tomas, P. V. Pugliese, G. G. Tronco, C. Love, C. J. Palestro, and K. J. Nichols, "Pinhole versus parallel-hole collimators for parathyroid imaging: an intraindividual comparison," *Journal of Nuclear Medicine Technology*, vol. 36, no. 4, pp. 189–194, 2008.

[21] M. Lorberboym, I. Minski, S. Macadziob, G. Nikolov, and P. Schachter, "Incremental diagnostic value of preoperative 99mTc-MIBI SPECT in patients with a parathyroid adenoma," *Journal of Nuclear Medicine*, vol. 44, no. 6, pp. 904–908, 2003.

[22] D. Moka, E. Voth, M. Dietlein, A. Larena-Avellaneda, and H. Schicha, "Technetium 99m-MIBI-SPECT: a highly sensitive diagnostic tool for localization of parathyroid adenomas," *Surgery*, vol. 128, no. 1, pp. 29–35, 2000.

[23] A. Slater and F. V. Gleeson, "Increased sensitivity and confidence of SPECT over planar imaging in dual-phase sestamibi for parathyroid adenoma detection," *Clinical Nuclear Medicine*, vol. 30, no. 1, pp. 1–3, 2005.

[24] D. L. Thomas, T. Bartel, Y. Menda, J. Howe, M. M. Graham, and M. E. Juweid, "Single photon emission computed tomography (SPECT) should be routinely performed for the detection of parathyroid abnormalities utilizing technetium-99m sestamibi parathyroid scintigraphy," *Clinical Nuclear Medicine*, vol. 34, no. 10, pp. 651–655, 2009.

[25] L. Harris, J. Yoo, A. Driedger et al., "Accuracy of technetium-99M SPECT-CT hybrid images in predicting the precise intraoperative anatomical location of parathyroid adenomas," *Head and Neck*, vol. 30, no. 4, pp. 509–517, 2008.

[26] D. R. Neumann, N. A. Obuchowski, and F. P. DiFilippo, "Preoperative 123I/99mTc-sestamibi subtraction SPECT and SPECT/CT in primary hyperparathyroidism," *Journal of Nuclear Medicine*, vol. 49, no. 12, pp. 2012–2017, 2008.

[27] D. Papathanassiou, J. B. Flament, J. M. Pochart et al., "SPECT/CT in localization of parathyroid adenoma or hyperplasia in patients with previous neck surgery," *Clinical Nuclear Medicine*, vol. 33, no. 6, pp. 394–397, 2008.

[28] R. Prommegger, G. Wimmer, C. Profanter et al., "Virtual neck exploration: a new method for localizing abnormal parathyroid glands," *Annals of Surgery*, vol. 250, no. 5, pp. 761–765, 2009.

[29] P. J. Roach, G. P. Schembri, I. A. Ho Shon, E. A. Bailey, and D. L. Bailey, "SPECT/CT imaging using a spiral CT scanner for anatomical localization: impact on diagnostic accuracy and reporter confidence in clinical practice," *Nuclear Medicine Communications*, vol. 27, no. 12, pp. 977–987, 2006.

[30] A. Serra, P. Bolasco, L. Satta, A. Nicolosi, A. Uccheddu, and M. Piga, "Role of SPECT/CT in the preoperative assessment of hyperparathyroid patients," *Radiologia Medica*, vol. 111, no. 7, pp. 999–1008, 2006.

[31] M. L. Taubman, M. Goldfarb, and J. I. Lew, "Role of SPECT and SPECT/CT in the surgical treatment of primary hyperparathyroidism," *International Journal of Molecular Imaging*, vol. 2011, Article ID 141593, 2011.

[32] G. Wimmer, C. Profanter, P. Kovacs et al., "CT-MIBI-SPECT image fusion predicts multiglandular disease in hyperparathyroidism," *Langenbeck's Archives of Surgery*, vol. 395, no. 1, pp. 73–80, 2010.

[33] G. Pata, C. Casella, S. Besuzio, F. Mittempergher, and B. Salerni, "Clinical appraisal of 99mTechnetium-sestamibi SPECT/CT compared to conventional SPECT in patients with primary hyperparathyroidism and concomitant nodular goiter," *Thyroid*, vol. 20, no. 10, pp. 1121–1127, 2010.

[34] G. Pata, C. Casella, G. C. Magri, S. Lucchini, M. B. Panarotto, N. Crea et al., "Financial and clinical implications of low-energy CT combined with 99m Technetium-sestamibi SPECT for primary hyperparathyroidism," *Annals of Surgical Oncology*, vol. 18, pp. 2555–2563, 2011.

[35] I. W. Gayed, E. E. Kim, W. F. Broussard et al., "The value of 99mTc-sestamibi SPECT/CT over conventional SPECT in the evaluation of parathyroid adenomas or hyperplasia," *Journal of Nuclear Medicine*, vol. 46, no. 2, pp. 248–252, 2005.

[36] J. Ruf, D. Seehofer, T. Denecke et al., "Impact of image fusion and attenuation correction by SPECT-CT on the scintigraphic detection of parathyroid adenomas," *NuklearMedizin*, vol. 46, no. 1, pp. 15–21, 2007.

[37] C. Billotey, A. Aurengo, Y. Najean et al., "Identifying abnormal parathyroid glands in the thyroid uptake area using technetium-99m-sestamibi and factor analysis of dynamic structures," *Journal of Nuclear Medicine*, vol. 35, no. 10, pp. 1631–1636, 1994.

[38] Y. Krausz, E. Shiloni, M. Bocher, S. Agranovicz, B. Manos, and R. Chisin, "Diagnostic dilemmas in parathyroid scintigraphy," *Clinical Nuclear Medicine*, vol. 26, no. 12, pp. 997–1001, 2001.

[39] R. Phitayakorn and C. R. McHenry, "Incidence and location of ectopic abnormal parathyroid glands," *American Journal of Surgery*, vol. 191, no. 3, pp. 418–423, 2006.

[40] A. C. Perkins, D. R. Whalley, and J. G. Hardy, "Physical approach for the reduction of dual radionuclide image subtraction artefacts in immunoscintigraphy," *Nuclear Medicine Communications*, vol. 5, no. 8, pp. 501–512, 1984.

Publication III. Unpublished manuscript

Virpi Tunninen, Pekka Varjo, Tomi Kauppinen, Anu Holm, Hannu Eskola, Marko Seppänen. Tc-99m-sestamibi/I-123 subtraction SPECT/CT in parathyroid scintigraphy: Is additional pinhole imaging useful?

Tc-99m-sestamibi/I-123 subtraction SPECT/CT in parathyroid scintigraphy: Is additional pinhole imaging useful?

Virpi Tunninen Tech.Lic[1], Pekka Varjo, MD[1], Tomi Kauppinen, PhD[2], Anu Holm, PhD[1], Hannu Eskola, PhD[3], Marko Seppänen, D.Med.Sc.[4,5]

[1]Department of Nuclear Medicine, Satakunta Central Hospital, Sairaalantie 3, 28500 Pori, Finland, [2]Helsinki University Hospital/HUS Medical Imaging Center, Helsinki, P.O. Box 340, 00029 HUS, Finland, [3]Faculty of Biomedical Sciences, Tampere University of Technology, P.O. Box 692, 33101 Tampere, Finland and Regional Imaging Center, Tampere University Hospital, P.O. Box 2000, 33521 Tampere, [4]Turku PET Centre, Turku University Hospital, P.O. Box 52, 20521 Turku, Finland, [5]Department of Clinical Physiology and Nuclear Medicine, Turku University Hospital, P.O. Box 52, 20521 Turku, Finland

Author responsible for correspondence concerning the manuscript:

Chief Physicist Virpi Tunninen
The Department of Nuclear Medicine
Satakunta Central Hospital, 28500 Pori, Finland
Tel. +358(0)44 707 7366, Fax. +358(0)2 627 7370
E-mail: virpi.tunninen@satshp.fi

There are no conflicts of interest or sources of funding to disclose

Short Title: Parathyroid Scintigraphy

ABSTRACT

Purpose: Tc-99m-sestamibi/I-123 subtraction SPECT/CT is a modern protocol for localization of parathyroid adenomas. This retrospective study evaluated whether the use of additional anterior Tc-99m-sestamibi/I-123 pinhole imaging improves the outcome of Tc-99m-sestamibi/I-123 subtraction SPECT/CT in parathyroid scintigraphy (PS).

Materials and Methods: PS using simultaneous dual isotope subtraction methods with Tc-99m-sestamibi and I-123 and an acquisition protocol combining SPECT/CT and planar pinhole imaging was performed between March 2011 and June 2016 for 175 patients with primary or secondary hyperparathyroidism. All patients who proceeded to surgery with complete post-surgery laboratory findings were included in this study. SPECT/CT images alone and combined with pinhole images were evaluated.

Results: There were 111 adenomas of which 104 and 108 adenomas were correctly visualized by SPECT/CT (7 false positive) or SPECT/CT with pinhole (3 false positive), respectively. Both sensitivity and specificity were higher with combined SPECT/CT with pinhole than with SPECT/CT alone (97% vs. 94% and 99% vs. 98%, respectively, not significant). The false-positive rate was 6% with SPECT/CT and decreased to 3% using combined SPECT/CT with pinhole.

Conclusion: Tc-99m-sestamibi/I-123 subtraction SPECT/CT is a highly sensitive and specific protocol for PS. The use of additional anterior pinhole imaging increases both sensitivity and specificity of PS, although this increase is not statistically significant. Given the low cost and time required for this additional imaging with no additional radiation dose to the patient, we feel that the use of this additional pinhole imaging is justified to achieve the highest possible sensitivity and specificity for each patient to avoid reoperation.

Key Words: parathyroid, SPECT/CT, pinhole, dual-isotope

Primary hyperparathyroidism is a common endocrine disorder caused by one or more hyperfunctioning parathyroid glands. Hyperfunctioning parathyroid glands secrete excess amounts of parathyroid hormone, which raises the blood calcium level. Secondary hyperparathyroidism, which is most commonly seen in patients with chronic kidney failure, refers to parathyroid gland hyperfunction in response to low blood calcium levels. Patient symptoms and laboratory findings contribute to identifying candidates for surgery, which is the only curative treatment for these indications (1).

Preoperative localization of hyperfunctioning parathyroid glands is highly recommended to define surgical strategy, select patients for minimally invasive surgery, and reduce the rate of surgical conversion or failure. Imaging protocols should effectively provide morphologic and functional information in a noninvasive and cost effective manner (2).

Today, scintigraphic imaging is usually performed using the dual-phase method, where only Tc-99m-sestamibi is used with early and late phase acquisitions. This method is based on the assumption that the kinetics of Tc-99m-sestamibi is different in thyroid and parathyroid glands, thereby revealing hyperfunctioning parathyroid glands in late phase images. This dual-phase method is attractive for its technical simplicity and low cost (3). Unfortunately, this technique has limits for detecting parathyroid adenomas with rapid Tc-99m-sestamibi clearance and low sensitivity for localizing multiple parathyroid glands due to parathyroid hyperplasia or differentiating thyroid nodules from parathyroid lesions (4).

These pitfalls can be avoided with more technically demanding dual-isotope subtraction methods with I-123 and Tc-99m-sestamibi. Thyroid-seeking I-123 is acquired simultaneously with Tc-99m-sestamibi, and normalized I-123 images are subtracted from Tc-99m-sestamibi images. Residual activity in subtraction images reveals hyperfunctioning parathyroid glands. The advantages of this method have been shown in several recent studies, and it is also recommended in the European Association of Nuclear Medicine (EANM) guidelines (5-10).

Several acquisition techniques can be used with each method. Both planar imaging (with parallel hole or pinhole collimators) and three-dimensional (3D) imaging (SPECT and SPECT/CT) are widely used. Although the trend is towards using 3D acquisition techniques, pinhole imaging remains a recommended part of any parathyroid imaging protocol and it is still considered superior owing to its much higher spatial resolution (9-14).

However, pinhole imaging lacks the 3D anatomical information offered by modern SPECT/CT imaging which may be very helpful in planning the surgical approach and even in shortening surgical times (4, 14, 15). These techniques are often combined in clinical practice to increase sensitivity (3, 12, 16, 17).

It would be tempting to simplify the parathyroid imaging protocol using only SPECT/CT imaging, but this would have to be performed without compromising on sensitivity or

specificity. Some preliminary results have already been published using the dual-isotope method where SPECT/CT results were equivalent or even better than pinhole (7, 11, 18). However, contrasting data showing pinhole imaging alone yielded better results than SPECT/CT alone or even combined with pinhole have been reported (13).

The aim of this study was to compare two protocols for parathyroid scintigraphy in the same patients with primary or secondary hyperparathyroidism: Tc-99m-sestamibi/I-123 subtraction SPECT/CT alone or combined with additional pinhole imaging.

PATIENTS AND METHODS

Patients

From March 2011 through June 2016, 175 patients were referred for parathyroid scintigraphy. All patients had biochemical evidence of hyperparathyroidism (elevated total serum calcium (Ca-ion) and parathyroid hormone level [PTH]). From this original cohort, patient data were included in this retrospective study if the patient proceeded to surgery and if post-operative Ca-ion and PTH results were available. Surgical and histopathological findings with post-operative Ca-ion and PTH levels were used as the gold standard.

The final study group consisted of 94 patients (27 men and 67 women) with a mean age of 64.0 years (range, 22.3–83.6 years). Of these, 84 patients had primary hyperparathyroidism (pHPT), and 10 had secondary hyperparathyroidism (sHPT). This study was exempt from approval by the institutional review board. The requirement for informed consent was waived.

Parathyroid Scintigraphy Protocols

Patients received 20 MBq (0.54 mCi) of I-123 intravenously. Two hours later, 750 MBq (20.3 mCi) of Tc-99m-sestamibi was injected. SPECT/CT acquisition was started 10 minutes after the Tc-99m-sestamibi administration. All SPECT/CT acquisitions were performed with Siemens Symbia T or Siemens Intevo T2 imaging systems (Siemens, Erlangen, Germany). Immediately after the SPECT/CT acquisition, a static pinhole image of the neck was acquired with a SKYLight gamma camera (Philips Healthcare, USA) or with Siemens Symbia or Intevo T2 systems (Siemens, Erlangen, Germany) beginning in 2015. All acquisition parameters are shown in Table 1.

TABLE 1. Acquisition parameters for SPECT/CT and pinhole imaging

Acquisition Parameter	SPECT/CT	Pinhole
Detector Configuration	180°	-
Orbit	Body-contour	-
Distance from the patient skin	-	10cm
Collimators	LEHR	Pinhole, 5mm opening
Matrix	128×128 matrix	256×256
Zoom	1	2,19
Pixel Size	4.8 mm	
Acquisition Mode	Step-and-Shoot	Static
Views Over 360°	96 (3,75° per projection)	-
Time Per Projection or Frame	33 s	10 min
Energy Windows	140 keV 10% 167 keV 10%	140 keV 10% 167 keV 10%
Voltage	130kVp	-
Collimation	2×2.5 mm	-
Rotation Time	0.8 s,	-
Pitch	1,5	-
Dose Modulation	CARE Dose AEC+DOM	-
Reference Exposure	80 mAs	-

Surgery and histologic analysis

An endocrine surgeon performed all operations and was aware of all initial scintigraphic results prior to surgery. The mean interval between scintigraphy and surgery was 164 days (range, 8–1065 days). Histopathological analysis was performed on all excised tissue.

Image processing

Tc-99m-sestamibi and I-123 SPECT images (with attenuation correction) were anonymized and reconstructed on the Siemens Syngo workstation using the FLASH 3D-algorithm (8 iterations, 8 subsets, Gaussian 9.00 filter). I-123 SPECT images were multiplied by a normalization factor (defined as the ratio of the corresponding thyroid maximum voxel counts in Tc-99m-sestamibi and I-123 SPECT images with manual adjustment based on visual evaluation, if necessary) to create normalized I-123 SPECT images, that were then subtracted from Tc-99m-sestamibi SPECT images. The final image sets consisted of Tc-99m-sestamibi SPECT images, I-123 SPECT images, and subtraction SPECT images. Images were displayed in 3 axes (transverse, coronal, and sagittal) alone, fused together (as I-123 fused with subtraction images), or fused with CT images. Static pinhole images were anonymized and processed in a Siemens Syngo workstation. Subtraction images were created in a similar manner as previously described. The final image set consisted of Tc-99m-sestamibi images,

I-123 images, and subtraction images. All image processing was performed by an experienced medical physicist.

Image Interpretation

Anonymized imaging data were reviewed for the purpose of this study by an experienced nuclear medicine physician who had no previous knowledge of images, patient information, or surgery results. The review was performed in two phases: the SPECT/CT data were reviewed first and each quadrant in relation to the thyroid gland (right upper, right lower, left upper, left lower, other/ectopic) was classified on a 2-point scale (negative or positive). The image review criteria for positive finding were as follows: clear abnormal residual activity on the subtraction SPECT images that had an anatomic correlation in the CT-images. Thereafter, the pinhole images were added next to the SPECT/CT data and images were reviewed together again in similar manner.

To estimate the sensitivity, specificity, and accuracy for the localization for each image set, findings were classified as true-positive, false-positive, true-negative, or false-negative with histologic analysis and post-operative laboratory findings as the reference standard. For each patient, 5 scores, one for each quadrant plus other (referring as ectopic), were assigned. The false-positive image rate was defined as the ratio of false-positives to the sum of true-positives plus false-positives.

Statistical Analysis

The sensitivity, specificity, and accuracy of each image set were calculated. McNemar test was performed to compare the sensitivities, specificities, and accuracies between the two image sets. A p-value less than 0.05 was considered statistically significant. Statistical analyses were conducted using SPSS v.21 (IBM Corp., Armonk, NY).

RESULTS

Surgical and histological findings

Altogether, 111 enlarged glands were found in 94 patients in surgery. Seventy-nine patients had a solitary parathyroid adenoma, 1 had parathyroid carcinoma, 12 had double adenomas, and 2 had multiglandular disease (1 with 3 enlarged glands and 1 with 4 enlarged glands). The mean weight of the abnormal parathyroid glands was 1.42 g (0.07–11 g). The smallest visible gland was 0.07 g in both image sets.

Imaging Results

Tc-99m-sestamibi/I-123 subtraction SPECT/CT was able to locate 104 enlarged glands correctly, and missed 7 enlarged glands that were located in surgery. Combined Tc-99m-sestamibi/I-123 subtraction SPECT/CT with additional pinhole imaging was able to locate

108 enlarged glands and missed 3 enlarged glands. A typical patient case with a true-positive finding is shown in Figure 1.

FIGURE 1. An example of a true-positive finding with SPECT/CT and with pinhole in primary hyperparathyroidism. **A**, Fusion SPECT/CT images. **B**, Anterior pinhole images (*Left*: Tc-99m-sestamibi image; *middle*: I-123 image; *right*: subtraction image). A 230 mg adenoma (arrows) was resected behind the lower right quadrant of the thyroid.

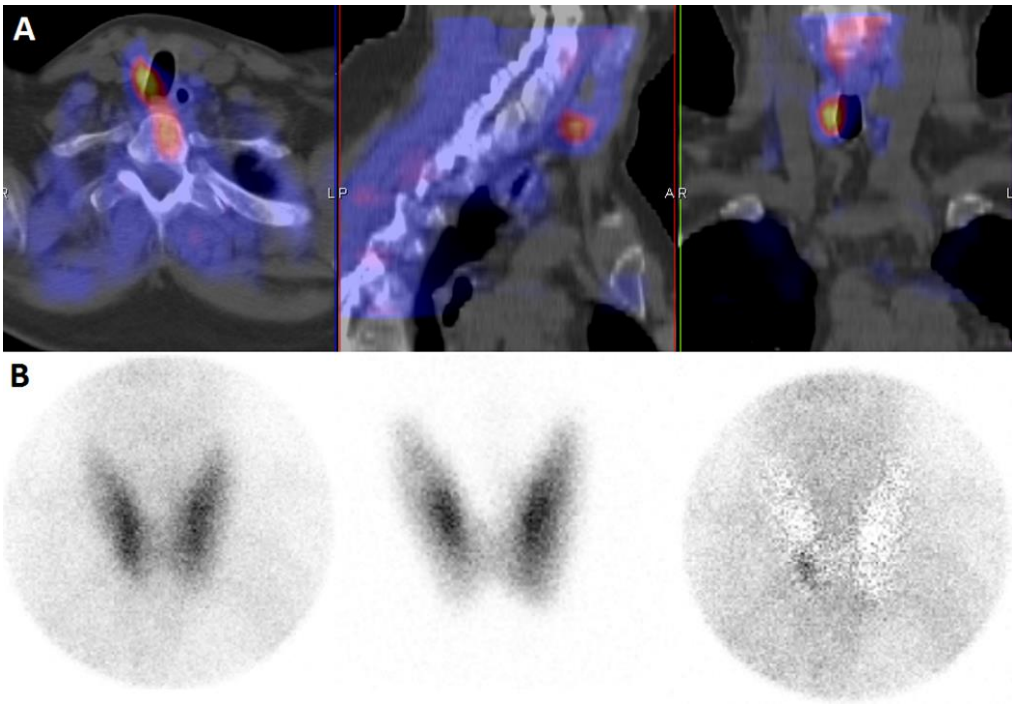

The sensitivity and specificity were slightly higher with SPECT/CT and pinhole combined than with SPECT/CT alone, but the difference was not significant. The false-positive rate was 6% with SPECT/CT and decreased to 3% with combined SPECT/CT and pinhole. Sensitivity and specificity were also calculated separately for patients with sHPT or pHPT. As expected, sensitivity was lower for patients with sHPT compared to patients with pHPT. There were no false positive findings in patients with sHPT. Results are depicted in Table 2.

TABLE 2. Sensitivity and specificity of Tc-99m –sestamibi/I-123 subtraction SPECT/CT and combined SPECT/CT with anterior planar pinhole imaging for all patients

Patient group	Sensitivity/Specificity	SPECT/CT	SPECT/CT with pinhole	*p*
All patients	Sensitivity	94%	97%	*NS*
	Specificity	98%	99%	*NS*
Primary hyper-parathyreosis	Sensitivity	95%	98%	*NS*
	Specificity	98%	99%	*NS*
Secondary hyper-parathyreosis	Sensitivity	89%	94%	*NS*
	Specificity	100%	100%	*NS*

NS indicates not statistically significant

False Negative Findings

Four parathyroid glands were classified falsely as negative with SPECT/CT alone, but they were correctly classified as true positive with additional pinhole imaging. Three parathyroid glands were falsely classified as negative in SPECT/CT and were also not visible in pinhole images. Two of these were small hyperplastic glands, and 1 was a small atypical adenoma. These 3 patients had more than 1 hyperplastic gland or adenoma, and smallest glands were not visualized in these cases.

False Positive Findings

Four parathyroid glands were classified falsely as positive with SPECT/CT alone, but were correctly classified as true-negative with additional pinhole imaging. Two of these were owing to uneven iodine uptake, with iodine-negative thyroid nodules more clearly visible in pinhole images. Two false-positive findings were subtraction artifacts, not visible in pinhole images.

Three false-positive findings in patients with complex multi-glandular disease that were classified with SPECT/CT alone remained falsely classified with the additional pinhole imaging.

Patient 1 had a true-positive adenoma at the upper left quadrant that was attached to a large thyroid cyst. There was weak residual activity at the lower left quadrant on both SPECT/CT and pinhole imaging classified as positive, but no adenoma was found during

surgery (normal parathyroid gland was seen). There was also a small adenoma at upper right quadrant, but it was not visible in either SPECT/CT or pinhole imaging and was classified as a false negative. Post-operative Ca-ion and PTH were normalized for this patient.

Patient 2 had 3 positive findings with both SPECT/CT and pinhole imaging. The upper right gland (small hyperplastic gland) was removed in surgery and classified as true-positive. Lower glands were visualized in surgery but not removed. Post-operative Ca-ion and PTH levels were normal. These 2 false-positive findings were classified as subtraction artifacts.

DISCUSSION

This retrospective study compared Tc-99m-sestamibi/I-123 –protocols using SPECT/CT alone or combined with an additional anterior pinhole image. The results indicate high sensitivity and specificity for both protocols. The use of the additional anterior pinhole image with SPECT/CT was able to improve both sensitivity and specificity, although the difference was not significant. The sensitivity and specificity of Tc-99m-sestamibi/I-123 –protocols using SPECT/CT alone or with pinhole imaging were equivalent in 2 recent studies (7, 18). However, no comparison to a combination of these protocols was made in either of the studies.

Interesting results were published recently by Bhatt and colleagues showing that a Tc-99m-sestamibi/I-123 pinhole protocol detected more adenomas than the Tc-99m-sestamibi/I-123 SPECT/CT protocol and missed fewer adenomas than either the Tc-99m-sestamibi/I-123 SPECT-CT protocol or the combined pinhole and SPECT-CT protocol (13). As Bhatt and colleagues suggested, one explanation for this result might be the rapid washout-phenomena since the SPECT/CT was started 45 minutes after sestamibi injection in comparison to 5 minutes in this study. Another explanation could be related to the acquisition parameters of the SPECT, since imaging was performed with quite a large angular sampling (5.6°). SPECT reconstruction parameters could also have had some effect, but this possibility cannot be evaluated because the parameters were not published. We have seen in our clinical work that reader's level of experience has a great effect on the sensitivity and specificity of Tc-99m-sestamibi/I-123 SPECT/CT. This could possibly have had some effect in the study by Bhatt and colleagues, since their study was conducted soon after the installation of SPECT/CT and the reader may not have had sufficient time to train with the new protocol.

The Importance of Pinhole Imaging

The EANM parathyroid guidelines stated in 2009 that "*Although SPECT and SPECT/CT imaging are becoming very helpful, they cannot replace the standard planar and "pinhole" protocols that are still essential for optimal resolution in the thyroid bed region and for a*

correct diagnosis" (10). This is still true, since the spatial resolution of the pinhole collimator cannot be reached with any parallel-hole collimator. The highest achievable resolution is important especially for detecting the thyroid nodules, especially the Tc-MIBI-Hot/I-123-Cold phenotype which may indicate thyroid malignancy (19, 20). This phenotype also results in false-positive residual activity in subtraction images, which can be easily interpreted as parathyroid adenoma.

The importance of pinhole imaging was also highlighted in this study, as both sensitivity and specificity were higher with the combined pinhole protocol although the difference was not statistically significant. However, it should be noted that the number of false-positive findings decreased to half and 4 more adenomas were correctly localized with the pinhole imaging. Although not statistically significant, there was a change in the final outcome of this study for 8 patients. The use of the additional pinhole imaging is fast, it does not increase the patient radiation dose or add to the total cost of the study. Thus we feel that the use of the additional pinhole imaging is justified to gain the highest possible sensitivity and specificity for each patient to avoid reoperation.

The Edge Artifact

Even optimal processing of Tc-99m and I-123 images does not give a flawless subtraction image, but leaves some activity around the edges of thyroid lobes; this activity is called the "edge artifact" (7). According to phantom measurements performed in our laboratory, this phenomenon could be reduced with careful implementation of acquisition and processing parameters, scatter/cross-contamination correction, and collimator selection. However, further studies are needed in order to implement this solution in clinical practice.

False-Negative Findings

There were only 3 enlarged parathyroid glands that were not visualized even with the additional pinhole image. Two of these were small hyperplastic glands, 1 was a small adenoma (0.14 g) which was a part of a complicated patient case with a true-positive finding, true-negative finding, false-positive finding, and a false-negative finding (the patient had a thyroid cyst and a double adenoma).

False-Positive Findings

It has been suggested that SPECT/CT is superior to SPECT alone because the specificity of SPECT/CT is significantly greater than that of SPECT alone. The false positive rate in this study with SPECT/CT was 6% which was in line with a Finnish study (6).
In addition to multimodality imaging, the use of I-123 and subtraction images fused together gives a strong suggestion of the nature of the lesion in subtraction images. Also with additional pinhole imaging, we were able to avoid all false-positive findings due to iodine-cold nodules in the thyroid.

The Effect of Reconstruction

It has been shown in several publications that there are significant differences in image quality between commercially available algorithms and correction methods (21-23). The effect of reconstruction parameters were not studied here. To further improve the quality of Tc-99m-sestamibi/I-123 SPECT/CT in parathyroid imaging, the final step is to optimize the protocol to include reconstruction and the correction methods for scatter, attenuation, depth-dependent resolution, and cross-contamination.

Limitations of the Study

Three different cameras were used in this study. All SPECT/CT acquisitions were performed with Siemens cameras (Symbia/Intevo) and, according to clinical quality control measurements, there were no differences in image quality. Pinhole acquisitions were performed with older Philips SKYLight with Siemens cameras. According to quality control measurements, there was no significant difference in image quality (resolution, sensitivity) between these cameras and thus no effect on results. The main bias in this study is probably the large variation in the time between scintigraphy and surgery.

CONCLUSION

This study indicates that Tc-99m-sestamibi/I-123 subtraction SPECT/CT is a highly sensitive and specific protocol for parathyroid scintigraphy. The use of additional anterior pinhole imaging increases both sensitivity and specificity of parathyroid scintigraphy, although this increase is not significant in this cohort. Given the low cost and short time required for additional imaging with no added radiation dose to the patient, we believe that the use of this additional pinhole imaging is justified to achieve the highest possible sensitivity and specificity for each patient to avoid reoperation.

ACKNOWLEDGEMENTS

We thank the staff of the Department of Nuclear Medicine at Satakunta Central Hospital.

REFERENCES

1. Bilezikian JP, Brandi ML, Eastell R, et al. Guidelines for the management of asymptomatic primary hyperparathyroidism: summary statement from the Fourth International Workshop. *J Clin Endocrinol Metab*. 2014;99:3561-3569.
2. Hindie E, Zanotti-Fregonara P, Tabarin A, et al. The Role of Radionuclide Imaging in the Surgical Management of Primary Hyperparathyroidism. *J Nucl Med*. 2015;56:737-744.
3. Bahador FM, Latifi HR, Grossman SJ, et al. Optimal interpretative strategy for preoperative parathyroid scintigraphy. *Clin Nucl Med*. 2015;40:116-122.
4. Taieb D, Hindie E, Grassetto G, et al. Parathyroid scintigraphy: when, how, and why? A concise systematic review. *Clin Nucl Med*. 2012;37:568-574.
5. Krakauer M, Wieslander B, Myschetzky PS, et al. A Prospective Comparative Study of Parathyroid Dual-Phase Scintigraphy, Dual-Isotope Subtraction Scintigraphy, 4D-CT, and Ultrasonography in Primary Hyperparathyroidism. *Clin Nucl Med*. 2015.
6. Ryhanen EM, Schildt J, Heiskanen I, et al. (99m)Technetium Sestamibi-(123)Iodine Scintigraphy Is More Accurate Than (99m)Technetium Sestamibi Alone before Surgery for Primary Hyperparathyroidism. *Int J Mol Imaging*. 2015;2015:391625.
7. Tunninen V, Varjo P, Schildt J, et al. Comparison of Five Parathyroid Scintigraphic Protocols. *International Journal of Molecular Imaging*. 2013;2013:12.
8. Caveny SA, Klingensmith WC, 3rd, Martin WE, et al. Parathyroid imaging: the importance of dual-radiopharmaceutical simultaneous acquisition with 99mTc-sestamibi and 123I. *J Nucl Med Technol*. 2012;40:104-110.
9. Klingensmith WC, Koo PJ, Summerlin A, et al. Parathyroid Imaging: The Importance of Pinhole Collimation with Both Single- and Dual-Tracer Acquisition. *Journal of Nuclear Medicine Technology*. 2013.
10. Hindie E, Ugur O, Fuster D, et al. 2009 EANM parathyroid guidelines. *Eur J Nucl Med Mol Imaging*. 2009;36:1201-1216.
11. Dontu VS, Kettle AG, O'Doherty MJ, et al. Optimization of parathyroid imaging by simultaneous dual energy planar and single photon emission tomography. *Nucl Med Commun*. 2004;25:1089-1093.
12. Taieb D, Hassad R, Sebag F, et al. Tomoscintigraphy improves the determination of the embryologic origin of parathyroid adenomas, especially in apparently inferior glands: imaging features and surgical implications. *J Nucl Med Technol*. 2007;35:135-139.
13. Bhatt PR, Klingensmith WC, 3rd, Bagrosky BM, et al. Parathyroid Imaging with Simultaneous Acquisition of 99mTc-Sestamibi and 123I: The Relative Merits of Pinhole Collimation and SPECT/CT. *J Nucl Med Technol*. 2015;43:275-281.
14. Taieb D, Urena-Torres P, Zanotti-Fregonara P, et al. Parathyroid Scintigraphy in Renal Hyperparathyroidism: The Added Diagnostic Value of SPECT and SPECT/CT. *Clin Nucl Med*. 2013;38:630-635.
15. Wong KK, Fig LM, Gross MD, et al. Parathyroid adenoma localization with 99mTc-sestamibi SPECT/CT: a meta-analysis. *Nucl Med Commun*. 2015;36:363-375.
16. Nichols KJ, Tomas MB, Tronco GG, et al. Preoperative parathyroid scintigraphic lesion localization: accuracy of various types of readings. *Radiology*. 2008;248:221-232.

17. Heiba SI, Jiang M, Rivera J, et al. Direct Comparison of Neck Pinhole Dual-Tracer and Dual-Phase MIBI Accuracies With and Without SPECT/CT for Parathyroid Adenoma Detection and Localization. *Clin Nucl Med*. 2015.

18. Hassler S, Ben-Sellem D, Hubele F, et al. Dual-Isotope 99mTc-MIBI/123I Parathyroid Scintigraphy in Primary Hyperparathyroidism: Comparison of Subtraction SPECT/CT and Pinhole Planar Scan. *Clin Nucl Med*. 2013.

19. Onkendi EO, Richards ML, Thompson GB, et al. Thyroid cancer detection with dual-isotope parathyroid scintigraphy in primary hyperparathyroidism. *Ann Surg Oncol*. 2012;19:1446-1452.

20. Greilsamer T, Blanchard C, Christou N, et al. Management of thyroid nodules incidentally discovered on MIBI scanning for primary hyperparathyroidism. *Langenbecks Arch Surg*. 2015;400:313-318.

21. van Hoorn RA, Vriens D, Postema JW, et al. The influence of SPECT reconstruction algorithms on image quality and diagnostic accuracy in phantom measurements and 99mTc-sestamibi parathyroid scintigraphy. *Nucl Med Commun*. 2013.

22. Ekjeen T, Tocharoenchai C, Pusuwan P, et al. Optimization and evaluation of reconstruction-based compensation methods and reconstruction parameters for Tc-99m MIBI parathyroid SPECT. *Physica medica : PM : an international journal devoted to the applications of physics to medicine and biology : official journal of the Italian Association of Biomedical Physics*. 2015;31:159-166.

23. Nichols KJ, Tronco GG, Palestro CJ. Effect of reconstruction algorithms on the accuracy of (99m)Tc sestamibi SPECT/CT parathyroid imaging. *American journal of nuclear medicine and molecular imaging*. 2015;5:195-203.

Publication IV

Tunninen V., Kauppinen T., Eskola H. (2018) Physical characteristics of collimators for dual-isotope imaging with 99mTc and 123I. In: Eskola H., Väisänen O., Viik J., Hyttinen J. (eds) EMBEC & NBC 2017. EMBEC 2017, NBC 2017. IFMBE Proceedings, vol 65. Springer, Singapore.

Physical characteristics of collimators for dual-isotope imaging with ^{99m}Tc and ^{123}I

V. Tunninen[1], T. Kauppinen[2] and H. Eskola[3,4]

[1]Satakunta Central Hospital/Department of Nuclear Medicine, Pori, Finland
[2]Helsinki University Hospital/HUS Medical Imaging Center, Helsinki, Finland
[3]Faculty of Biomedical Sciences and Engineering, Tampere University of Technology, Tampere, Finland
[4]Department of Radiology, Tampere University Hospital, Tampere, Finland

Abstract—**The purpose of this study was to compare the physical characteristics of Low Energy High Resolution (LEHR), Low Energy Ultra High Resolution (LEUHR) and Medium Energy Low Penetration (MELP) collimators for simultaneous ^{99m}Tc and ^{123}I imaging. MELP collimator performed well with ^{123}I high-energy gamma photons, but low resolution makes it unsuitable to use for acquisition of small structures such as parathyroid adenomas. LEUHR collimators optimized for ^{99m}Tc have highest resolution, but the differences in septal penetration and sensitivity in favor of LEHR collimator needs to be tested with specific parathyroid phantoms.**

Keywords—**dual-isotope, ^{99m}Tc, ^{123}I, collimator, SPECT/CT.**

I. Introduction

Modern SPECT/CT is a standard clinical tool for various nuclear medicine procedures. Clinical work is usually performed with one radiopharmaceutical, but there are some applications using simultaneous dual-isotope imaging such as parathyroid scintigraphy with ^{123}I and ^{99m}Tc-sestamibi. Simultaneous use of ^{99m}Tc and ^{123}I is particularly challenging because of the close proximity of the photon energies (140keV and 158keV) and with limited energy resolution of a gamma camera.

Collimator selection for dual-isotope applications is always a compromise in terms of resolution, sensitivity and septal penetration of photons. It has been shown previously that "*the physical characteristics for ^{123}I imaging and dual-isotope imaging differ even between low energy collimators that provide similar sensitivity and spatial resolution*" [1].

The use of medium energy (ME) collimators reduces the influence of septal penetration of high-energy gamma photons of ^{123}I. However, ME collimators generally provide lower spatial resolution compared to that of low energy (LE) collimator, which may influence the detection of small structures such as parathyroid adenomas [1,2]. If the LE collimator is used to acquire good quality ^{99m}Tc images, the septal penetration of ^{123}I photons may be elevated and image contrast will be degraded [3]. The energy window selection, the contamination of one radionuclide photon into the energy window of the other (cross contamination), energy-dependent uniformity and sensitivity also need to be examined [4].

Several approaches are suggested for simultaneous ^{123}I/^{99m}Tc-imaging, e.g.:

1. Using narrow or asymmetric energy windows [5,6]
2. Using a subtraction method based on a single crossover factor [7]
3. Using a scatter correction method (TEW) [8]
4. Using complex and time-consuming model-based correction methods [9].

The septal penetration of high-energy photons of ^{123}I is also a potential cause of artefacts. It also effects on ^{123}I sensitivity as a function of distance, as high-energy photons penetrate through the lead into the crystal and behave as camera would be without collimator [2]. That is why suggested the physical characteristics should be investigated for each camera-collimator system used for dual-isotope imaging [1,3].

The aim of this study was to compare the physical characteristics of Low Energy High Resolution (LEHR), Low Energy Ultra High Resolution (LEUHR) and Medium Energy Low Penetration (MELP) collimators for ^{99m}Tc and ^{123}I imaging.

II. Materials and Methods

A Siemens Symbia Intevo T2 SPECT/CT (Siemens, Erlangen, Germany) in the Department of Nuclear Medicine of Satakunta Central Hospital was used in this study. All measurements were performed with three sets of collimators: LEHR, LEUHR and MELP (Table 1).

Table 1 Collimator specifications according to manufacturer

Collimator	MELP	LEHR	LEUHR
Hole length (mm)	40,64	24,05	35,8
Septal thickness (mm)	1,14	0,16	0,13
Hole Diameter (mm)	2,94	1,11	1,16
Sensitivity @ 10 cm (cpm/μCi)	275	202	100
System resolution @ 10 cm (mm)	12,5	7,5	6,0

H. Eskola et al. (eds.), *EMBEC & NBC 2017*,
IFMBE Proceedings 65,
DOI: 10.1007/978-981-10-5122-7_62

Intrinsic uniformity was measured separately with ^{99m}Tc and ^{123}I according to the quality control routine by Siemens. ^{99m}Tc was measured using 140 keV 10% energy window and ^{123}I was measured using symmetric (158 keV, 10%) and asymmetric (167keV, 10%) energy windows. 60 million counts were collected for each measurement.

System sensitivity was measured for each collimator following the NEMA guidelines [10], using a 100mm plastic dish into which calibrated activity of (about 37MBq) each isotope (^{99m}Tc or ^{123}I) was instilled. Measurements were performed separately for each isotope using the above-mentioned energy windows with 10 cm distance from the collimator surface. Sensitivity was calculated as cpm/μCi.

System spatial resolution was measured in air with ^{99m}Tc and ^{123}I separately for each collimator following the NEMA guidelines [10]. A tube of 1mm inner diameter was filled with ^{99m}Tc or ^{123}I solution and placed at various distances from detector surface (0 cm, 10cm, 20 cm, 30cm, and 40 cm) parallel to the x axis of the camera using non-scattering material as a spacer. Images were collected on a 1024x1024 matrix with above-mentioned energy window settings.

SPECT spatial resolution and uniformity with scatter were measured with Jaszczak phantom with hot spot insert (Data Spectrum Corporation, Durham, North Carolina). The phantom was filled with 1,5GBq of ^{99m}Tc and acquired with clinical SPECT/CT acquisition protocol for all collimators (a noncircular orbit, 180° detector configuration, 128×128 matrix; 140 keV 10%, step-and-shoot, 48 views for each detector, 33 s/projection).

The CT acquisition was acquired after the SPECT acquisition without moving the phantom and using the same scan area as for SPECT (130 kVp, 2×2.5 mm collimation, 0.8 s rotation time, 1.5 pitch, CARE Dose AEC+DOM, with the ref. exposure 80 mAs). ^{99m}Tc images (with attenuation correction) were reconstructed on the Siemens Syngo workstation using the FLASH 3D-algorithm with four different parameter settings (6, 8, 16 or 32 iterations, 8 subsets, Gaussian 9.00 filter, with TEW scatter correction).

SPECT spatial resolution was evaluated visually, according to the visibility of the hollow channels (12,7mm (1), 11,1mm (2), 9,5mm (3), 7,9mm (4), 6,4mm (5) and 4,8mm (6)). To evaluate uniformity, a large circular ROI was drawn in uniform part of the phantom. The percent root mean square noise (%RMS) was calculated using the formula:

$$\%rms = \frac{SD}{mean} \times 100\% \quad [1]$$

Spectrum for both isotopes was measured in air and with scatter separately for each collimator at various distances (10cm, 20cm, 30cm and 40cm). Measurements were repeated also with scatter (5cm water as scattering material) between the source and the detector.

Scatter-to-photopeak –ratio was measured using ^{99m}Tc and ^{123}I point sources of equal activity (80MBq) in air separately for each collimator at various distances (10cm, 20cm, 30cm and 40cm). Photopeak and scatter windows were set to 20% (photopeak and scatter windows being equal width in keV). Acquisition time per frame for each collimator was selected to avoid pixel overflow in any measurement. Uniformity correction was set off to avoid any adjustment of counts. Background counts were subtracted. Measurements were repeated also with scatter (5cm water as scattering material) between the source and the detector.

Cross-contamination was measured using two identical 1000 ml bottles filled with ^{99m}Tc and ^{123}I (~40MBq of each). A SPECT acquisition was performed with each bottle using previously mentioned acquisition protocol with both energy window settings and for all collimators. The cross-contamination was expressed as percentage of ^{99m}Tc counts in ^{123}I window of ^{99m}Tc counts in ^{99m}Tc window. The ^{123}I cross-contamination in ^{99m}Tc window was calculated in a similar manner.

III. Results

Integral uniformity at the useful field of view (UFOV) with symmetric energy windows were 3,1% and 2,2% with ^{99m}Tc and ^{123}I, respectively. With asymmetric ^{123}I energy window the uniformity was 11,9%.

System sensitivity with ^{99m}Tc was well in line with specifications given by Siemens. Sensitivity with ^{123}I symmetric energy window was higher with low-energy collimators compared to sensitivity with ^{99m}Tc, which is caused by septal penetration of high-energy gamma photons of ^{123}I. Asymmetric energy window with ^{123}I reduced sensitivity 15,0%-43,2% compared to symmetric energy window. System sensitivity results are presented in Table 2.

Table 2 System sensitivity for LEHR, LEUHR and MELP collimators measured with ^{99m}Tc and ^{123}I using symmetric and asymmetric energy windows.

Collimator	^{99m}Tc (cpm/μCi)	^{123}I symmetric (cpm/μCi)	^{123}I asymmetric (cpm/μCi)
MELP	220	205	117
LEHR	159	282	231
LEUHR	72	149	127

Measured FWHM for was similar for ^{99m}Tc and ^{123}I. For MELP collimator there was no difference in FWTM values for ^{99m}Tc and ^{123}I. For LE collimators, FWTM was larger with ^{123}I than that with ^{99m}Tc. There was no difference with symmetric and asymmetric energy windows for ^{123}I. The results are presented in Table 3.

Table 3 System spatial resolution at 20cm for LEHR, LEUHR and MELP collimators measured with ^{99m}Tc and ^{123}I using symmetric and asymmetric energy windows.

Collimator	FWHM (mm)		FWTM (mm)	
	^{99m}Tc	^{123}I	^{99m}Tc	^{123}I
MELP	17,3	16,8	30,0	29,9
LEHR	11,3	11,5	20,1	23,0
LEUHR	8,3	7,6	14,8	16,0

SPECT spatial resolution with MELP collimators was inadequate for acquisition of small structures. Only two largest channels could be identified. LEHR and LEUHR collimators performed better, as channels in sectors 3 and 4 could be identified, respectively. SPECT uniformity decreased with increasing resolution and number of iterations. The results are presented in Table 4.

Table 4 SPECT resolution and uniformity for LEHR, LEUHR and MELP collimators measured with ^{99m}Tc and ^{123}I using symmetric and asymmetric energy windows.

		Iterations			
		6	8	16	32
MELP	Resolution	1	1	2	2
	Uniformity (%rms)	3	3,3	4,2	5,9
LEHR	Resolution	3	3	3	3
	Uniformity (%rms)	3,1	3,4	4,4	5,6
LEUHR	Resolution	4	4	4	4
	Uniformity (%rms)	3,5	3,9	5,1	6,2

The shape of the spectrum in air for ^{99m}Tc was similar for all collimators and distances. Scattering material increased the amount of scatter, but there was no change in the shape as a function of distance or between collimators. Spectrum for ^{123}I in air was different for collimators (Figure 1) and also varied as a function of distance (Figure 2).

Scatter to photopeak –ratio in air with ^{99m}Tc was 13,0%-14,7% for all collimators and distances. With scatter, the ratio increased to 46,8%-49,3%. Distance between the source and collimator surface did not have any significant effect. Scatter to photopeak –ratio with ^{123}I was very different for all collimators and also as a function of distance (Table 5).

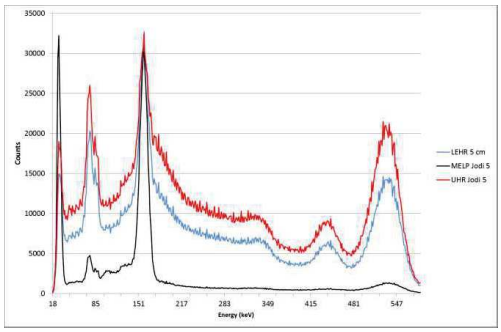

Figure 1. Spectrum of ^{123}I at 5 cm from detector in air for LEHR (blue), LEUHR (red) and MELP (black) collimators.

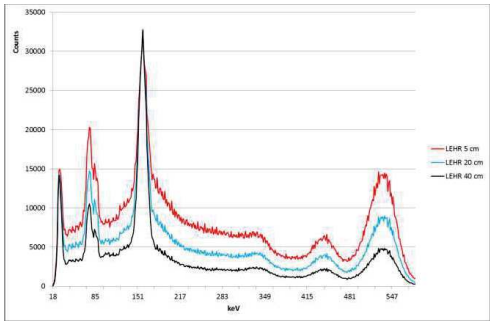

Figure 2. Spectrum of ^{123}I with LEHR collimator at 5 cm (red), 20cm (blue) and 40cm (black) from detector.

Table 5. Scatter to photopeak –ratio with ^{123}I for collimators in air and with scatter with 10cm, 20cm, 30cm, and 40 cm distance between source and collimator surface.

Collimator	10cm	20cm	30cm	40cm
MELP, air	20,0	18,9	17,9	16,7
MELP, scatter	58,1	57,5	57,2	57,0
LEHR, air	42,1	35,4	30,6	26,6
LEHR, scatter	57,9	54,7	52,0	50,2
UHR, air	53,4	47,0	41,7	36,7
UHR, scatter	67,0	64,5	62,5	60,9

Cross-contamination measurements showed similar contamination of ^{99m}Tc in ^{123}I window for all collimators. Asymmetric energy window for ^{123}I was reduced to approximately half when using asymmetrical energy window. ^{123}I contamination in ^{99m}Tc window was highest with LEUHR collimator and lowest with MELP collimator (Table 6).

Table 6 Cross-contamination of ^{99m}Tc and ^{123}I.

	^{99m}Tc-contamination in		^{123}I contamination in
	^{123}I symmetric	^{123}I asymmetric	^{99m}Tc
MELP	4,7 %	1,8 %	28,3 %
LEHR	4,7 %	2,0 %	40,7 %
LEUHR	5,1 %	2,6 %	50,6 %

IV. Discussion

The advantages of dual isotope method with ^{99m}Tc-sestamibi and ^{123}I for parathyroid scintigraphy have been acknowledged in several studies and is also recommended in the European Association of Nuclear Medicine (EANM) guideline for parathyroid scintigraphy [11]. Unfortunately dual isotope imaging with ^{99m}Tc and ^{123}I is a challenging task. Collimators optimized for ^{99m}Tc have problems with ^{123}I high energy photon septal penetration. ME collimators have less septal penetration, but the resolution is inadequate for detecting small structures as shown in this study.

SPECT acquisitions are performed with elliptical orbit in order to gain highest resolution possible. However, as shown in this study, both sensitivity and cross contamination of ^{123}I into ^{99m}Tc window are dependent on the distance between the source and the collimator which degrades the quantitative precision. Cross contamination of ^{99m}Tc into ^{123}I window is low. Although the injected activity of ^{123}I in clinical study is much lower than the activity of the ^{99m}Tc-sestamibi, the uptake of iodine in the thyroid gland is higher. The average activities of ^{123}I and ^{99m}Tc in the thyroid gland are thus comparable and the contamination of ^{99m}Tc in ^{123}I image is not significant. Shifting the ^{123}I window to the right decreases the amount of cross contamination and allows for wider scatter window between ^{99m}Tc and ^{123}I photopeak but in the expense of uniformity. The contamination of ^{123}I in ^{99m}Tc image is much higher regardless of the collimator. Shifting the ^{99m}Tc window to the left was not tested here, as being shown inappropriate previously [2].

The most important information in parathyroid scintigraphy is in the ^{99m}Tc-sestamibi image. The ^{123}I image is mainly used for removal of the thyroid gland. Although ^{99m}Tc image is contaminated with ^{123}I photons, their spatial distribution is different as parathyroid glands are separated from thyroid glands (excluding rare cases of intrathyroidal parathyroid glands). High resolution images are thus of high importance.

The choice of the collimator for simultaneous dual-isotope imaging is a compromise. LEUHR collimator has highest spatial resolution, but due to thinner septa the ^{123}I contamination in ^{99m}Tc image is higher. LEHR collimators has twice the sensitivity but in the expense of resolution. The suitability of both LE collimators for parathyroid imaging needs to be tested with specific phantoms in order to resolve the suitability for clinical work.

V. Conclusions

MELP collimator performed well with ^{123}I, but low resolution makes it unsuitable to use for acquisition of small structures. LEUHR collimators optimized for ^{99m}Tc have highest resolution, but the small difference in septal penetration in favor of LEHR collimator needs to be tested with specific parathyroid phantoms. This study pointed out that thorough testing before clinical application is of high importance in order to understand physical limitations of the imaging process.

Conflict of Interest

The authors declare that they have no conflict of interest.

References

1. Inoue Y, Shirouzu I, Machida T, et al (2003). Physical characteristics of low and medium energy collimators for ^{123}I imaging and simultaneous dual-isotope imaging. Nucl Med Commun, 24(11), 1195-1202.
2. Dobbeleir A, Hambye A, Franken P (1999). Influence of high-energy photons on the spectrum of iodine-123 with low- and medium-energy collimators: consequences for imaging with ^{123}I-labelled compounds in clinical practice. Eur J Nucl Med, 26(6), 655-658.
3. Ivanovic M, Weber D, Loncaric S, et al (1994). Feasibility of dual radionuclide brain imaging with I-123 and Tc-99m. Med Phys, 21(5), 667-674.
4. Madsen M, O'Leary D, Andreasen N, et.al (1993). Dual isotope brain SPECT imaging for monitoring cognitive activation: physical considerations. Nucl Med Commun, 14(5), 391-396.
5. Devous M Sr, Lowe J, & Payne J (1992). Dual-isotope brain SPECT imaging with technetium-99m and iodine-123: validation by phantom studies. J Nucl Med, 33(11), 2030-2035.
6. Neumann D, Obuchowski N, & Difilippo F. (2008). Preoperative ^{123}I/^{99m}Tc-Sestamibi Subtraction SPECT and SPECT/CT in Primary Hyperparathyroidism. J Nucl Med, 49(12), 2012-2017.
7. Neumann D, Esselstyn C Jr, Go R, et al (1997). Comparison of double-phase ^{99m}Tc-sestamibi with ^{123}I-^{99m}Tc-sestamibi subtrac-

tion SPECT in hyperparathyroidism. AJR Am J Roentgenol, 169(6), 1671-1674
8. Ogasawara K, Hashimoto J, Ogawa K, et al (1998). Simultaneous acquisition of iodine-123 emission and technetium-99m transmission data for quantitative brain single-photon emission tomographic imaging. Eur J Nucl Med, 25(11), 1537-1544.
9. Shcherbinin S, Chamoiseau S, & Celler A (2012). Quantitative image reconstruction for dual-isotope parathyroid SPECT/CT: phantom experiments and sample patient studies. Phys Med Biol, 57(15), 4755-4769.
10. NEMA National Electrical Manufacturers Association, NEMA Standards Publication NU 1 (2007): Performance measurements of scintillation cameras.NEMA, Rosslyn, VA
11. Hindie E, Ugur O, Fuster D, et al (2009). 2009 EANM parathyroid guidelines. Eur J Nucl Med Mol Imaging; 36:1201-1216.

Author: Virpi Tunninen, chief physicist
Institute: Satakunta Central Hospital,
Department of Nuclear Medicine
Street: Sairaalantie 3
City: 28500 Pori
Country: Finland
Email: Virpi.tunninen@satshp.fi

Publication V

Tunninen V., Kauppinen T., Eskola H. (2018) Optimization of 99mTc-sestamibi/123I subtraction SPECT/CT protocol for parathyroid scintigraphy. In: Eskola H., Väisänen O., Viik J., Hyttinen J. (eds) EMBEC & NBC 2017. EMBEC 2017, NBC 2017. IFMBE Proceedings, vol 65. Springer, Singapore.
.

Optimization of ^{99m}Tc-sestamibi/^{123}I subtraction SPECT/CT protocol for parathyroid scintigraphy

V. Tunninen[1], T. Kauppinen[2] and H. Eskola[3,4]

[1]Satakunta Central Hospital/Department of Nuclear Medicine, Pori, Finland
[2]Helsinki University Hospital/HUS Medical Imaging Center, Helsinki, Finland
[3]Faculty of Biomedical Sciences and Engineering, Tampere University of Technology, Tampere, Finland
[4]Deparment of Radiology, Tampere University Hospital, Tampere, Finland

Abstract—**The purpose of this study was to optimize effective, but technically challenging ^{99m}Tc-sestamibi/^{123}I subtraction SPECT/CT protocol for parathyroid scintigraphy. An anthropomorphic parathyroid phantom was set up using a small sphere, a thyroid phantom and a thorax phantom with clinical range of activities of ^{123}I and ^{99m}Tc. SPECT/CT acquisitions were performed using three collimators (Low Energy High Resolution (LEHR), Low Energy Ultra High Resolution (LEUHR) and Medium Energy Low Penetration (MELP)) and two energy window settings. Images were reconstructed with a combination of four different numbers of iterations and with or without scatter correction. Images were subjected to visual and quantitative evaluation. The effect of collimator, energy window selection and reconstruction parameters had a significant effect on visual appearance and adenoma contrast in parathyroid ^{99m}Tc-sestamibi/^{123}I subtraction SPECT/CT. Symmetrical energy windows and ultra-high resolution collimator yielded best results with some improvement with scatter correction.**

Keywords— **parathyroid, SPECT/CT, phantom, optimization, dual-isotope.**

I. Introduction

The diagnosis of hyperparathyroidism is based on laboratory findings, with ionized calcium and parathormone levels being elevated. Patient should be referred for parathyroid scintigraphy only when above-mentioned diagnostic criteria are met. Parathyroid scintigraphy is thus not a diagnostic study, but a localization one. Localization of hyperfunctioning parathyroid glands before surgery is highly recommended to define surgical strategy.

The only tracer available for parathyroid scintigraphy, ^{99m}Tc-sestamibi is not parathyroid-specific but taken up also by adjacent thyroid tissue. This problem can be solved by using either a single isotope (dual-phase) or a dual-isotope method.

The dual-phase method assumes that thyroid and parathyroid tissue have different washout kinetics for ^{99m}Tc-sestamibi. By acquiring images immediately after the injection and 2-3 hours later, the focally increasing uptake will reveal hyperfunctioning parathyroid gland. In the dual-isotope method, ^{99m}Tc-sestamibi is used together with ^{123}I, which is taken up by the thyroid gland only. Subtracting the ^{123}I image from the ^{99m}Tc-sestamibi image leaves only enlarged parathyroid glands in the subtraction image. Imaging findings are based on a visual appearance of subtraction image, confirmed with anatomical reference in the CT image.

The advantages of dual-isotope method with ^{99m}Tc-sestamibi and ^{123}I for parathyroid scintigraphy have been acknowledged in several studies and are recommended in the European Association of Nuclear Medicine (EANM) guideline for parathyroid scintigraphy [1]. This method has been applied in Finland, as all nuclear medicine departments performing parathyroid scintigraphy are now using dual-isotope method with ^{99m}Tc-sestamibi and ^{123}I as their first method of choice in parathyroid scintigraphy [2].

Both planar and tomographic acquisition techniques are used clinically. Planar pinhole acquisition has its advantages due to superior spatial resolution, but modern SPECT/CT imaging offers three-dimensional images together with exact anatomical information. These techniques are often combined to increase sensitivity and specificity [3-4]. However, acquisition of an additional image requires the change of the collimator and increases the total length of the study. Thus, it would be attempting to simplify imaging protocol but this has to be done without decreasing image quality. It should be noted that a large, active parathyroid adenoma is clearly visible regardless of the imaging protocol used. The current clinical problem are patients with secondary hyperparathyroidism with relatively inactive hyperplastic glands, and patients with multiglandular disease, where patient has more than one enlarged parathyroid glands [5].

^{99m}Tc-sestamibi/^{123}I subtraction SPECT/CT is technically challenging. Close proximity of the photon energies (140keV and 158keV) with limited energy resolution of a gamma camera detector leads to cross-contamination of isotopes. Asymmetric energy window for ^{123}I is generally used to reduce ^{99m}Tc contamination in ^{123}I energy window, [6-7]. The septal penetration of high-energy photons of ^{123}I is also a potential cause of artefacts in subtraction images. The selection of collimator (due to different septal thick-

H. Eskola et al. (eds.), *EMBEC & NBC 2017*,
IFMBE Proceedings 65,
DOI: 10.1007/978-981-10-5122-7_212

ness, resolution and sensitivity) has thus a marked effect on the final results [8]. Reconstruction parameters and the use of scatter correction will also have effect [9-10].

The purpose of this study was to optimize the parathyroid scintigraphy ^{99m}Tc-sestamibi/^{123}I subtraction SPECT/CT - protocol using an anthropomorphic phantom. The effect of collimator choice, energy window settings and the reconstruction parameters (number of iterations, scatter correction) were studied.

II. Materials and Methods

For the purpose of this study, a phantom mimicking parathyroid patient with a small, low intensity adenoma was set up (Figure 1). A thyroid gland phantom (Radiology Support Devices) was filled with ^{123}I and ^{99m}Tc (concentration of 500 kBq/ml). A small sphere with inner diameter of 7.86mm (Micro Hollow Sphere, Data Spectrum) was filled with lower ^{99m}Tc –concentration as thyroid gland (~300kBq/ml) to mimic small parathyroid adenoma or hyperplastic gland (0.25ml with ~125kBq of ^{99m}Tc) and attached behind the thyroid gland. The thyroid and parathyroids were inserted into the thorax phantom (Radiology Support Devices), which was then filled with 350MBq of ^{99m}Tc. Activities were measured using a VIK-202 ionization chamber (Veenstra) used in clinical work and subjected to strict daily quality control measures.

A series of SPECT/CT scans were performed with three sets of collimators: Low Energy High Resolution (LEHR), Low Energy Ultra High Resolution (LEUHR) and Medium Energy Low Penetration (MELP) and with two energy window settings, clinical and test windows (Table I).

SPECT was acquired using normal clinical acquisition protocol (a noncircular orbit, 180° detector configuration, 128×128 matrix; 4.8 mm pixel size; step-and-shoot, 48 views for each detector, 33 s/projection).

Figure 1. Thorax phantom, the thyroid gland and spherical phantom mimicking parathyroid adenoma. Images are not in scale.

Table 1 Energy window settings

Energy Window Setting	Energy Window	Photopeak at	Window Width (%)	Window Limits (keV)
Clinical	Scatter	-	15%	112 – 133
	^{99m}Tc	140 keV	10%	133 – 147
	Scatter	-	7%	147 – 156
	^{123}I	167 keV	10%	159 – 175
Test	Scatter	-	15%	112 – 133
	^{99m}Tc	140 keV	10%	133 – 147
	Scatter	-	2%	147 – 149
	^{123}I	158 keV	10%	150 – 165

The CT acquisition for attenuation correction and image fusion was acquired after the SPECT acquisition without moving the phantom and using the same scan area as for SPECT (130 kVp, 2×2.5 mm collimation, 0.8 s rotation time, 1.5 pitch, CARE Dose AEC+DOM, with the ref. exposure 80 mAs). All acquisitions were performed with Siemens Symbia Intevo T2 SPECT/CT ((Siemens, Erlangen, Germany) in the Department of Nuclear Medicine of Satakunta Central Hospital.

^{99m}Tc-sestamibi and ^{123}I SPECT images (with attenuation correction) were reconstructed on the Siemens Syngo workstation using the FLASH 3D-algorithm with eight parameter settings (6, 8, 16 or 32 iterations, 8 subsets, Gaussian 9.00 filter, with and without TEW scatter correction).

^{123}I SPECT images were multiplied by a normalization factor (as the ratio of the thyroid maximum voxel counts in ^{99m}Tc and ^{123}I SPECT images to create normalized ^{123}I SPECT images, which were then subtracted from ^{99m}Tc SPECT images. All images were subjected to visual and quantitative evaluation. Image processing and evaluation was performed by an experienced medical physicist. All images were anonymized (no knowledge of collimator or acquisition or processing parameters) and scored from 0 to 5. Scoring was based on clinical appearance (the intensity of adenoma, the presence of artefacts).

For quantitative analysis, a VOI was drawn around the sphere using the fused CT image as a reference (with corresponding background VOI). An image contrast C for sphere was calculated using the formula (1):

$$C = \frac{C_{adenoma} - C_{background}}{C_{background}} \times 100\% \qquad [1]$$

where:

$C_{adenoma}$ is the number of counts in the sphere,

$C_{background}$ is the number of counts in the background area

The mean values for contrast and visual scores were calculated for each collimator (all energy windows and processing parameters), for each energy window setting (all collimators and processing parameters) and for scatter correction (all collimators, energy windows and processing parameters).

III. Results

The calculated contrast for adenoma was between 0,4%-80,9%. The visual scores were between 0-5. The contrast and visual scores were in correlation (Figure 2). The mean values for contrast and visual scores were highest for LEUHR collimator and for test energy windows settings. Contrast values were higher with scatter correction, but visual scores were lower (Table 2).

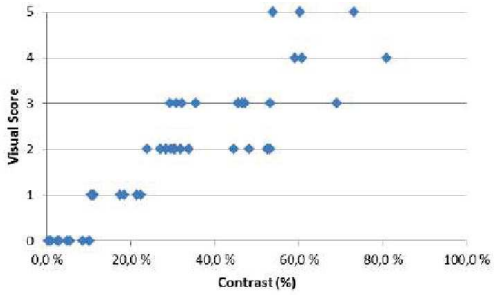

Figure 2. Visual score as a function of contrast.

Table 2 Mean contrast values and visual scores calculated for collimators, energy window settings and with or without scatter correction

	$Contrast_{mean}$	$Visual_{mean}$
MELP	18 %	0,9
LEHR	26 %	1,8
LEUHR	47 %	2,9
Clinical	18 %	0,8
Test	43 %	2,9
SC-	28 %	1,9
SC+	32 %	1,8

The mean values for contrast for reconstruction parameters (for all collimators and energy window settings) were higher with an increasing number of iterations. However, visual scores were highest with 16 iterations, increasing iterations to 32 decreased the visual appearance of the images (Table 3).

Table 3 Mean contrast values and visual scores calculated for eight reconstruction parameter settings for all collimators

Iteration, SC-/SC+	$Contrast_{mean}$	$Visual_{mean}$
6, SC-	24 %	1, 7
8, SC-	26 %	1,7
16, SC-	30 %	2,2
32, SC-	33 %	2,0
6, SC+	22 %	1,5
8, SC+	27 %	1,7
16, SC+	36 %	2,2
32, SC+	47 %	2,0

The mean values for contrast for each combination of collimator, energy window and scatter correction are presented in Table 4. The highest mean values for contrast and visual scores were with LEUHR collimator with not-corrected test energy window. Phantom images with highest visual scores and with current clinical protocol are presented in Figure 3.

Table 4 Mean contrast values and visual scores calculated for collimators with two energy window settings and with or without scatter correction

Collimator, Energy Window, Correction	$Contrast_{mean}$	$Visual_{mean}$
MELP, Clinical, SC+	2 %	0,0
MELP, Clinical, SC-	9 %	0,0
MELP, Test, SC-	25 %	1,5
MELP, Test, SC+	37 %	2,3
LEHR, Clinical, SC-	9 %	0,5
LEHR, Clinical, SC+	9 %	0,5
LEHR, Test, SC-	30%	2,5
LEHR, Test, SC+	55 %	3,5
LEUHR, Clinical, SC-	30 %	2,0
LEUHR, Clinical, SC+	50 %	2,0
LEUHR, Test, SC-	67 %	4,8
LEUHR, Test, SC+	4 %	2,8

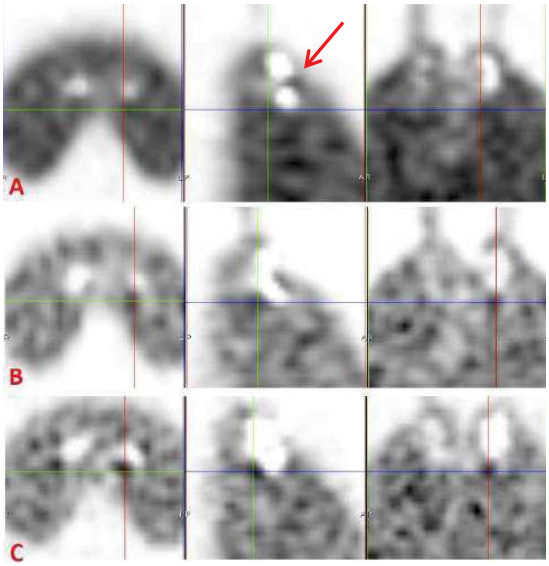

Figure 3. From left to right, transverse, sagittal, and coronal images of the phantom (an adenoma is located at the crosshair). A) LEHR Clinical, 8 iterations, no scatter correction (current clinical protocol), B) LEHR Test, 16 iterations, scatter correction, and C) LEUHR Test, 16 iterations, no scatter correction. The red arrow is showing "the edge artefact".

IV. Discussion

The findings of this study confirmed that the selection of collimator, energy window positioning and reconstruction parameters have a significant effect on the visual appearance of images. Collimators with higher resolution yielded better results, as did increasing iterations in reconstruction. The energy window setting had a significant effect on the appearance of subtraction images, as symmetric window for ^{123}I was always better than asymmetric window. Scatter correction increased calculated contrast, but at the same time, the visual appearance was decreased due to increased noise.

Current clinical protocol for parathyroid scintigraphy with LEHR collimator, asymmetric energy window without scatter correction was able to visualize adenoma only faintly. Switching to symmetric energy window for ^{123}I and applying scatter correction with more iterations was able to increase visual score from 0,5 to 3,5. MELP collimator would be attempting choice for imaging with ^{123}I due to thicker septa, but low spatial resolution is not adequate when searching for small, relatively inactive parathyroid gland. LEUHR collimator with symmetric energy windows had best contrast and visual scores. The scatter correction in fact decreased these results, probably due to statistics as LEUHR collimator has sensitivity of approximately 50% compared to LEHR collimator and subtraction-based scatter correction reduces counts even further. The visual effect of increasing noise is visible in the Figure 3, where the artifactual "blobs" have a similar appearance to parathyroid adenoma. However, this misinterpretation can be avoided with the use of CT, and the search of the anatomical reference.

The so-called edge artefact [11] is currently the main cause of false positive findings in ^{99m}Tc-sestamibi/^{123}I subtraction SPECT/CT (Figure 3). According to the results of this study, the edge-artefact is more present with lower resolution image and with asymmetric ^{123}I window. LEUHR symmetric window images did not include any marked artefact.

According to the results of this study, increasing the number of iterations to more than 16 decreased the visual scores due to increased noise. However, it should be noted that this is highly dependent on camera and collimator specifications, acquisition parameters and activity of ^{99m}Tc-sestamibi and ^{123}I used.

Due to large variation of adenoma contrast and visual scores in this study, we find that the protocols used in clinical practice should be thoroughly tested using phantoms. Although clinical situation is different when comparing to phantom studies (patient movement, breathing, extra thyroid ^{99m}Tc-sestamibi activity), the ultimate detection limit should be resolved.

V. Conclusions

The effect of collimator, energy window selection and reconstruction parameters have a significant effect on visual appearance and adenoma contrast in parathyroid ^{99m}Tc-sestamibi/^{123}I subtraction SPECT/CT. Symmetrical energy windows and high-resolution collimator yielded best results with some improvement with scatter correction.

Conflict of Interest

The authors declare that they have no conflict of interest.

References

1. Hindie E, Ugur O, Fuster D, et al (2009). 2009 EANM parathyroid guidelines. Eur J Nucl Med Mol Imaging; 36:1201-1216.
2. Tunninen V, Varjo P, Kauppinen T. Towards harmonization in parathyroid scintigraphy in Finland – A seven year follow-up study (2016). EJNMMI 43; Suppl 2.

3. Bahador FM, Latifi HR, Grossman SJ, et al (2015). Optimal interpretative strategy for preoperative parathyroid scintigraphy. Clin Nucl Med;40:116-122
4. Hassler S, Ben-Sellem D, Hubele F, et al. (2013). Dual-Isotope ^{99m}Tc-MIBI/^{123}I Parathyroid Scintigraphy in Primary Hyperparathyroidism: Comparison of Subtraction SPECT/CT and Pinhole Planar Scan. Clin Nucl Med; 39(1):32-6
5. Hindie E, Zanotti-Fregonara P, Tabarin A, et al (2015). The Role of Radionuclide Imaging in the Surgical Management of Primary Hyperparathyroidism. J Nucl Med;56:737-744
6. Neumann DR, Obuchowski NA, Difilippo FP (2008). Preoperative ^{123}I/^{99m}Tc-Sestamibi Subtraction SPECT and SPECT/CT in Primary Hyperparathyroidism. J Nucl Med;49:2012-2017.
7. Dontu VS, Kettle AG, O'Doherty MJ, et al. (2004). Optimization of parathyroid imaging by simultaneous dual energy planar and single photon emission tomography. Nucl Med Commun ;25:1089-1093
8. Inoue Y, Shirouzu I, Machida T, et al. (2003). Physical characteristics of low and medium energy collimators for ^{123}I imaging and simultaneous dual-isotope imaging. Nucl Med Comm (24); 1195-1202.
9. Nichols KJ, Tronco GG, Palestro CJ (2015). Effect of reconstruction algorithms on the accuracy of (^{99m})Tc sestamibi SPECT/CT parathyroid imaging. Am J Nucl Med Mol Imaging. 5:195-203
10. van Hoorn RA, Vriens D, Postema JW, et al. (2013). The influence of SPECT reconstruction algorithms on image quality and diagnostic accuracy in phantom measurements and ^{99m}Tc-sestamibi parathyroid scintigraphy. Nucl Med Commun; 35; 64-72.
11. Tunninen V, Varjo P, Schildt J, et al (2013). Comparison of Five Parathyroid Scintigraphic Protocols. Int J Mol Imaging, Article ID 921260, 12 pages, 2013. doi:10.1155/2013/921260

Author: Virpi Tunninen, Chief Physicist
Institute: Satakunta Central Hospital,
Department of Nuclear Medicine
Street: Sairaalantie 3
City: 28500 Pori
Country: Finland
Email: virpi.tunninen@satshp.fi

Tampereen teknillinen yliopisto
PL 527
33101 Tampere

Tampere University of Technology
P.O.B. 527
FI-33101 Tampere, Finland

ISBN 978-952-15-4011-0
ISSN 1459-2045